Universität Rostock Traditio et Innovatio

Dissertation

Spectral Characteristics of Photocatalytic Constant for Titania

Submitted by:

Adwaa Ahmed

born on 10.10.1979 in Taiz - Yemen

Matriculation number: 214207773

In fulfillment of the requirement of the degree
of Doctor in Natural Sciences (Dr. rer. nat.)

Submitted on:

26.06.2020

Supervisor

Prof. Dr. Eberhard Burkel

https://doi.org/10.18453/rosdok_id00002963

Universität Rostock | Mathematisch-Naturwissenschaftliche Fakultät
Institut für Physik
Albert-Einstein-Straße 23–24, 18059 Rostock

Dieses Werk ist lizenziert unter einer
Creative Commons Namensnennung 4.0 International Lizenz.

Gutachter:
1- Prof. Dr. Eberhard Burkel, Universitaet Rostock, Institut fuer Physik.

2- Prof. Dr. Igor Khmelinskii, Universitaet der Algarve, Fakultaet fuer Naturwissenschaften und Technik.

Jahr der Einreichung: 26.06.2020.
Jahr der Verteidigung: 20.11.2020

Adwaa
Ahmed

DATE OF BIRTH:
10/10/1979

CONTACT

Nationality: Yemeni

Gender: Female

Justus-Von-Liebig-Weg 6A,
Room 214
18059 Rostock, Germany

yemenaa@gmail.com

(+49) 17628652979

LinkedIn: https://www.linkedin.com/in/adwaa-ahmed-04446b1a4/

Skype: Adwaa Ahmed

europass

WORK EXPERIENCE

Faro , Portugal

Good experience in some Micro and nanofabrication methods, Chemical Vapor Depositions , Thermal evaporation, Sputtering, ion milling, etc).

PhD student

Good experience in UV-Visible Spectroscopy and High-performance liquid chromatography (HPLC)

Rostock , Germany

Good experience in X- Rays Diffractions and Micromeritics ASAP-Physisorption Analyzer 2020

PhD student

EDUCATION AND TRAINING

06/07/2015 – Albert-Einstein-Straße 23–24, , Rostock, Germany

PhD

Institute of physics

Field(s) of study

- Natural sciences, mathematics and statistics : *Physics*

https://www.physik.uni-rostock.de/

06/06/2018 – 06/06/2019 – Faro, Portugal

International scholar (internship)

Algarve University

Field(s) of study

- Natural sciences, mathematics and statistics

01/05/2014 – 24/12/2014 – Taiz , Yemen

Assistant Lecturer

Taiz University

2010 – 27/04/2014 – Riyadh, Saudi Arabia

Master of science In Physics

Faculty of science- King Saud University

Field(s) of study

- Natural sciences, mathematics and statistics

Taiz, Yemen

Demonstrator in Physics department

Taiz University

Exercise classes,

laboratories, and lectures.

Field(s) of study

- Natural sciences, mathematics and statistics

2000 – 07/2003 – Taiz , Yemen

B.Sc. in physics

Faculty of science - Taiz university

Field(s) of study

- Natural sciences, mathematics and statistics

1995 – 1997 – Taiz , Yemen

High school

Asmaa school

LANGUAGE SKILLS

MOTHER TONGUE(S): Arabic

OTHER LANGUAGE(S):

English

Listening	Reading	Spoken production	Spoken interaction	Writing
C1	C1	C1	C1	C1

Deutsch

Listening	Reading	Spoken production	Spoken interaction	Writing
A2	A2	A2	A2	A2

DIGITAL SKILLS

■ Good experience in project management and team co-ordination / Good Experience in Microsoft Office / Ability to use Comsol, Mathematica, , Labview, and Nova electrochemical characterization software / Good experience in Phython / Good experience in Maud program, spectroscopy, Origin, Latex program, Linux, and WIEN2K program

PUBLICATIONS

First-principle analysis of the electronic and optical properties of ,boron and nitrogen doped carbon mono-layer graphenes

2015 https://www.sciencedirect.com/science/article/pii/S0008622314008999
Amel Laref

RECOMMENDATIONS

Prof.Dr. Eberhard Burkel – Supervisor – eberhard.burkel@uni-rostock.de
My first supervisor

Prof. Dr. Valentin Bessergenev – Supervisor – vbess@ualg.pt
My second supervisor in PhD

Pro.Dr.Conceicao Mateus – mcmateus@ualg.pt
My supervisor in lab

Pro. Amel Laref – amel_la06@yahoo.fr
My supervisor in Master degree.

PAPERS ARE PREPARING

I still have two papers under preparations

Paper (1): Spectral characteristics of Photocatalytic constant for Titania.

Paper (2): Photocatalytic decomposition of different dyes by photoelectrochemical.

DEDICATION

This work is dedicated to all my family.

Especially:

My parents, who supported me along the years of my studies.

My lover, who encouraged me and supported me along all the way.

My beloved sister Salwa.

Contents

Contents i
List of Figures . . . ii

List of Figures iii

List of Tables v

1 Introduction 1
1.1 Objectives . . . 2
1.2 Literature review . . . 4
1.2.1 Principle of photocatalysis . . . 6
1.2.2 Titanium dioxide (TiO_2) as a photocatalyst . . . 9
1.2.3 Doped TiO_2 . . . 11
1.2.4 Electrolysis . . . 12
1.3 Overview of the thesis . . . 14

2 Methods and experimental setup 15
2.1 Characterization . . . 16
2.1.1 X-Ray Diffraction . . . 16
2.1.2 Surface area and porosity . . . 17
2.1.2.1 Qualitative analysis . . . 19
2.1.2.2 Experimental details . . . 20
2.1.3 Photocatalytic activity setup . . . 21
2.1.3.1 Experimental setup . . . 21
2.1.4 UV-Visible Spectroscopy . . . 24
2.2 TiO_2 nanoparticles synthesis . . . 25
2.2.1 TiO_2 powders . . . 25
2.2.1.1 TiO_2 prepared by Sol-gel method . . . 25
2.2.1.2 TiO_2 doped with Cobalt(Co) . . . 28
2.3 TiO_2 thin film samples . . . 28
2.3.1 TiO_2 thin film deposition . . . 29
2.3.2 Photocatalytic activity of TiO_2 thin film . . . 32
2.3.3 Dye materials . . . 32

3 Results 36
3.1 Powder samples . . . 37
3.1.1 X-ray diffraction . . . 37

3.1.2 Surface Area . . . 41
3.1.3 UV-Visible absorption spectra . . . 44
3.1.4 Photocatalytic activity of TiO_2 nanopowders . . . 47
3.1.4.1 Using mercury lamp . . . 47
3.1.4.2 Using different wavelengths . . . 49
3.2 TiO_2 thin film . . . 52
3.2.1 X-ray diffraction . . . 52
3.2.2 Photocatalytic activity of TiO_2 thin film . . . 53

4 Discussion **60**
4.1 Surface area and porosity . . . 61
4.2 Analysis of energy gap . . . 62
4.3 The photocatalytic activity of TiO_2 nanopowders with using mercury lamp . . . 64
4.3.1 Spectral properties of the photocatalytic constant . . . 65
4.4 Photocatalytic decomposition of different dyes . . . 68

5 Summary and Conclusion **74**

A Appendix **78**
A.1
Appendix A . . . 79

Bibliography **81**

List of Figures

1.1 Solar radiation spectrum of the sun at sea level. 5
1.2 Spectra absorption of mercury lamp 5
1.3 Photocatalysis mechanism 8
1.4 Crystal structures of TiO_2 11

2.1 The types of isotherm for catalysts material. 18
2.2 The hysteresis shapes for mesoporous catalysts material. 19
2.3 The experimental setup for study the photocatalytic activity of TiO_2 powders. 23
2.4 Scheme of the sol-gel synthesis 27
2.5 CC-CVD setup of TiO_2 thin film. 31
2.6 Schematic diagram of a photoelectrochemical cell used within this work 34
2.7 Molecular structures of different dyes 35

3.1 XRD patterns of sample TiO_2 powders. 39
3.2 XRD patterns of P25 Degussa and Co-doped TiO_2 powders. 40
3.3 Typically N_2 isotherms of studied powders. 42
3.4 Pore size distribution of TiO_2 studied samples. 43
3.5 UV-Visible absorption spectra of selected powders. 45
3.6 Analysis of the optical energy gap of studied samples 46
3.7 Degradation of selected powders under UV illumination. 48
3.8 Photocatalytic degradation curves of selected powders under low wavelengths. 50
3.9 Photocatalytic degradation curves of selected powders under high wavelengths. 51
3.10 XRD pattern of the TiO_2 thin film deposited by the Chemical Vapor Deposited method. 53
3.11 UV-Vis absorption spectra of different dyes without thin film under dark. 55
3.12 UV-Vis absorption spectra of different dyes under UV illumanation without TiO_2 thin film. 56
3.13 Absorption spectra of Methanol Blue and Brilliant Green under the different effects. 57
3.14 Absorption spectra of Methyl Orange and Gentian Violet under the different effects. 58
3.15 The photocatalytic constant of different dyes with TiO_2 thin film under different effects. 59

4.1 The optical energy gap (E_g) of different samples. 63
4.2 The photocatalytic constants of the studied samples under UV illumination. 65
4.3 Photocatalytic constant (K) as a function of different wavelengths. . . 67
4.4 Schematic diagram of dyes 69
4.5 Relationship between the kinetic rate constant of TiO_2 thin film and different effects. 72

A.1.1UV-Vis absorption spectra of Eosin with TiO_2 thin film under different effects. 79
A.1.2The photocatalytic constant of TiO_2 thin film with Eosin (OS) under three effects. 80

List of Tables

1.1 The crystal structure of TiO_2 phases 10

2.1 The parameters of preparation for sol-gel powders. 27
2.2 Molar concentrations of different dyes and H_2O. 33

3.1 XRD results of selected powders. 38
3.2 Results calculated of specific surface area and pore size analysis 42
3.3 Wavelengths and the optical energy gap of selected powders. 45
3.4 Results calculated of the photocatalytic constant of selected powders under UV illumination. 47
3.5 Results calculated of the photocatalytic constant for different TiO_2 nanopowders under different wavelengths. 50
3.6 Results calculated of the photocatalytic constant for different dyes with TiO_2 thin film under different effects. 55

4.1 The results normalization of K constant for the sample powders . . . 68

List of Abbreviations and units

AOPs	Advanced oxidation processes
TiO_2	Titanium dioxide
CVD	Chemical Vapor Deposition
O_2	Oxygen
H_2	Hydrogen
A	anatase
R	rutile
Co	Cobalt
UV	UltraViolet
h^+	hole
e^-	electron
e-h	electron-hole
E_g	energy gap (eV)
VB	valence band
Å	Angstrom
CB	conduction band
UV-Vis	UV-Visible
PEC	Photoelectrochemical cell
K	kinetic constant
MB	Methanol Blue
GV	Gentian Violet
BG	Brilliant Green
MO	Methyl orange
EO	Eosin
XRD	X-Ray Diffraction
GofF	Refinement parameter

SA	Surface area(m^2g^{-1})
BET	Brunauer-Emmett-Teller
N_a	Avogadro number (mol^{-1})
HPLC	High-performance liquid chromatography
0°C	degree celcius
C	Current integrated peak at different time
C_0	Initial integrated peak
K	Photocatalytic constant (h^{-1})
h	Hour
I_0	Initial absorbance
I	Current absorbance after t time.
E	Electric field
K_{UV}	The photocatalytic constant under UV illumination
$K_{Darkness}$	The photocatalytic constant in darkness
K_{UV+E}	The photocatalytic constant by using UV illumination with electric field together

Acknowledgments

First and foremost I am grateful the Almighty Allah, the most generous for enabling me to complete my Ph.D. thesis.

I am heartily thankful to my supervisor Prof. Dr. Eberhard Burkel for giving me this opportunity to do my PhD in his group.
I'm gratefully appreciated all the time he gave motivation, patience, guidance, enthusiasm and also helping me getting scholarship which enabled me finishing this work .

I am heartily thankful to my co-supervisor Prof. Dr. Valentin Bessergenev from the Department of Physics and Center for Marine Sciences (CCMar), Faculty of Science and Technology (FCT) and Center for Marine Sciences (CCMAR) in Algarve university.
I would like to express my deep gratitude to him for continuous support, encouragement, help, patience, enthusiasm and giving immense knowledge in my work.

I am thankful to Prof. Conceicao Mateus from the department of Chemistry, FCT and Research Center in Algarve university.
I would like to express my deep gratitude and great respect to her for giving me a lot of her time and do everything in her power to overcome the obstacles and her good remarks and advice during the preparation of this research.
I would like to express my deep gratitude to her for support and permission me to work in her laboratory.

I owe big thanks to the technical staff in the department of physics in Rostock university and departments of physics and chemical in Algarve University for their continuous help.

I am grateful to Dr. Hanan Atia from Leibniz Institute for Catalysis at the University of Rostock.
I would like to express my deep gratitude to her for support and helping me.

Special thanks to all my friends and colleagues for reading this thesis.

I am grateful to all my family for encouraging and supporting me during my study. So, my gratitude and thanks to the Yemeni Embassy represented by the cultural attached and all embassy staff and Special thanks to Taiz University which supported me.
Many thanks to Mr. Daniel Reinecke, the responsible for the erasmus$^+$ program at Rostock University for his appreciated cooperation.
This Ph.D. project was funded by the Taiz University of Yemen and the erasmus$^+$ program at Rostock University.

Abstract

Advanced oxidation processes (AOPs), namely photocatalytic reactions can be successfully used in the field of wastewater treatment to reduce toxicity and reach the complete mineralization of the organic pollutants. AOPs are the multistep photochemical processes that start with electron-hole excitation by absorbing light on the surface of photocatalyst. This process subsequents water splitting in H^+ and OH^- active radicals. These radicals interact with organic pollutants presented in water which in turn result in mineralization of pollutants.

Titanium dioxide (TiO_2) is considered one of the most effective photocatalysts. It is a semiconductor that has a wide energy gap and three crystalline forms.
These are anatase which considered as the most active photocatalyst, rutile and brookite.

Great efforts have been done during the last decades to improve photocatalytic properties of TiO_2 which was prepared by different synthetic procedures in different morphological forms, like pure nanopowders, thin films and doped powders.
Many efforts were done in attempts to increase photocatalytic efficiency in the visible light region.

In this work, we perform systematic studies for the spectral dependence of photocatalytic constant of TiO_2 fabricated by different methods.
P25 Degussa nanopowder was used as a reference photocatalyst. On the other hand, other samples were prepared by the sol-gel process followed by instead of with different annealing procedures.
In addition, P25 Degussa powders were doped with different concentrations of cobalt. Furthermore, the thin films were prepared by Chemical Vapor Deposition (CVD) method.

It was shown that for all wavelengths used in this study (365, 405, 436, 546, and 690 nm) the photocatalytic constant is not zero but instead it increased in the shorter wavelengths for all TiO_2 nanopowders (the energy gap is about 3.2 eV that corresponds to 387 nm).
Our findings are that nanopowders have some electronic states inside the energy gap between valence and conduction bands. These states can be excited by light and the electrons and holes resulting from this excitation play a significant role in photocatalysis.

Another approach for increasing the photocatalytic efficiency is by increasing the lifetime of electron-hole pairs before recombination. This can be achieved by introducing local impurities or likewise local perturbation caused by the electric field inside the photocatalysts crystal matrix or by applying an external electrical field. Different commercial dyes were used to verify their purification efficiency from water. It was shown that two simultaneous effects occur in water.
One is the electrochemical removing of the pollutant and the other is the photocatalytic degradation of the pollutant. Furthermore, the existence of the synergetic effect is confirmed. This effect can be interpreted in the framework of e-h pairs separation in the electric field which results in lifetime increase, even when this field was relatively small.

Chapter 1

Introduction

1.1 Objectives

The worldwide growth of industry is accompanied by serious issues that affect the environment. Among the top of these issues comes the problem of the contaminated water. Hence, it is not surprising that many scientists work on producing research that may help in solving this problem. For instance, the discovery of water splitting effect by Fujishima and Honda paved the way for developing advanced oxidation processes, in particular the photo-induced processes of water purification [1].

TiO_2 is considered as one of the most attractive transition metal oxide material in the photocatalytic application due to its unique properties such as high photostability, strong oxidation activity, highly photoactive and transparency to visible light. The commercially available for TiO_2 is P25 Degussa powder. This powder consists of two phases 80% anatase and 20% rutile [2].

Despite the intensive studies dedicated to photocatalysis [3], the mechanisms of such processes are not completely understood.
Probably, it should be taken into account that a photocatalytic transformation is essentially dynamic and multi-steps process in which typical time intervals lie in the nanoscale level.

As it is supposed, initially absorbed photons result in e-h pairs formation.
These pairs can be recombined or can migrate to the semiconductor surface where they interact with water molecules creating H^+ and OH^- species. These species can in turn destroy organic contaminants adsorbed on the catalyst surface.
Defects of various types can play a very important role in enhancing the photocatalytic activity by creating additional electron levels that take positions between the valence and conduction bands.
Oxygen vacancies and various dopants (metallic and nonmetallic) inclusions are examples of such defects. Existence of additional electron levels can manifest itself in spectral dependencies of photocatalytic constant or in presence of the photocatalytic activity, when the wavelength of excitation light is higher than the energy gap nearly which corresponds to 387 nm for TiO_2.

To the best of our knowledge, the spectral dependence of photocatalytic activity has not been studied yet.
Therefore, two main strategies are chosen to be investigated throughout this work.

The first one is used to understand the spectral dependence of photocatalytic constant for different TiO_2 systems. This helps to understand the influence of electronic states inside the energy gap of the electronic structure.

The second one is used to separate e-h pairs in order to increase life time before recombination. Additionally, applying electrical field simultaneously with photoexcitation also provokes photoelectrochemical processes of water splitting[4].
Several methods have been used to prepare TiO_2 nanoparticles.

In this thesis, our focus is mainly on sol-gel method due to its advantages such as cost efficiency, relatively low temperature synthesis, stability and production of nanoparticles which have high photocatalytic activity.

Consequently, the main overall objective of this work is to prepare pure TiO_2 nanoparticles with different surface areas.

Other samples used here employed the commercially available P25 Degussa powder with different concentrations of cobalt dopant.

The thin film samples used for photoelectrochemical studies were prepared by Chemical Vapor Deposition(CVD)[5] using titanium isopropoxide on Si:B p-type wafer as a substrate.

1.2 Literature review

A rather simplistic description of heterogeneous photocatalysis is based on the initial absorption of light by semiconductor materials.
Sunlight is a clean and natural source of light that can be utilized in the photocatalytic processes. Its wavelengths window ranges from 10^2 to 10^5 nm.
A wide of these wavelengths arrive at earth in the form of 5% UV, 50% visible light and 45% infrared.
The UV wavelength window ranges between 280 nm to 400 nm. Its wavelengths can pass through atmospheric layers and it has the possibility for a photochemical process.

TiO_2 photocatalyst has an indirect energy gap equal to 3.23 eV and 3.0 eV for anatase and rutile crystal modifications, respectively[1, 6].
Depending on these energy gap structures, the absorption thresholds for anatase and rutile are 383 and 413 nm, respectively.
This means that pure TiO_2 is only active in the UV region which is 5% of the solar spectrum whereas the visible region consists of 40% of the spectrum as referred in figure 1.1.
Several studies have employed light waves with λ longer than 400 nm or solar light without filtering [7, 8, 9, 10].
However, to our knowledge, the spectral dependence of photocatalysis constant has not been investigated yet.

This part is devoted to studying the photocatalytic constant by using a high-pressure mercury lamp as UV illumination and also visible lines. Different optical filters are also used to separate the lamp spectrum into different wavelengths as displayed in figure 1.2.

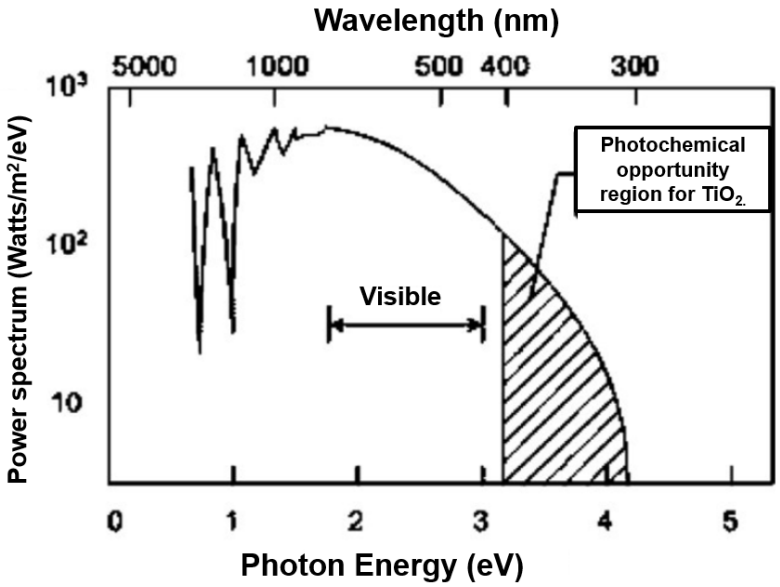

Figure 1.1: Solar radiation spectrum of the sun at sea level at zenith. TiO_2 is capable of receiving excitation in the ultraviolet region of the solar spectrum which is smaller than 5 % of the total solar intensity[11].

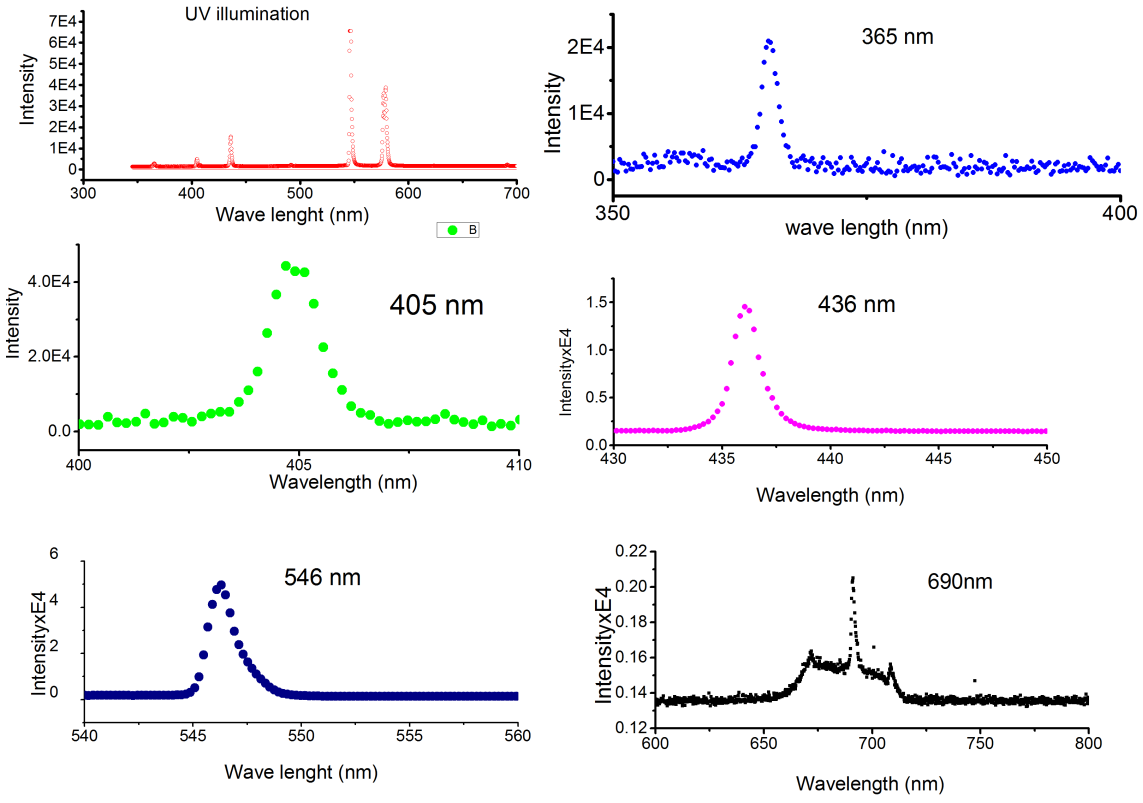

Figure 1.2: Spectral absorption of mercury lamp used as a light source. Different wavelengths are shown here, 365, 405,436, 546 and 690 nm obtained by UV-visible spectrometer.

1.2.1 Principle of photocatalysis

Photocatalysis is considered as the most effective process for water and air purification from organic pollutants. This process is known as advanced oxidation process (AOPs). This process depends on the in-situ generation of highly reactive radical species, mainly hydroxyl radicals and superoxides ions which is created by photogenerated holes (h^+) and electrons (e^-) and consequent chemical reaction by adsorbing on the surface of photocatalyst for organic compounds[12].
This process has the ability to oxidize the organic material and mineralize the intermediates to a non-hazardous form such as carbon dioxide, nitrates and water.
Moreover, it has several advantages compared to other processes. The most important advantages are:

1. The AOP chemical reactions can be placed at relatively mild conditions, require less chemical input and the reaction time may be smaller including the temperature and pressure at ambient conditions.

2. Low cost and formation of harmless products.

3. High potential to destroy toxic compounds in various wastewater streams.

4. Complete mineralization[13].

It should be noted that the catalysis, as well as, photocatalysis is widely referred to the process that accelerates chemical reaction without consuming the photocatalyst[14].

TiO_2 is the most preferred material used in photocatalysis due to its numerous advantages, such as chemical stability, low cost, easy availability and high photoactivity[14, 15].
Due to its aforementioned properties, TiO_2 is considered an excellent photocatalyst. As depicted in figure 1.3, the mechanism of the photocatalytic reaction goes through three steps:

1. The incident photon that has the energy greater than or equal to energy gap ($h\nu \geq E_g$) of the metal oxide can excite an electron from valence to conduction bands and can form photoexcited e^-/h^+ in the bulk (equation1.1).
   A common chain reaction describing this process is

$$\text{Photocatalyst} + h\nu \rightarrow h^+_{VB} + e^-_{CB} \tag{1.1}$$

2. The photoexcited carriers can recombine and dissipate energy (equation1.2) or these charge carriers can be trapped by Ti^{3+} and O^- defect sites in TiO_2 lattice [16, 17, 18].

$$h^+_{VB} + e^-_{CB} \rightarrow \text{energy} \tag{1.2}$$

3. The charge carriers can migrate to the catalyst surface and initiate redox reaction with adsorbates [19, 20].

   The photoexcited electron in the conduction band can interact with oxygen to form superoxide radicals (Equation1.3) and produce reactive form of oxygen may interact with hydrogen ion to form hydroxyl radicals (Equation 1.4).

$$e^-_{CB} + O_2 \rightarrow O_2^{-\cdot} \tag{1.3}$$

$$O_2^{-\cdot} + H^+ \rightarrow HOO^{\cdot} \tag{1.4}$$

These hydroxyl radicals react with electron to form hydroperoxide ions (equation 1.5)

$$HOO^{\cdot} + e^- \rightarrow HOO^- \tag{1.5}$$

Furthermore, these ions react with hydrogen ions to form hydrogen peroxide (equation 1.6).
Hydroxyl radicals and hydroxide ions are formed from the hydrogen peroxide reacting with the electron in the conduction band equation1.7

$$HOO^- + H^+ \rightarrow H_2O_2 \tag{1.6}$$

$$H_2O_2 + e^- \rightarrow OH^- + OH^{\cdot} \tag{1.7}$$

In the valence band, the adsorbed water on the surface reacts with the positively charged hole to form hydroxyl radicals and hydrogen ions equation 1.8.

$$h^+ + H_2O \rightarrow H^+ + OH^{\cdot} \tag{1.8}$$

Lastly, those holes are directly oxidized on the catalyst surface to form hydrogen ions and hydroxyl radicals.
These radicals play an important role to oxidize the organic compounds and decompose pollutants in equations(1.9 and 1.10).

$$h^+ + \text{organics} \rightarrow CO_2 + H_2O \tag{1.9}$$

$$OH^{\cdot} + \text{organics} \rightarrow CO_2 + H_2O \tag{1.10}$$

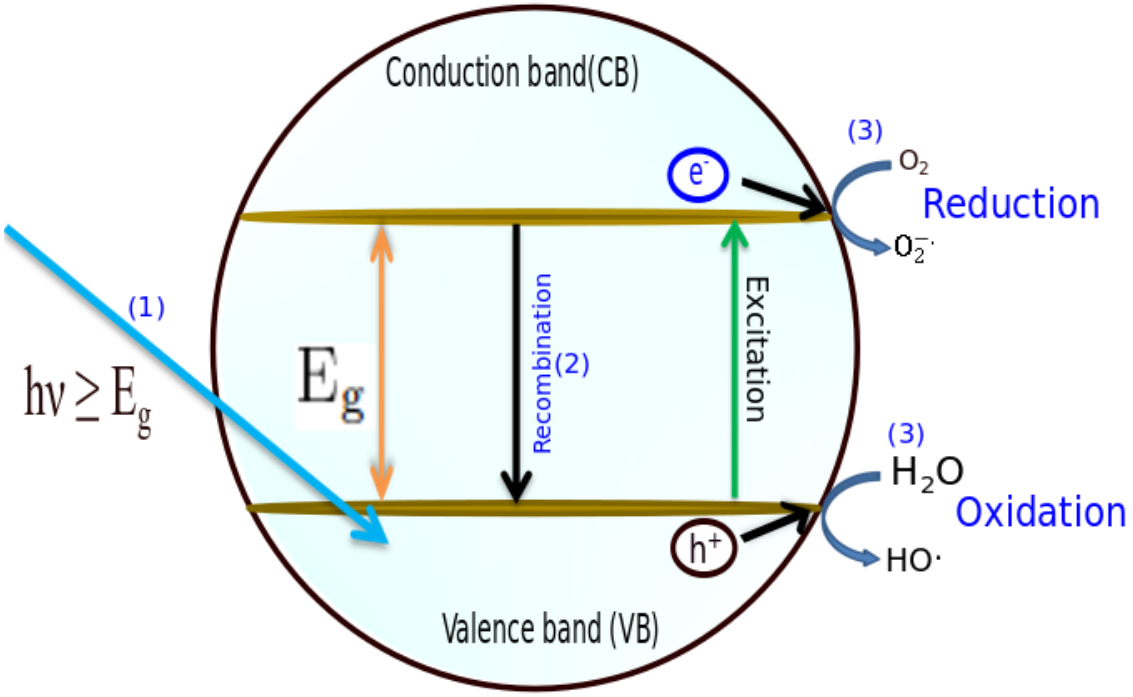

Figure 1.3: Schematic diagram illustrating the mechanism of TiO_2 photocatalysis. This mechanism consists of two processes. The oxidation in the valence band and a reduction in the conduction band when photons have energies greater than energy gap (E_g).

1.2.2 Titanium dioxide (TiO_2) as a photocatalyst

TiO_2 which also known as a Titania was used as a white pigment as it has high brightness and high refractive index[21]. It is also classified as a transition metal oxide[22].
In 1972, Fujishima and Honda discovered the water splitting in the photoelectrochemical cell using TiO_2 rutile single crystal as one of the potential electrode[1].
Recently, TiO_2 has attracted immense interest as an ideal photocatalyst compared to its counterpart metal oxides. It is insoluble in water, thermal stability, being cheap, inert biological and chemical nature, nontoxic and non-flammable.
Besides its photostability, it is not exposed to photoanodic corrosion, TiO_2 is highly photoactive and transparent to visible light[23, 24, 25].
Furthermore, TiO_2 is applicable in many fields at large industrial scale such as self cleaning, catalyst support, dye-sensitized photoelectrochemical solar cell and in consumer goods.
It is also used in the pharmaceuticals sector for example, in antibacterial agent because it has strong oxidation activity and superhydrophilicity[26].

Naturally, TiO_2 exists in three crystalline forms; anatase, rutile and brookite. Figure1.4 demonstrates the units cell of these three forms of TiO_2.
These structures consist of titanium Ti^{4+} ions surrounded by six oxygen O^{-2} ions to form TiO_6 octahedral configurations. These three crystal structures are different in the arrangement of the distortion with each octahedral units and in the assembly patterns of the octahedral chains [27, 28].
Although both anatase and rutile have tetrahedral structures, there are some features that differentiate them from each other. Namely, in the anatase form the octahedrals are shared with their vertices while in the rutile structure the edges are shared.
Moreover, the arrangement of TiO_6 octahedron is slightly larger in the anatase phase compared to the rutile phase. In anatase the Ti-Ti distances are larger whereas the Ti-O distances are shorter than in rutile.
On the other hand, the structure of brookite is different as it is orthorhombic where the vertices and edges are shared [29].
Thermodynamically, the rutile phase is the most stable. The anatase and brookite phases are metastable and they can be transformed to rutile phase under heating to $(600 - 700°C)$[30, 31].

It is very important to bear in mind that TiO_2 is n-type semiconductor because the valence band is composed of 2p orbitals of O_2 hybridized with the 3d orbitals of titanium, whereas the 3d orbitals of titanium are responsible for the conduction band [28].
Table1.1 shows the parameters of the crystal structure of different phases of TiO_2.
The anatase phase reveals the best photocatalytic activity because it has the larger surface area and porosity which produces higher number of hydroxyl groups and the catalytic sites increase.
In addition, the optimum energy gap and recombination of the e-h pair at lower rates.

Furthermore, the electron transfer from the conduction band to O_2 is easier at the surface because the conduction band in the anatase phase has higher energy than that of rutile phase[32, 33].
The brookite form is not used in the experiments because it is difficult to prepare it as a pure form. Furthermore, it is unstable and it can barely be produced[34].

The photocatalytic properties of TiO_2 occur when photogenerated charge carriers (holes and electrons) formed upon the absorption of the light[35, 36, 37].
In the valence band, photogenerated holes react with the molecules of adsorbed water to form the hydroxyl radicals (equation 1.8) [36].
These holes and hydroxyl radicals oxidize the organic molecules on the TiO_2 surface. Superoxide radical anions are formed when the electrons in the conduction band react with the molecules of O_2 (equation1.3).
In addition, TiO_2 surface under the UV light becomes superhydrophilic[38, 39].

Table 1.1: The crystal structure of anatase, rutile and brookite phases. a, b and c represent the cell parameters in the x, y, and z directions, respectively. [29].

Properties	Anatase	Rutile	Brookite
Crystal structure	Tetragonal	Tetragonal	Orthorhombic
Space group	D_{4h}^{19}-$4_1/amd$	D_{2h}^{15}-Pbca	Pbca
Lattice constant Å	a = b = 3.784 c = 9.515	a = b = 4.593 c = 2.959	a =9.184 , b =5.447 c =5.145
Energy gap (eV)	3.23	3.02	3.13
Wavelength (nm)	< 390	< 415	
Applications	Photocatalyst	White paint	Dye-sensitized solar cell

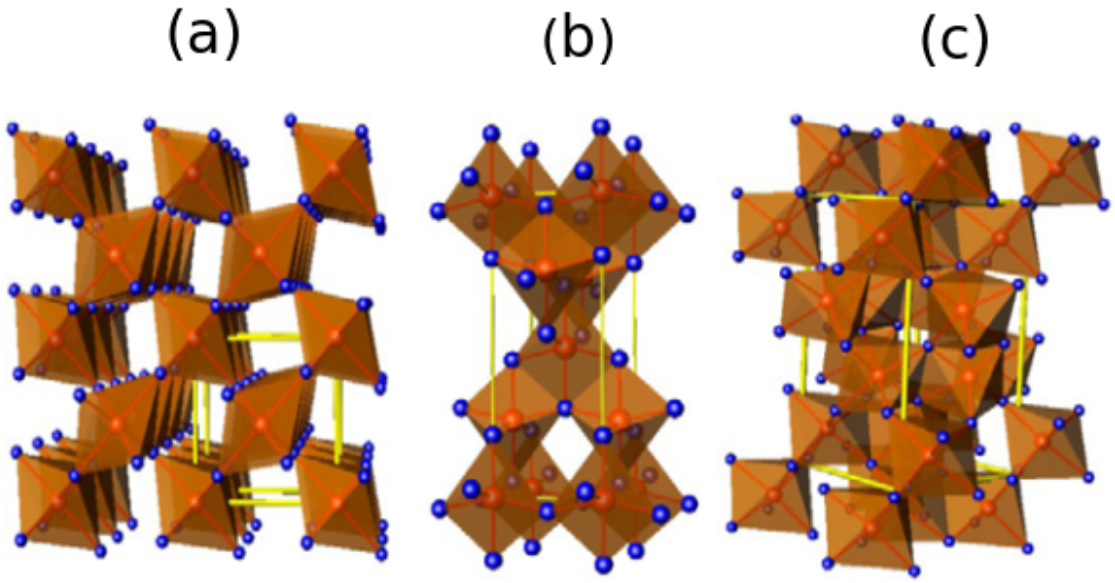

Figure 1.4: Crystal structures of TiO_2 crystalline forms: (a) rutile, (b) anatase and (c) brookite; red spheres are shown in Ti^{4+}, blue spheres are shown in O^{2-} and the unit are shown in yellow lines[28].

1.2.3 Doped TiO_2

As mentioned above, TiO_2 has energy gap of 3.23 eV and 3.0 eV for anatase and rutile, respectively.
Several methods can be used to modify the band structure such as creation of composite semiconductors and doping.
The goal of this modification is necessary to reduce the e-h recombination and increase wavelength of the absorbed light in order to allow the occurrence of photocatalytic processes utilizing the natural sunlight[40, 41].

TiO_2 can be doped with transition and rare earth metals such as Fe, Ni, Co, V, and Lanthanides at Ti sites and non metals (like N and F) at O_2 sites.
These will create trapping sites which reduce e-h pair recombination.
This facilitate the absorption in the visible region and improves the photocatalytic performance compared to the undoped photocatalyst[42, 43, 44].
Previous studies showed that doping TiO_2 with transition metals (V, Fe, and Co) improved the spectral response in the visible light.
This is due to the substitution of Ti^{4+} by metallic ions in the TiO_2 lattice is allowing energy states inside the energy gap structure.
Therefore, the photoactive transition is attained due to the promotion of an electron from mid-energy gap into the conduction band or excitation of an electron from the valence band of TiO_2 to the mid-level of energy gap.
The dopant ions also play role on the trapping sites creation in order to reduce the recombination rate[45, 46, 47, 48, 49].

1.2.4 Electrolysis

The electrolysis of water is a process that is used to decompose water (H_2O) into oxygen (O_2) and hydrogen (H_2) components.
In this process, all the products are safe or non-polluting compared to the process of steam reforming which produces carbon dioxide[50].
Electrolysis occurs when a sufficient energy is applied to drive the process.
In the case of the electrolytic water splitting, this energy is provided by an electric current passing through the water between anode and cathode during the electrochemical reaction[50].
The water electrolysis was first studied by using an electrostatic generator between gold electrodes to produce an electrostatic discharge[51].
Afterwards, the electrolytes of aqueous alkaline solutions were used technology still used until now[52, 53].
Later, Fujishima and Honda for the first time demonstrated photocatalytic water splitting by a photoelectrochemical cell (PEC) using TiO_2[1].
The PEC water splitting has attracted a lot of attention mostly with the aim to improve the production of efficient H_2[54, 55].

Other studies were dedicated to investigate the photoelectrochemical reactions on the surface of electrodes[4].
The photocatalytic water splitting by PEC has unique advantages compared to the other processes. These include the low costs and reasonable solar to H_2 efficiency.
One more advantage is that it requires a relatively small reactor. Additionally, PEC allows H_2 and O_2 to be easily separated during the reaction[56].

PEC is classified into two types depending on the type of photocatalyst used in the reaction. One type is used as a photochemical cell with the powder as suspended particles in solution. Another type is the photoelectrochemical cell in which the thin film is deposited and used as photocatalyst materials to form a photoanode for performing the water splitting reaction in the solution [56].
In figure 2.6, the anode consists of Si:B p-type semiconductor substrate with TiO_2 photocatalyst thin film deposited on the surface by CVD.
This TiO_2 photocatalyst is used as an anode which absorbs the light and a gold wire is used as a cathode.

As known, the mechanistic model of PEC involves four steps that are performed consequently:

- Photo energy absorption, e-h pairs are generated during the process of the excitation an electron from the valence band to conduction band.
- At the photoanode, water is splitted to generate H^+ and OH^- species by interaction with the e-h pairs.
- Photogenerated species are passed through an internal circuit solution to the cathode.
- At the cathode, H^+ ions are reduced to H_2 on the TiO_2 surface[57, 58].

Surprisingly, according to our knowledge, this process was not to be used for water purification for some industrial dyes instead of photocatalytic process or in parallel with the photocatalytic process.

In this thesis, electrolysis and photocatalysis processes were studied where both processes simultaneously occur. The electric field was applied and the photocatalytic constant (K) was investigated in dark and under illumination with UV light for the different dyes.

1.3 Overview of the thesis

This thesis is organized into five chapters as follows:

Chapter 1 elaborates the objectives of this thesis. The photocatalysis phenomenon and its mechanism is illustrated.
Then, the basic features of TiO_2 are discussed. The importance of doping on TiO_2 and its influence on the properties and TiO_2 structure is also explained.
Finally, a brief introduction of the photoelectrochemical is addressed.

Chapter 2 describes the techniques used to characterize the physical properties of prepared pure and doped TiO_2 photocatalyst powders and TiO_2 thin film.
Also, this chapter focuses on the preparation of pure TiO_2 powders from titanium tetraisopropoxide as a precursor (TTIP) by the sol-gel method and doped TiO_2 powders using the tris(diethylditiocarbamato)Co(III) (CoDtc- $Co[C_2H_5)2NCS_2]3$).
Details regarding the preparation method of TiO_2 thin film by the Chemical Vapor Deposition(CVD) process are presented.
Finally, this chapter addresses the basic concepts of different dyes. These include Methanol Blue(MB), Gentian Violet(GV), Brilliant Green(BG), Methyl orange(MO) and Eosin(OS) which are used as electrolytes in the photochemical cell(PEC).

Chapter 3 presents the main results obtained for pure and doped TiO_2 powder materials and TiO_2 thin film.

Chapter 4 includes the discussion and the analysis of the results obtained in this work presented in the previous chapter.
The influence of dopant ions on TiO_2 particle size, specific surface area, phase transformation and energy gap are investigated.
In addition, there are discussions on the results of photocatalytic activity of TiO_2 thin films deposited on Si:B substrate (that represent p-type semiconductor) by using electrochemical cell and different types of dyes under different effects.
These effects are UV illumination(UV), electric field(E) applied between TiO_2 thin film and gold electrode and both UV illumination and electric field(UV+E).
The influence of these effects on different dyes by TiO_2 thin film was investigated.

Chapter 5 provides the general conclusions of this thesis.

Chapter 2

Methods and experimental setup

2.1 Characterization

2.1.1 X-Ray Diffraction

X-ray diffraction technique (XRD) was used to analyze and identify TiO_2 phase formation and investigate crystallographic information of the samples.
XRD patterns of TiO_2 sol- gel powder were obtained by Bruker D8 Discover model diffractometer using Cu-Kα-radiation (λ =0.154 nm) at room temperature, operated at 40 kV and 40 mA from (17–63)°C in the lab of Rostock university.
The crystal structures of the cobalt-doped P25 Degussa have been analyzed by XRD technique at the Faculdade de Ciencias Technologia of Algarve university in Faro, Portugal.
Also, the crystalline phases of the thin film investigated by a high resolution PANanalytical XRD using Cu-Kα radiation(λ = 0.154 nm).
The accelerating voltage and the applied current were 45 kV and 30 mA, respectively.
The high resolution PANanalytical XRD setup is used in Θ - 2Θ configuration.

All experimental data obtained from XRD experiments were collected using MAUD program and refined by Rietveld refinement method[59, 60].
All parameters such as crystal structures, phases, lattice parameters, crystal sizes and percentage of crystallinity of all samples were refined.
It is usually difficult to obtain detailed information about the structure of a polycrystalline sample because this information is lost due to the overlap of independent diffraction peaks for powders which prevents extracting any structure information. Also, the random orientation of the crystalline makes it more difficult to get structure information[61, 62, 63].
This method has worked together with Fourier analysis for broader peaks.
Other parameters such as Caglioti Paoletti and Ricci formula are replaced by crystallite size, shape and root mean square considering them as fitting parameters[63, 64].
These parameters can be refined and minimized to the residual function by using the non-linear squares algorithm which is described in this equation 2.1 :

$$y = \sum_{i=1} w_i (I_i^{exp} - I_i^{cal})^2 \tag{2.1}$$

with w_i

$$w_i = \frac{1}{I_i^{exp}} \tag{2.2}$$

Where I_i^{cal} and I_i^{exp} are measured XRD experiment and theoretical calculated diffraction intensities from the powder, respectively. The calculated diffraction intensity of the powders can be expressed as:

$$I_i^{cal} = S_F \sum_{j=1}^{n} \frac{f_i}{(V_j)^2} \sum_{k=1}^{nL_k} |F_{K,j}|^2 S_j(2\Theta_i - 2\Theta_{k,j}) P_{k,j} A_j + bkg(2\Theta_i) \tag{2.3}$$

Where S_F is the beam intensity, f_i is the phase volume fraction, V_j is the phase cell volume andS_j is the phase scale factor, respectively.

L_k is Lorentz polarization factor which depends on experimental parameters such as detector, geometry, position and the sample angle.
$F_{K,j}$ is the structure factor and it depends on the number of atoms, atomic scattering factor and the atom coordinates.
A_j is the absorption coefficient of the sample. It depends on the sample thickness. And the phase have k = 1 to n and j correlates peaks for the factors.
$P_{K,j}$ is the texture which depends on the angle between the crystallographic plane hkl and the preferred orientation vector.
$bkg_{2\Theta_i}$ is the background of the polynomial function in 2Θ.

Finally, the quality of refinement can be checked by two factors: R_{wp} and R_{exp}. GofF is obtained from the best fit and is must be <1.
This is described in the equation below:

$$\mathrm{GofF} = \frac{R_{wp}}{R_{exp}} \tag{2.4}$$

The parameters R_{wp} and R_{exp} can be described by the following equations:

$$R_{exp} = \sqrt{\frac{(N-P)}{\sum_{i=1}^{N}[w_i I_i^{exp}]^2}} \tag{2.5}$$

$$R_{wp} = \sqrt{\frac{\sum_{i=1}^{N}[w_i(I_i^{exp} - I_i^{cal})]^2}{\sum_{i=1}^{N}[w_i I_i^{exp}]^2}} \tag{2.6}$$

Where N and P are the number of points and parameters, respectively[63].

2.1.2 Surface area and porosity

Surface area and porosity are two important physical properties that depend on morphology of the nanostructure powders. They play a important role in photocatalysis are studied by N_2 adsorption.
The gas adsorption can be classified into physisorption and chemisorption which are depending upon the bonding type.
The physisorption is the phenomenon that is used to study the morphology because it has a characteristics which makes it the most suitable for surface area determinations.
Both adsorption and desorption processes are reversible. However, it may lead to coverage the surface by multilayer adsorbate and it occurs at low temperature.
Moreover, these processes do not require activation energy and they can achieve equilibrium rapidly. As result, it is easy to calculate the surface area since the molecules are not restricted to specific sites and they are free to cover the entire surface[65, 66].

Since the late 1940s, N_2 adsorption is used to determine the surface area and characteristics of porous texture for catalyst at N_2 liquid temperature 77 K at 1 atm pressure[67, 68].
The adsorbed volume of N_2 gas versus the relative pressure ($\frac{p}{p_o}$) is used to obtain isotherm shape.
This isotherm is classified in six types according to the IUPAC classification.
Mainly four of these types are used in the catalyst characterization [69, 70].
The main type of isotherm is Π isotherm 2.1 with a H_3 hysteresis characteristic as shown in 2.2.
This type belongs to the transition-metal oxide powders such as TiO_2.
Furthermore, IUPAC has classified the pore to three types depend on their size [70, 71].

- Micropores: Size$\leq$2 nm.
- Ultramicropores: Size$<$0.7 nm.
- Mesopores: 2$<$Size$\leq$ 50 nm.
- Macropores: Size $>$50 nm.

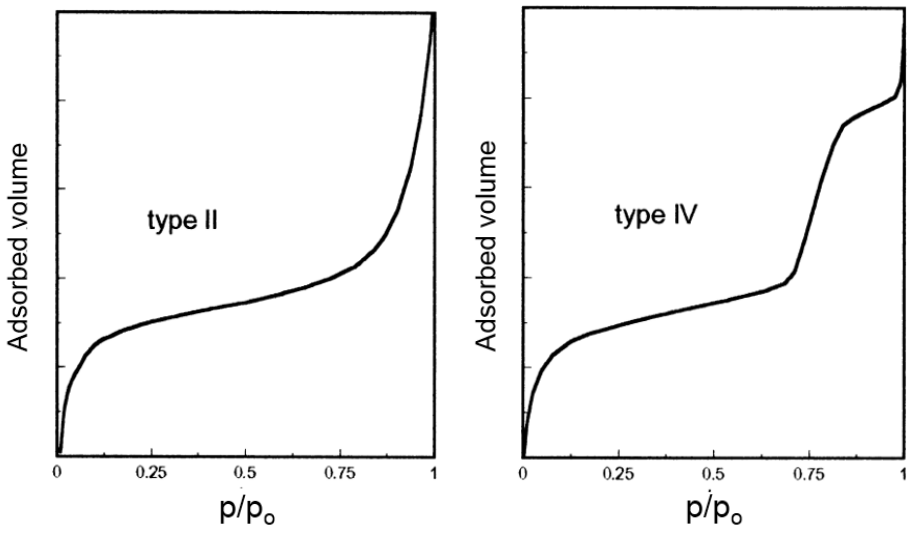

(a) Mesoporous. **(b)** Mesoporous.

Figure 2.1: The types of isotherm for a mesoporous catalysts material, adapted from reference[70].

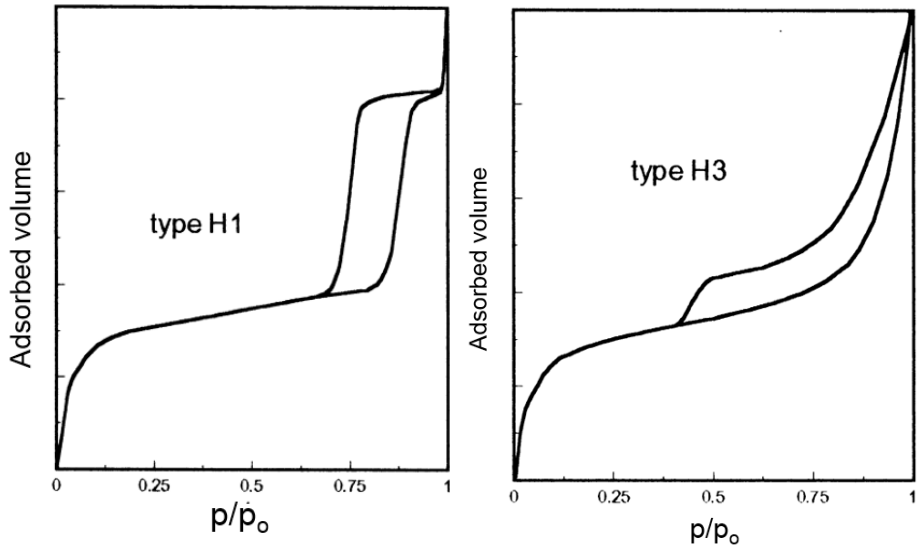

(a) Uniform size. **(b)** Non-uniform size.

Figure 2.2: The hysteresis shapes of isotherm for mesoporous catalysts material, adapted from reference[70].

Typical isotherms for mesoporous materials are shown in figures 2.1and 2.2. They are characterized by a steady slope of adsorbed gas, especially between $0.05 \leq \frac{p}{p_o} \leq 0.8$. The presence of a hysteresis means the presence of open pores or different between adsorption-desorption isotherm. Inside open pores, capillary effects lead to locally higher pressure compared to the outside and capillary condensation. Therefore, the amount of gas molecules layers on the surface is not uniform and the desorption branch is not equal to the adsorption branch. The shape of the hysteresis defines the shape of the open pores, whether they are cylindrical, ink bottled or slit shaped[70].

2.1.2.1 Qualitative analysis

Brunauer-Emmett-Teller (BET) is the most common process used to obtain surface area and the pore size distribution. It is based on gas adsorption on the surface. The amount of gas adsorbed at a given pressure allows determining the surface area of the material[71]. This method is a cheap, fast and reliable. Also, it is very well understood and applicable in many fields. The simple form of this equation that forms the basis of the BET method for the determination of the surface area for solids can be written:

$$\frac{p}{n_a(p_o - p)} = \frac{1}{n_{max}.c} + \frac{c-1}{n_{max}.c}.\frac{p}{p_o} \tag{2.7}$$

Where n_{max} is the amount of adsorbed at the relative pressure $\frac{p}{p_o}$ which can be calculated by the law of ideal gas[68]. This is shown below in the equation 2.8

$$n_a = \frac{RT}{(p_{inlet} - p_{equi}).V_{tube}} \tag{2.8}$$

Where V_{tube} is the volume of the sample tube. p_{inlet} and p_{equi} are the pressure when the N_2 adsorbs on the materials and the pressure inside the tube which is controlled until it reaches a constant value, respectively.
n_{max} is the monolayer capacity of the adsorbate. p and p_o are the saturated vapor and the output pressure for the adsorbate, respectively, at N_2 liquid temperature.
c is a constant value which depends on the isotherm shape[68, 72].
According to the equation 2.7, a linear relation is obtained when$(\frac{p}{n_a(p_o-p)})$ is plotted against $\frac{p}{p_o}$, from fit the line slope s and the intercept i can be determined.

The equations 2.9 and 2.10 describe n_{max} and c constant.

$$n_{max} = \frac{1}{s+i} \tag{2.9}$$

$$c = \frac{s}{i} + 1. \tag{2.10}$$

Now, it is easy to calculate the surface area (SA) of the materials by the following equation:

$$SA = (\frac{n_{max}}{22414})N_a\sigma \tag{2.11}$$

Where N_a is Avogadro number ($6.023x10^{23}$ molecules mol^{-1}) and σ is the area of one molecule of N_2 which is occupied on the monolayer. This value $\sigma = 0.0162$ nm^2 and 22414 cm^3gm^{-1} is the volume under standard conditions of one N_2 molecule which is adsorbed[73, 70].

2.1.2.2 Experimental details

Micromeritics ASAP-Physisorption Analyzer 2020 is used to obtain the surface area and the pore size distribution for pure P25 Degussa, doped P25 Degussa with different concentrations of cobalt. The samples were prepared by the sol-gel method. The weights of sample powders were determined before and after the measurement. Before the measurement, the samples were degassed at 300°C for 2 hours at 10 mmHg pressure. Then, the samples were placed at 77K temperature using N_2 gas to get the isotherm shape.
Finally, the BET equation is used to calculate the specific surface area in the range of $0.05 \leq \frac{p}{p_o} < 0.25$.
The pore size distributions and pore areas are derived by the Barret-Joyner-Halenda (BJH) analysis with Halsey corrections in the range of $0.42 \leq \frac{p}{p_o} < 1$ of the adsorption branches for N_2 on the powders surface.

2.1.3 Photocatalytic activity setup

The photocatalytic process is described in section 1.2.1.
The experimental setup used to study the photocatalytic activity of the powder samples is shown in figure2.3.
It consists of a circular reactor shown in figure2.3 (a) which consists of magnetic stirring, Aluminum plate and three holes.
One of these holes is used to inject and collect the samples from reactor while the other holes are used to pump air inside, as shown in figure2.3 (d).
The second part of the setup, shown in figure 2.3 (b), is the tube used to focus the radiation vertically onto the samples being studied. Also, it has a holder to fix the filters that are used in the experiments.
The third part is where the high-pressure mercury lamp (400 W, Germany) was used as a UV source shown in the figure 2.3 (c). This lamp has 5 wavelengths according to USB 4000 UV-Visible spectrometer that was used to analyze it. The wavelengths are 365 nm, 405 nm, 436 nm, 546 nm and 690 nm, respectively.
The mercury lamp was kept at approximately 14 cm away from the sample to perform the photocatalytic reaction.
Finally, syringes are used to inject the sample in the reactor and collect it for analysis. Small tubes used to collect the samples during the experiment.
This setup was built in Rostock university and all experiments were performed in chemistry department of Algarve university.

The photocatalytic degradation of Fenarimol follows the first order kinetic in equation2.12[74, 75, 76].

$$\mathrm{C} = \mathrm{C}_0 e^{-\mathrm{Kt}}. \tag{2.12}$$

Where C is initial HPLC (High-performance liquid chromatography) chromatographic integrated peak intensities at 220 nm after adsorption-desorption equilibrium. C_0 is current HPLC chromatographic integrated peak during the radiation time. t is the time in hours and $\mathrm{K}(\mathrm{h}^{-1})$ is the kinetic rate constant of the degradation. The total kinetic rate constant of photocatalytic degradation can be calculated by the sum of the degradation at catalyser $\mathrm{K_c}$ and a photolysis under the UV light $\mathrm{K_o}$.

$$\mathrm{K} = \mathrm{K_c} + \mathrm{K_o} \tag{2.13}$$

The kinetic rate constant of the chemical reaction $\mathrm{K_c}$ is determined for the different TiO_2 systems[75, 76].

2.1.3.1 Experimental setup

The photocatalytic activity experiments were prepared as follows:
Firstly, Fenarimol powder ($C_{17}H_{12}Cl_2N_2O$) as a reference was mixed with MilliQ H_2O.
The ratio and the amount of photocatalyst are:
Fenarimal:H_2O=5 mg : 1 Litre.
Then, this solution was heated at 40°C with ultrasonic about 15 minutes for several times and kept in a dark place for one day.

After that, 20 mg of TiO_2 powder was mixed with 100 ml of Fenarimal solution and kept in darkness for one day. Finally, 50 ml of the solution was injected into the reactor.
The reactor was bubbled continuously with external air under constant magnetic stirring throughout the experiment and the solution was left for 1 hour and 30 minutes in the darkness to allow saturation of the powder to establish an adsorption-desorption equilibrium.
After adsorption-desorption equilibrium, the first sample(T_0) is taken. A light source focuses vertically at the center inside the reactor to begin the experiment. Samples treated were withdrawn from the reactor at regular interval of (10, 15 and 30) minutes.
Before analysis the sample were filtered by 0.45μm filters to remove the photocatalyst particles. Photolytic and photocatalytic kinetics were followed using a HPLC chromatographer (Agilent, 1220 LC System) equipped with a C18 reverse phase column (lichrocart 125-4, Lichrose Rp-18e (5μ m), an arheodyne manual injector with the loop of 50μl and a variable UV detector.
Mobile phase composition consists of 65% Acetonitrile and 35% H_2O and it has a flow of approximately 1 ml/min.
The wavelength at maximum absorption peak, of each indicator compound is used to monitor degradation is 220 nm.

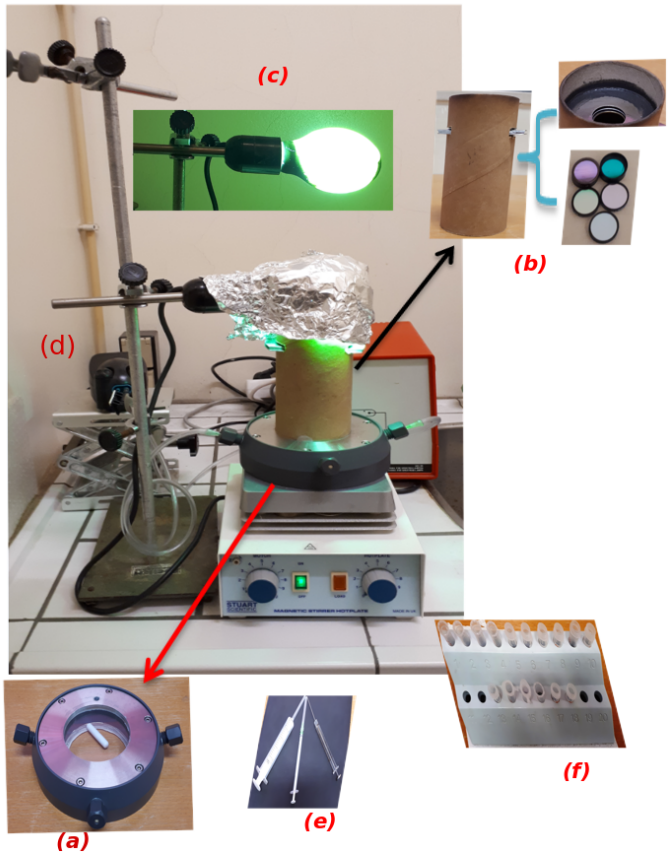

Figure 2.3: The experimental setup for studying the photocatalytic activity of TiO_2 powders. It consists of a circular reactor (a). A cylindrical tube to focus the radiation and hold the filters (b). The mercury lamp is used as a light source (c). Air pump is used to insert air to the reactor (d) and syringes to inject and collect sample (e). Plastic tubes are used to collect samples for analysis (f).

2.1.4 UV-Visible Spectroscopy

Ultraviolet-visible(UV-Vis) technique refers to absorbance and reflectance in the ultraviolet-visible spectral region.
UV-Vis absorption spectroscopy is used to measure the absorption spectra of organic dyes or powders at each wavelength.
UV-Vis technique is based on the principle of Beer-Lambert law which has the linear relationship between the absorbance and the solution concentration. It can be expressed as follows:

$$A = \varepsilon lc. \tag{2.14}$$

A is the absorption which depends on $\log(I_0/I)$. I_0 is the incident light intensity and I is the transmitted light intensity, ε is the molar absorptivity, l is the path length through the sample and c is the sample concentration in the solution.
This technique is usually done by scanning the wavelength for 2 seconds by recording the absorbance spectra.

In this thesis, UV-Vis spectrophotometer was used to measure the absorption spectra for the TiO_2 powders to study the degradation of different organic dyes by TiO_2 thin film photocatalyst.
For example, the absorption at maximum λ of methylene blue equals to 664nm and methyl orange equals to 466nm. The photocatalytic degradation and photocatalytic constant for the different dyes are calculated by using the equation2.15.

$$\ln\frac{I}{I_0} = -Kt \tag{2.15}$$

I_o is the initial absorbance in the darkness at the beginning t=0 minute and I is the absorbance after time t.
The plot $\ln\frac{I}{I_0}$ as a function of irradiation time exhibits a straight line, whose the slope is equal to photocataltyic constant K.

Additionally, UV-Vis technique is used to calculate the optical energy gap of the samples[77].
By using the relationship between the photon energy and wavelength:

$$E = hc/\lambda \tag{2.16}$$

where h is the Planck constant (6.626 $\times^{-34}$ Js), c is the speed light (2.998 $\times^{8}$ m/s and λ is the wavelength.
The optical energy gap of studied samples can be defined by equation2.17

$$E(eV) = 1239.8/\lambda \tag{2.17}$$

2.2 TiO_2 nanoparticles synthesis

In this thesis, The focus is on TiO_2 nanopowders and the nanostructured thin film. Thin films were prepared by the Chemical Vapor Deposition(CVD) method.
Three different powders were chosen: The first one is the commercial P25 Degussa powder which was used as a reference. The second samples are based on P25 Degussa doped with different concentrations of Co. The third samples series are these prepared by sol-gel method.

2.2.1 TiO_2 powders

2.2.1.1 TiO_2 prepared by Sol-gel method

Several techniques such as sol-gel, hydrothermal, chemical vapor, solvothermall and microwave are used for the TiO_2 materials synthesis of photocatalytic applications[29].
Among all these techniques, sol-gel method has generated a large scope of interest in the preparation of inorganic ceramic and it was classified as one of the most important chemical technique for TiO_2 nanoparticles synthesis[78].
This method has a lot of advantages such as cost effectivty, requires relatively low temperature for synthesis, it has versatility in processing, high stability and it is used in large scale application in catalyst preparation.
Due to these advantages, it has the potential to fabricate catalysts with high purity, homogeneity, fine scale and controllable morphology[79, 80].
Furthermore, this method can be classified into two different routes that are depending on the type of titanium precursor used.
There are non-alkoxide and alkoxide route. The non-alkoxide route uses inorganic salts such as (nitrates, chlorides, sulfates, carbonates, etc.) while the alkoxide route uses metal alkoxides which is starting from materials such as (titanium isopropoxide, titanium terra isopropoxide, titanium butoxide, titanium ethoxide, etc.)[81].
The sol-gel method depends on the reactions of inorganic polymerization[82].
Generally, the sol-gel method involves these steps:
Firstly, the homogenous solution was prepared by metal alkoxide precursor dissolved in an organic solvent like alcohols.
Then, a stable sol was formed by treating the homogenous solution with a suitable reagent by adding water with the acid.
After that, the sol was converted into gel which was calcinated to get the powder[83].
A lot of parameters play a role in the sol-gel method such as the solvent type, PH of acid, the amount of water and treatment temperature.
Therefore, these parameters are very important since they have direct affect on the physical properties of the final material.

Certainly, the final material is amorphous after the drying step, but heat treatment step is very necessary to convert this material into a crystalline material[84, 85, 86, 87].

In this thesis, alkoxide route is used for TiO_2 synthesis. Sol-gel process of metal alkoxide can be started with hydrolysis and condensation reactions and followed by aging and then by heat treatment to convert amorphous to crystalline nanoparticles. During hydrolysis, when water is added to TiO_2, a proton from the attacking nucleophile (water) is transferred to the alkoxide group so metal hydroxide and a small amount of alcohol are released, as illustrated in the equation2.18

$$M - OR + H_2O \rightarrow M - OH + R - OH \tag{2.18}$$

Also, a small amount of alcohol is released and acid play a role in Ti-alkoxide formation during the hydrolysis and condensation steps.
of powde And, adding the acid to the solvent enhances the reaction and splitting of Ti-OR bonds is accelerated, as shown in the equation 2.19.

$$M - OR + H^+ \rightarrow M^+ - OHR + HOH \tag{2.19}$$

In this acidic medium state, the rate of condensation reaction becomes very slow due to which this reaction occurs at the end of the chain rather than in the middle. During the condensation reaction the water and alcohol molecules are released, as shown monomers under the release of an alcohol molecule[80, 83].

$$M - OH + HO - M \rightarrow M - O - M + H_2O \tag{2.20}$$

$$M - OH + RO - M \rightarrow M - O - M + ROH \tag{2.21}$$

where M is the titanium and R is the alkyl group - C_nH_{2n+1}.
Additionally, a mutual solvent such as an alcohol is used because water and alkoxides are immiscible[88, 89].
When the gel is formed, it contains a lot of solvents that further being removed by drying.
The period between the gel formation and its drying is known as ageing.
In this period, the gel may keep undergoing hydrolysis or condensation. The aging step is crucial to obtain strength gel without changing the pore structure and an increase of the pore size reduces the surface area through dissolution and precipitation of the particles. A scheme of the detailed synthesis is given in figure 2.4.

In this thesis, three different series of sol-gel powders were prepared by varying temperature and in dependance on the addition of H_2O and HCl during the initial preparation, this is shown in table 2.1.

Table 2.1: The parameters of preparation sample series for sol-gel powders. The sample of series 1 added the H_2O firstly, then addition HCl. While series 2 and 4 started with acid firstly and changed temperature for series 4.

Sample	H_2O	HCl	Temperature
S1	First	Second	21°C
S2	Second	First	21°C
S4	Second	First	40°C

Firstly, a precursor titanium terra isopropoxide(TTIP)($C_{12}H_{28}O_4Ti$) was added to the solvent (Ethanol) and the solution was mixed under vigorous stirring.
After that, the deionized water by burette was added to the solution and stirred for approximately half an hour.
Then, acid HCl was mixed to the previous mixture and the solution product was stirred for 5 hours at room temperature.
The reagent ratios in mole are displayed in the equation:

TTIP : Ethanol : HCl : H_2O =10 : 10 : 0.3 : 10

Finally, drying the formed gel by spray drying process with a maximum temperature (inlet) of T_{max}= 180°C.
These sol-gel powders are placed in ceramic crucibles and heated in vacuum furnace. The pressure of this furnace is 2.5 x$\times 10^{-5}$ mbar and annealed temperature at 400°C for 3 h.

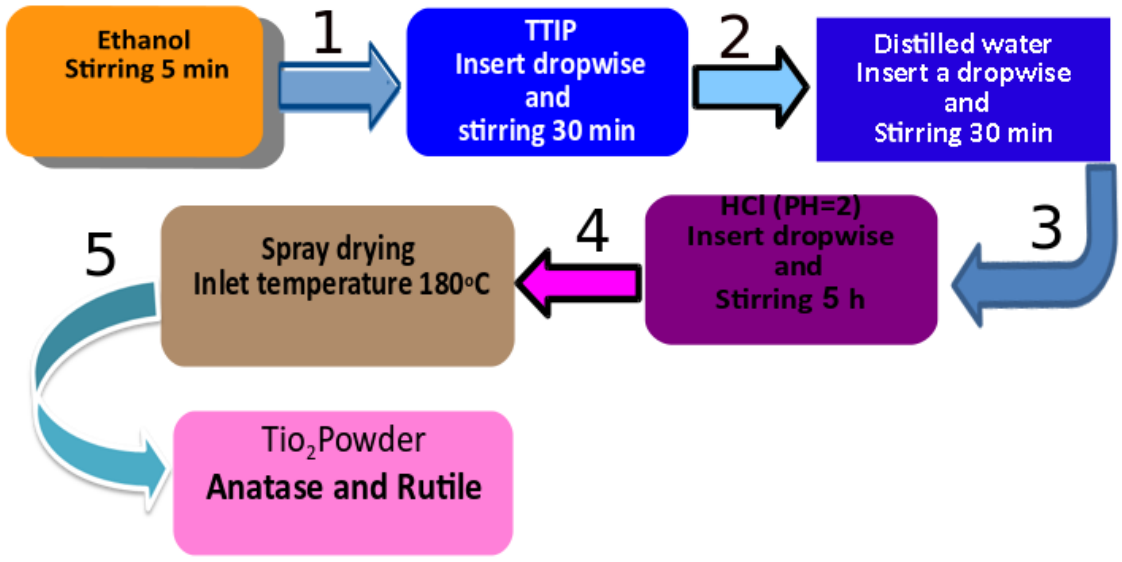

Figure 2.4: Scheme of sol-gel synthesis of titanium dioxide powder.

2.2.1.2 TiO_2 doped with Cobalt(Co)

TiO_2 doped by transition metals attracts a major interest due to its potential use in the spintronic and other electronic devices. Moreover, it is considered as one of the reducible oxides on which photocatalytic processes are based [90, 91, 92, 93].
P25 Deguass is doped with Co by using a simple approach based on the sintering of P25 Degussa nanopowder with Co. P25 Degussa powder usually contents 80% anatase and 20% rutile and it is used as a reference material.
On the other side, this powder was chosen due to its high photocatalytic performance, considered sometimes as a gold standard.

Synthesis of Co-doped TiO_2 nanoparticles is achieved following the preparation of the mixture of the P25 Degussa nanopowders with Co precipitate.
Four different series of P25 Degussa doped with Co were prepared which are labeled as P25:1% Co, P25:2% CO, P25:5 % Co and P25:10%Co.
These series were prepared in the following steps:
Firstly, Co precipitate was obtained by dissolving of Tris(diethylditiocarbamato)Co(III) (CoDtc- Co[C_2H_5)2NCS_2]3) in the chloroform ($CHCl_3$) and consequent mixture with P25. They are drying by evaporation of chloroform under heating in air at approximately 50°C.
Then, amounts of P25 and CoDtc were chosen to prepare four different Co contents in $Ti_{1-x}Co_xO_2$ (x= 0.01, 0.02, 0.05 and 0.10).
After that, powders were annealed in the furnace at 400°C for 30 min in the air in order to make decomposition of CoDtc and then they were milled after being cooled.
Finally, samples were annealed in air at 550°C for 100 hours in order to make the diffusion of the Co precipitate to the inside of TiO_2 particles.

2.3 TiO_2 thin film samples

TiO_2 has been a topic of significant interest since the beginning of the current century.
TiO_2 is a wide energy gap semiconductor and one of its remarkable properties is the ability for water splitting and, as consequence, the ability to be used as efficient photocatalyst for removing an organic waste from water and air.
This treatment is very important for reducing the toxic organic compounds to non-toxic compounds such as carbon dioxide, water, ammonium or nitrates and chloride ions[94].
Essentially, in an organic degradation, the use of thin films for water purification has some advantages in comparison to the use of nanopowders.
One of such advantages is that it excludes the stage of powder removal after organic compound degradation. It is also supposed that an application of external electric field can result in lowering the recombination rate between e-h pairs produced by absorbed photons and, thereby, improving the catalyst effciency[95].
To prepare uniform thin films, CVD process is widely used. This technique is one of the most modern processes to prepare thin films.

This technique is flexible and applicable to produce multilayer thin film or doped thin film structures.
Additionally, the CVD deposition technique has advantages to produce thin films such as a good quality, high growth rates and it can control the properties[96, 97]. The CVD technique is based on chemical reactions. This technique uses liquids, different gaseous and the chemical solids as a precursor. The deposition process depends on many conditions such as vapour pressure and temperature.
The CVD deposition used to prepare a wide range variety of amorphous, single crystalline and polycrystalline thin film including semiconductors of III-V and II-VI groups.
The CVD process is considered as a chemical reaction that consists of two precursors. One of them is a metal (precursor A) and the other is the precursor of Oxygen and Sulphur which is called precursor (B). This reaction is shown in equation 2.22.

$$\text{Precursor(A)} + \text{Precursor(B)} \rightarrow \text{AB}. \tag{2.22}$$

This reaction needs more than two precursors and the interfering secondary products are presented during the reaction. This normally leads in polluting the metaloxide thin film.
This problem can be overcome by using the complex compound in chemical vapour deposition (CC-CVD). An idea is that in every molecule of complex compound precursor is present already bonded metal and oxygen (or sulphur).
In this case, the chemical reaction of precursor decomposition has different kinetics when compare to classic CVD, that leads to more perfect crystallization during thin films growing[98].

$$\text{Precursor(AB)} \rightarrow \text{AB(+OR)} \tag{2.23}$$

here AB is the complex compound of the precursor and OR is the possible organic. The CC-CVD method has the advantage to prepare the metal oxide inside the organic precursor. The precursor is evaporated which leads to the removal of organic rests and a pure metal oxide molecule is deposited on the substrate in Si:B. Due to this advantage, TiO_2 thin films are prepared by CC-CVD method[98].

2.3.1 TiO_2 thin film deposition

To prepare the TiO_2 thin film, titanium[isopropoxide] Ti(OPri)4 (TTIP) is used as a precursor while a silicon wafer of p-type which has the resistivity of (0.002-0.005)Ωcm is used as a substrate.
The experimental setup of the CVD method, as shown in figure 2.5 consists of the following parts:
Firstly, a quartz tube with inner diameter of 35 mm, 40 mm the external diameter and the length about 300 mm is used[99].
This tube was fixed (a) inside standard vacuum apparatus with a turbo-molecular pump (ALCATEL TMP 5400 CP) creating vacuum down to 5 $\times 10^{-7}$ mbar.
Then, the tube heater was placed inside a titanium foil screen.

This heater consists of two halogen lamps (A Philips 1KW) used to heat the substrate. Also, four halogen lamps (500 W) used as a heater.
Before loading, the tube was cleaned in water by detergent and rinsed in distilled water. Whereas, the substrate was immersed in sulfuric acid (95%) for about 1 hour, rinsed by distilled water and washed with acetone.
Finally, it was dried by a flux of filtered air[94, 99].
TiO_2 thin film deposition is done by the following steps:
Firstly, the precursor is filled inside the circles of the evaporator which are at the bottom of the chamber while at the top of the chamber the substrate is fixed above the evaporator.
The cooling system was connected directly to the evaporator. The vapor source has a temperature in the range (90-210)°C.
Before the thermal treatment of the precursor, the chamber is pumped out to the pressure 1×10^{-5} mbar and the temperature of the substrate at 450°C to confirm the crystallization of theTiO_2 phase on the quartz glass substrate.
Secondly, during the deposition, when the temperature of the substrate has reached, the chamber is submerged by mixture Ar\$O_2$gas = 100\50 fluxes rates of gas 20 ml/min. As well, the pressure of deposition was changed from $1x\times10^{-1}$ mbar to 1.7×10^{-1} mbar. The mixture of argon-oxygen atmosphere should supply enough oxygen to guarantee the formation of TiO_2 molecules and the burning of organic rests to avoid contamination of the thin film.
Thirdly, the evaporator is heated up to 50°C and the shutter substrate is opened to begin the chemical deposition process.
During this process the pressure inside the chamber increases until the pressure of deposition is restored and at this pressure the precursor is completely evaporated and the deposition process is finished.

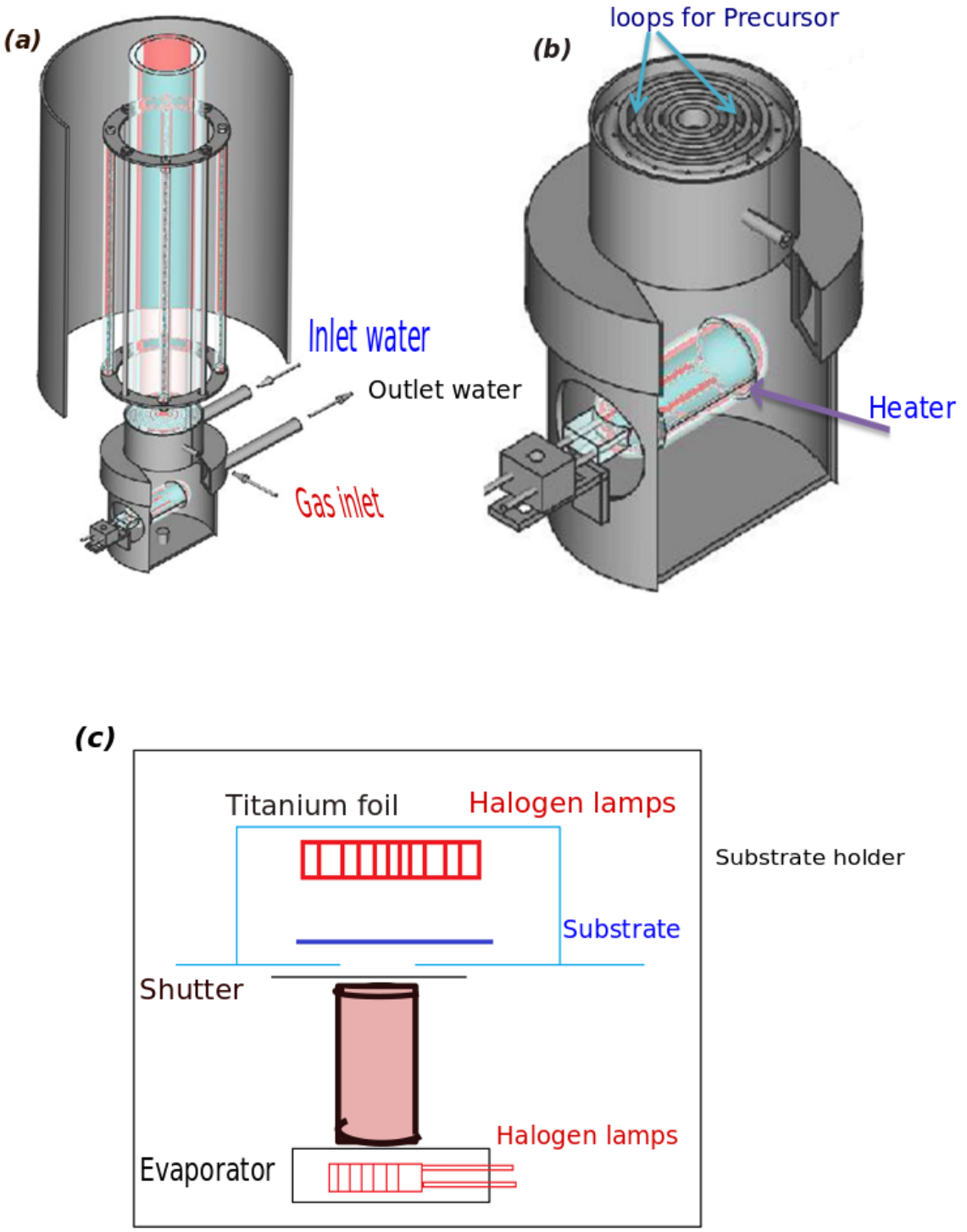

Figure 2.5: CC-CVD setup of TiO_2 thin film preparation. (a) Quartz is placed inside the chamber, (b) Evaporator and (c) Schematic diagram for preparing the TiO_2 thin film by CC-CVD process[99].

2.3.2 Photocatalytic activity of TiO_2 thin film

Recently, the dyes and commercial colorants have become the focus of environmental remediation because of their natural biodegradability [100, 101].
These dyes are ineffective in the traditional wastewater treatment methods because the dyes are highly soluble in water[102].

Many researchers studied the effect of visible and UV irradiation on photocatalytic degradation of these dyes on the semiconductor nanoparticles surface.
They found that photocatalytic reaction can take place due to electron and hole transfer that occur between dyes and semiconductors directly or through intermediate water splitting.
Consequently, these dyes can degrade to a smaller material and also mineralize it to water completely or other inorganic ions. Employing these methods to degrade colored organic pollutants such as dyes has important implications because of high efficiency use of visible light or UV radiation[103, 104].

2.3.3 Dye materials

In this work, five dyes were used as electrolytes to study the photocatalytic activity of TiO_2 thin film under UV irradiation of mercury lamp and applied electric field at potential difference of 15 Volts.
These dyes are Methanol Blue (MB), Gentian Violet (GV), Brilliant Green (BG), Methyl orange (MO) and Eosin (EO). The chemical structures of these dyes are shown in figure2.7.

Methylene blue is a cationic dye and medication. Commonly, it is used for dyeing cotton wools and coloring paper and colorant hair. The molecular formula of MB is $C_{16}H_{18}N_3SCl$. It has a green dark crystalline powder and easily soluble in water at room temperature.
Moreover, it has a strong adsorption characteristics on many surfaces and good resistance to light degradation[105, 106].

Methyl Orange is an azo dye which is used in textiles, pulp and papers, and leather industry. It has the molecular formula $C_{14}H_{14}N_3NaO_3S$. It is vastly used as an acid-base indicator in the textiles dyeing industry and experiments[107].

Gentian Violet is a dye used to distinguish and classify bacterial species, a histologial strain and also it was used as an antiseptic. The chemical formula of GV is $C_{25}H_{30}ClN_3$. This dye has different colors depending on the acidity degree of the solution. For example, this dye is green if the acidic solution is strong[108].

Furthermore, Brilliant Green is used as an antiseptic and it is very effective against gram-positive bacteria. The chemical formula of the dye is $C_{27}H_{33}N_2HO_4S$ and it is not resistant to light[108, 109].

Eosin is a fluorescent dye which connects salts with eosinophilic compounds containing positive charges. It is yellow in color and $C_{20}H_6$ $Br_4Na_2O_5$ is the chemical formula[110].
Commercially, it has several types but the most important is Eosin Y because it is easily soluble in water and alcohol. Eosin can be used to examine under the microscope because it has the ability to distinguish between the cytoplasm of different types of cell[111].

In this thesis, the setup contains the PEC cell. This cell consists of an anode and a cathode immersed in the solution (electrolyte) and connected to an external circuit shown in figure2.6.

The photo-electrochemical reactor (PEC) is made up from of quartz glass which has 75x25 mm dimensions. The capacity of this reactor is 42 ml but the total volume of the solution is used in the experiments is about 40 ml. At the bottom side of this reactor, there are inlets for air pump.
The reactor consists of an anode and a cathode. The anode is TiO_2 thin film prepared by CVD process which is connected with silver electrode glued on the top of Si:B substrate on which TiO_2 thin film is deposited.
The back side of the substrate as well as other sides were isolated from electrolyte by epoxide glue in order to provide electrical connection only through TiO_2 thin film. A gold metal is used as a cathode.
All these dyes were obtained through pharmacy market and are used as received. While solutions were prepared using water from a Millipore water purification unit. The concentrations of the dyes were determined in the range of validity domain of the Beer-Lambert law as mentioned in section 2.1.4 according to the sensing capability of the spectrophotometer.

Table 2.2: Molar concentrations of different dyes ($\times 10^{-5}$) mol and H_2O. The concentration of dyes and water is different according to the sensing capability of the spectrophotometer.

Name of dye	Dyes (mol)	H_2O (mol)
Methanol Blue	312	5.6
Methyl orange	1.5	28
Gentian Violet	29	28
Brilliant Green	12	28
Eosin	15	39

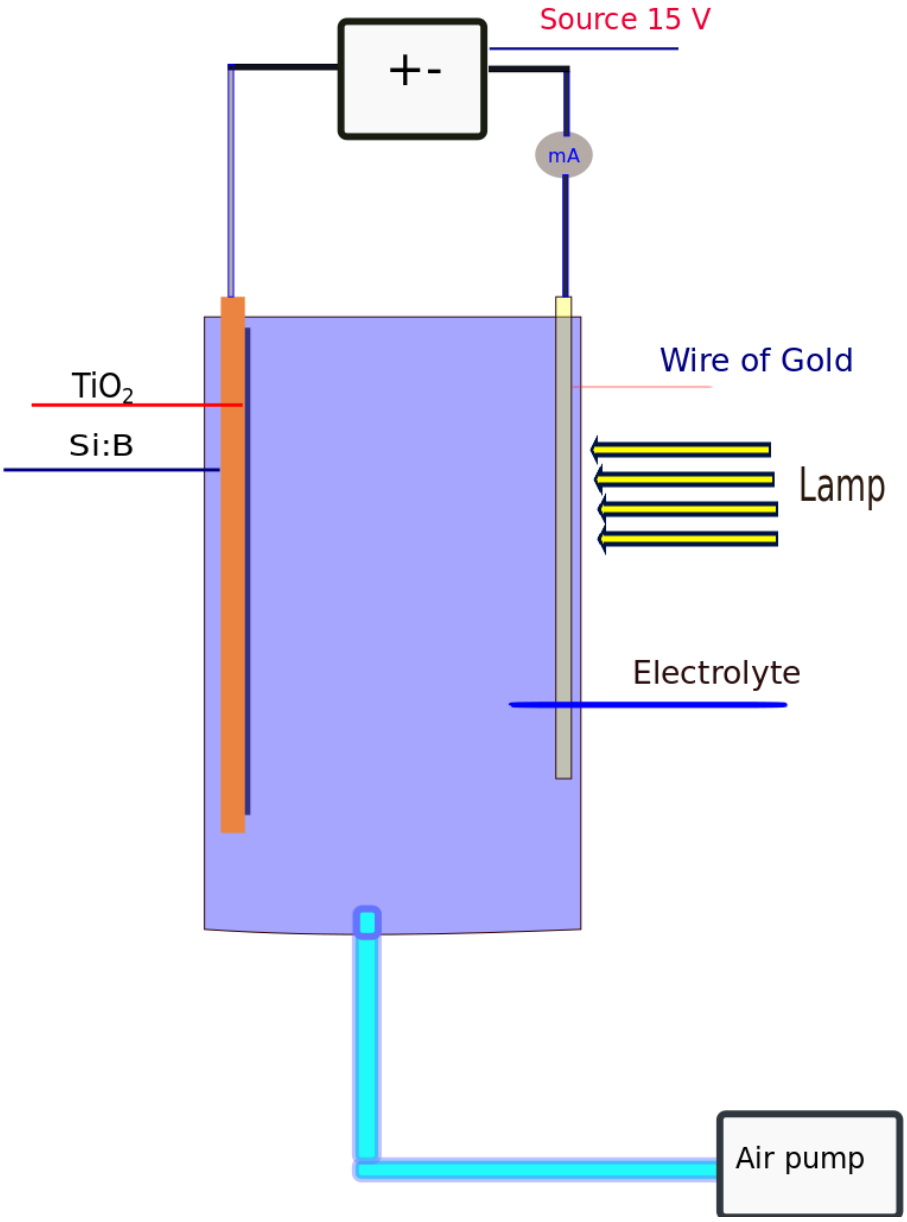

Figure 2.6: Schematic diagram of a photoelectrochemical cell(PEC) used within this work. This cell consists of an anode and a cathode. The photoanode is Si-B p-type semiconductor as a substrate with TiO_2 thin film photocatalyst deposited on its surface by CVD, where H_2O is oxidized. The photocathode is a gold metal where H^+ ion is reduced to H_2. Both are immersed in an electrolyte which consists of dye and connected to an external circuit.

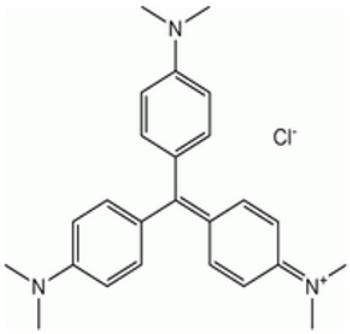

Gentian Violet

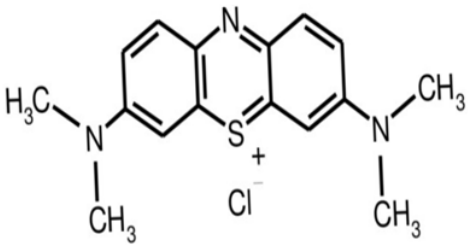

Methylene Blue

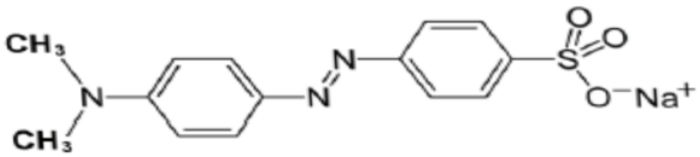

Methyl orange

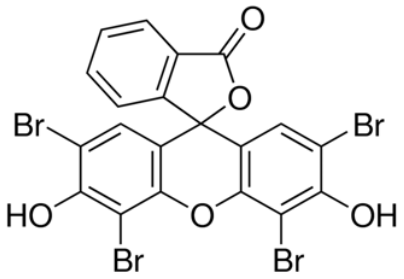

Eosin

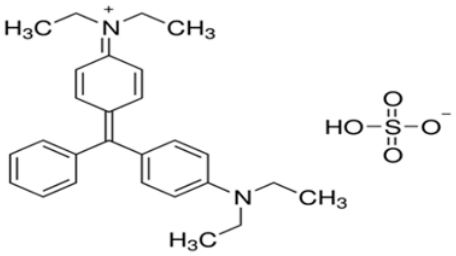

Brilliant Green

Figure 2.7: Molecular structures of different dyes which are used to study the photocatalytic decomposition within this work[108, 105, 107, 111, 109].

Chapter 3

Results

This chapter includes the results of sample characterization and photocatalytic activity studies for nanopowders prepared by sol-gel process and TiO_2 thin film materials.
These studies include: XRD results obtained for pure P25 Degussa and sol-gel powders. Also, P25:x%Co (P25 Degussa nanopowders doped with different concentrations of cobalt Co,(x= 1, 2, 5, and 10).
Furthermore, the results of surface area which based on TiO_2 nanopowder structure and the photocatalytic activity for TiO_2 different powders and different dyes by TiO_2 thin film is presented in details.
The samples were prepared as a powder by the sol-gel method and P25 Degussa doped with cobalt. These samples were used to study the photocatalytic activity by two methods. The first method uses a mercury lamp as a source at room temperature. The second method uses different optical filters to study spectral dependence of the photocatalytic constant for various wavelengths in the range from 365 nm to 690 nm.
On the other side, several kinds of organic pollutants were degraded by TiO_2 p-type thin film. The photocatalytic effect on the water includes the photocatalytic degradation of different dyes and electrochemical decomposing.

3.1 Powder samples

3.1.1 X-ray diffraction

XRD method is explained in chapter 2.1.1. The XRD patterns of pure P25 Degussa nanopowders, P25 doped with Cobalt(Co) and different samples of TiO_2 powders prepared by the sol-gel method. As well as, series of sol-gel powders calcined at 400°C in vacuum chamber are shown in table 3.1.
The XRD patterns for all synthesized powders via sol-gel method show broadening of peaks due to small crystallite size. This can be also be clearly seen when comparing diffraction patterns from TiO_2 sol-gel and $P25$ Degussa powders.
All the peaks shown in figure 3.1 confirm the presence of TiO_2 anatase and rutile phases (JCPDS: No $21-1272$) and (JCDS No$(21-1276)$), respectively[112].
Furthermore, the crystallite size of synthesized TiO_2 powders were found to be 24.4 nm, 10.75 nm and 33.98 nm for $S1$, $S2$ and $S4$, respectively.
In comparison to P25 Degussa which was 25.6 nm, this is much smaller, except for series $S4$. This sample has the largest crystallite size in compared to other samples for TiO_2 anatase phase.
Additionally, the crystallite size of P25 has 43.3 nm for rutile which was the largest of TiO_2 powders. The crystallite size for $S1$, $S2$ and $S4$ were 34.5 nm, 40.6 nm and 50.09 nm, respectively.
This significant changes in anatase and rutile phases can be taken place for the sample $S4$. It is higher than the other samples as shown in table 3.1.
Some peaks of diffraction patterns obtained for the samples P25:x%Co (where$x$ = 0.01, 0.02, 0.05 and 0.10) are shown in figure 3.2.
The patterns in figure 3.2 showed (101) (004) and (110) peaks.
Their peaks can be indexed as anatase and rutile phases of TiO_2.

Moreover, It was shown that there are no extra peaks present or additional Co-Ti-O phases were not detected conforming that the anatase phase isn't disturbed upon doping by cobalt ions in TiO_2 structure which confirms high purity of TiO_2 for Co doping and phase stability of the system.
By increasing Co concentration, the peaks of XRD pattern become slightly broader indicating lattice disordering.
The results shown by[113] confirm that Co ions substitute the Ti sites and have well been incorporated in host TiO_2 matrix. No signs of Co cluster phases through the whole range of Co contents were observed within the sensitivity of XRD.
The results are illustrated in table3.1, when Co content is increased, the rutile phase is decreased.
Whereas at concentration 10% of Co the relation between anatase and rutile phases is almost the same as for P25 Degussa powder.
Therefore, it seems that Co acts as inhibitor for anatase and rutile phases transformation. This result is in contradiction with the statement presented in[114] where Co is considered as promoter for such transformation.
However, it should be noted that Co position in the diagram of elements is close to the line that divides elements as promoters and inhibitors[114].

Table 3.1: XRD results of pure P25, sol-gel powders and P25:x%Co nanopowders that were annealed at 550° for 100 h

Samples	Anatase %	Rutile %
P25 Degussa	83.31±0.5	16.74±0.5
S1	52.98±0.3	47.03±0.4
S2	58.82 ±0.5	41.23±0.5
S4	74.82±0.4	25.23±0.5
P25:1%Co	75.61±0.6	24.40±0.5
P25:2%Co	78.02±0.5	22.02±0.5
P25:5 % Co	80.13 ±0.5	19.92 ±0.5
P25:10 % Co	83.02±0.4	17.01 ±0.4

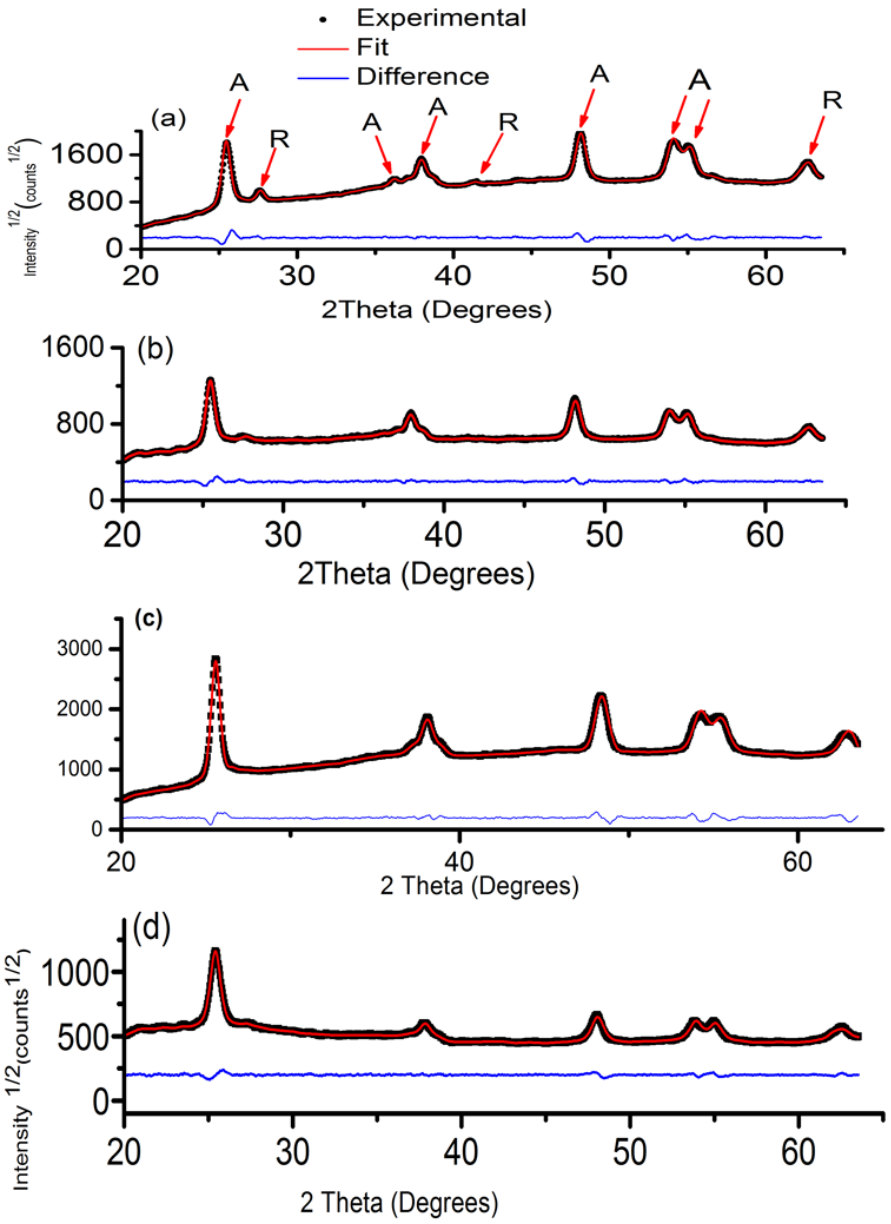

Figure 3.1: XRD patterns of sample powders (a) P25 Degussa as a reference and TiO_2 sol-gel powders (b-d).

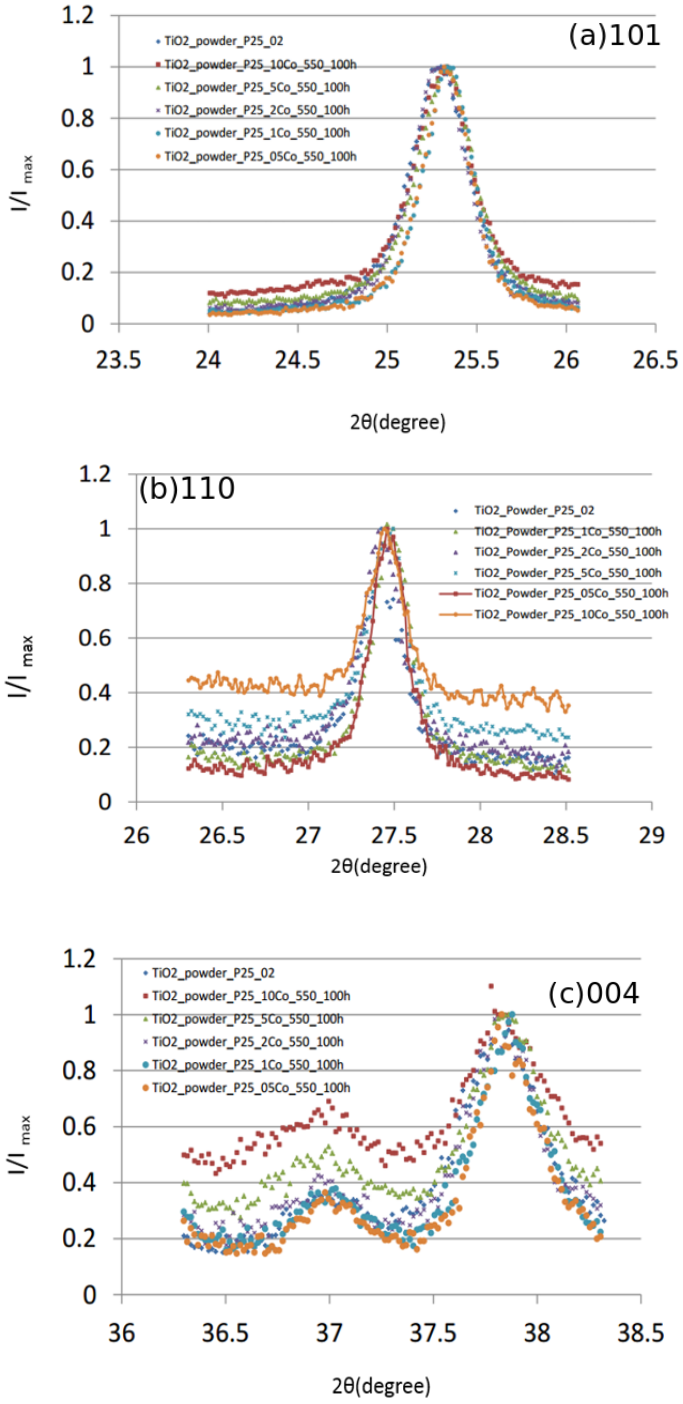

Figure 3.2: XRD patterns of P25 Degussa and Degussa P25:x%Co. The peaks can be indicated as TiO_2 anatase phase, there are 101, 110 and 004, respectively.

3.1.2 Surface Area

Figure 3.3 represents the typical isotherms of N_2 adsorption-desorption measured at 77 K of studied powders. There are P25 Degussa, sol- gel samples and P25:x%Co (x= 1, 2, 5 and 10) with different concentrations of Co.
All powders show a type Π isotherm which characterises the transition metal oxide with a H3 hysteresis.
All isotherms have a small slope from the B-point at $\frac{p}{p_o}$ which is referring to a unique characteristic of mesoporous material family.
For the adsorption branch, the slope of the powder increases from the $\frac{p}{p_o}$, where a monomolecular coverage is reached unital adsorbed quantity reaches to the maximum value at $\frac{p}{p_o} = 0.98$ [70, 71].
It can be noted that the adsorbed quantity of N_2 on powders directly decreases with decreasing of N_2 pressure during the desorption branch which formed a narrow hysteresis that is closed at$\frac{p}{p_o}$. This indicates mesoporous structures inside the powder samples.
The H3 hysteresis indicates that all studied powers are involving aggregates or agglomerates of particles forming a slit-shaped pores like cubes with nonuniform sizes and shapes[71].
According to figure 3.3, all powder samples show the same isotherm Π with type H3 hysteresis which is typical for $P25$ Degussa nanopowder[76].
The surface areas can be calculated for all samples by using equation 2.11.
In accordance with these calculations all the samples have surface area lower than that of P25 Degussa.
Furthermore, surface area increased and pore size decreased which indicates as aggregation of the particles being weaker.
According to these calculations, the sample S2 and P25:2%Co show a higher amount of N_2 adsorbed compared to the others samples which displays that these samples has the largest surface area as referred in the table 3.2.
In contrary, these samples have a larger pore volume and the slimmest hysteresis compared to the other.
On the other hand, the smaller surface area and lower pore volume of the samples indicate that aggregation of the particles is stronger.
Whereas, in figure3.4, it is shown that the pore size distribution was a broad for P25 doped similar to that of the mesoporous family and it was observed for all the powders being studied.
This organized porous structure might be significant in the photocatalytic process because they possess efficient transport pathways for reactant and product species.
The surface area parameters shown in table 3.2 indicate that surface area of P25 Degussa is higher than P25 Degussa doped .
Whereas, the surface area is increased when increasing the concentration of Co at lower concentrations.
In addition, the surface area of powders P25:5%Co and P25:10%Co is decreased compared to lower concentrations of Co.
From our results, the analysis of BET for doped powders showed that a specific area is not changed drastically.

Table 3.2: Results calculated of specific surface area, pore size and the pore volume for P25 Degussa, sol-gel samples and P25:x%Co doped powders. The errors are numerical errors from BET and BJH calculations

Sample	SA (m^2g^{-1})	Pore size (nm)	Pore volume(cm^3g^{-1})
P25Degussa	57±0.34	2.2±0.008	0.179 ±0.008
$S1$	6.4 ±0.096	10.8±0.009	0.01±0.006
$S2$	73.5 ± 1.06	2.37±0.001	0.08 ±0.011
$S4$	8.6 ±0.12	3.04±0.007	0.007±0.005
P25:1%Co	31.4 ±0.13	46.9±0.008	0.07±0.007
P25:2%Co	38.3 ±0.084	45.4±0.005	0.10±0.005
P25:5%Co	35.5 ±0.077	45.5±0.003	0.09±0.009
P25:10%Co	31.5 ±0.086	45.3±0.002	0.07±0.007

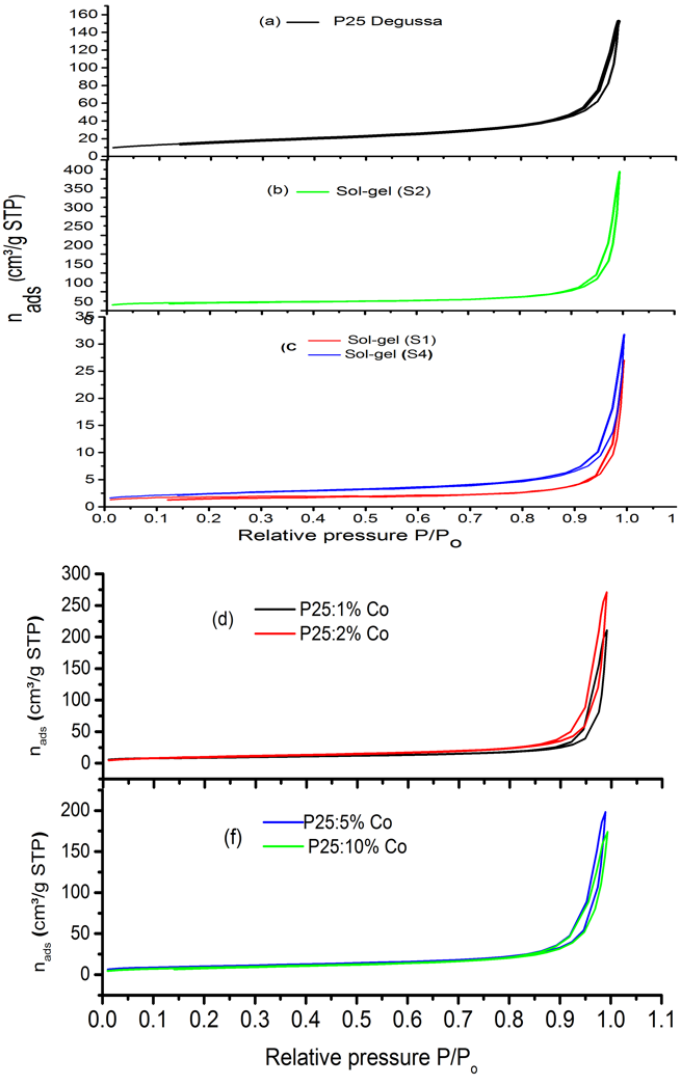

Figure 3.3: Typically N_2 adsorption-desorption isotherms of P25 Degussa (a). TiO_2 powders prepared via sol-gel method (b) and (d). P25 doped with different concentrations of Co (d) and (f). All these isotherms belong to the mesopores materials family.

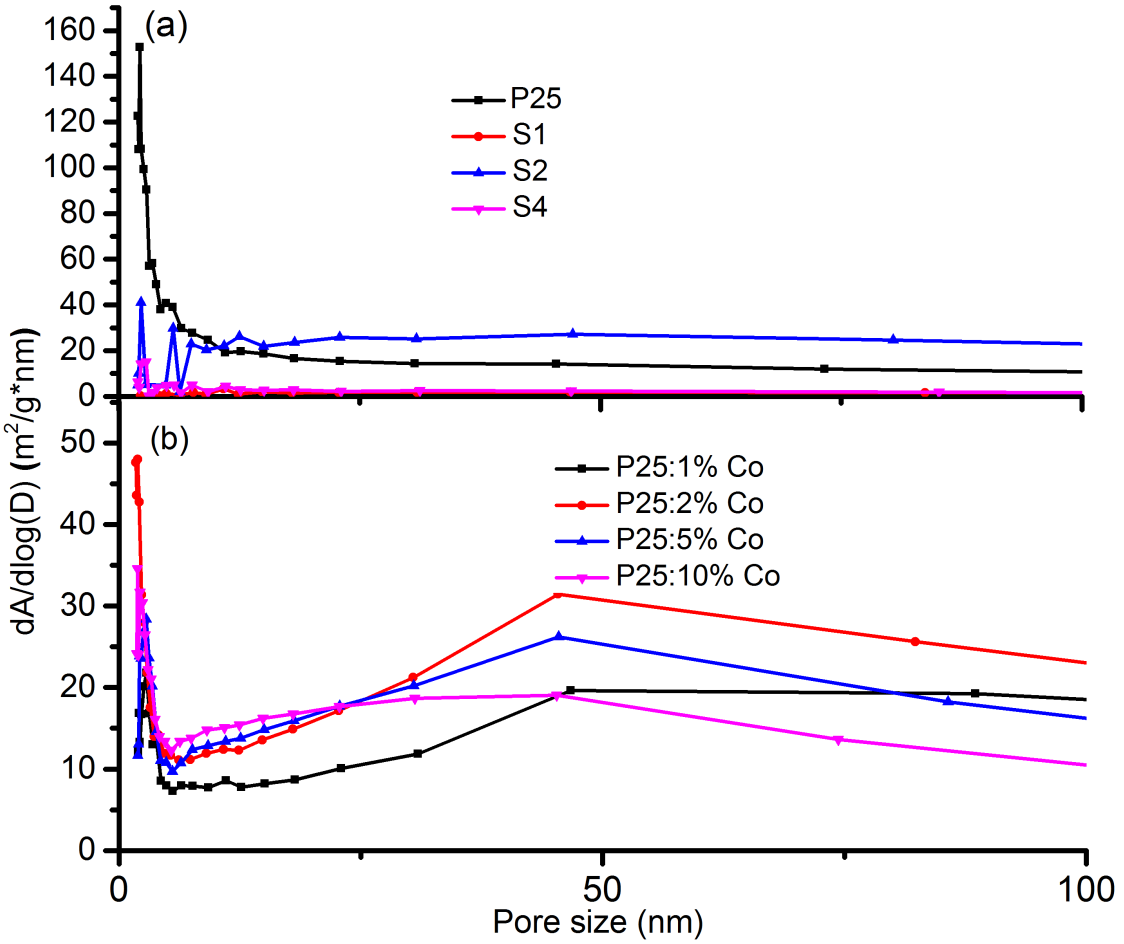

Figure 3.4: Pore size distribution of TiO_2 studied samples. There are pure P25 Degussa Powder, sol-gel powders and P25 doped with different concentrations of Co.

3.1.3 UV-Visible absorption spectra

The UV-Visible absorption spectra of the studied samples were investigated.
Figure 3.5 shows UV-Vis absorption spectra of P25 Degussa as a reference material and different concentrations of Co doped P25 Degussa as well as different samples prepared by sol-gel method.
The UV-Vis spectra of studied samples are recorded in the range of 250-700 nm at room temperature as shown in figure 3.5.
This absorption spectra is shifted for doped P25 Degussa samples with increasing the concentrations of Co. However, the absorption spectra of sol-gel powders also shift dependence on crystallite size.
The energy gap and wavelengths of absorption edge are summarized in table3.3.
The optical energy gap is calculated by extrapolation of the baseline and the absorption edge[77].
These energies gap were analyzed by using the relationship between photon energy and wavelength from equation 2.20 which are referred in figure 3.6
Figure 3.5 displays the spectrum absorption of P25 Degussa, P25:x%Co doped and sol-gel powder, respectively.
P25 Degussa has a sharp absorption edge at 387 nm, however, the absorption edge at(385 nm, 381 nm and 402 nm) for the series sol-gel powder were shifted towards the visible region. This shifting in absorption spectra may be enhanced the photocatalytic activity of sol-gel powder under visible light radiation.
Whilst, for the TiO_2 doped powders have the absorption thresholds at 399.39 nm, 401.12 nm, 397.57 nm and 380 nm for the concentrations 1%, 2%, 5% and 10% of cobalt, respectively.
The slight shift in absorption edge of doped samples at the concentration of Co increased.
Table 3.3 illustrates the decreasing in energy gap values when increasing in dopant concentrations. Whereas, the energy gap of S1 and S2 powders is slightly increased with comparing to P25 Degussa powder. While the energy gap for S4 is decreased.

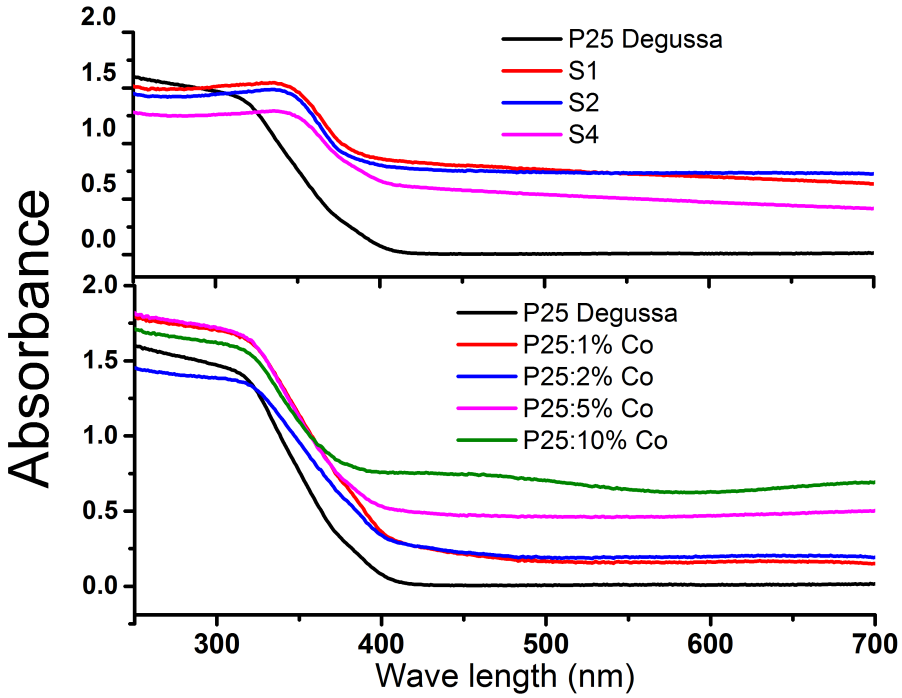

Figure 3.5: UV-Visible absorption spectra of P25 Degussa, P25 Degussa doped with Co and pure sol-gel powders, respectively.

Table 3.3: Wavelengths and the optical energy gap of P25 Degussa, P25 doped with different concentrations of Co and different of sol-gel powders.

Sample	Wavelengths (nm)	E_g(eV)
P25 Degussa	387.0	3.20
S1	385.2	3.22
S2	381.0	3.25
S4	402.3	3.08
P25:1%Co	399.5	3.10
P25:2%Co	401.1	3.09
P25:5%Co	397.7	3.21
P25:10%Co	380.0	3.26

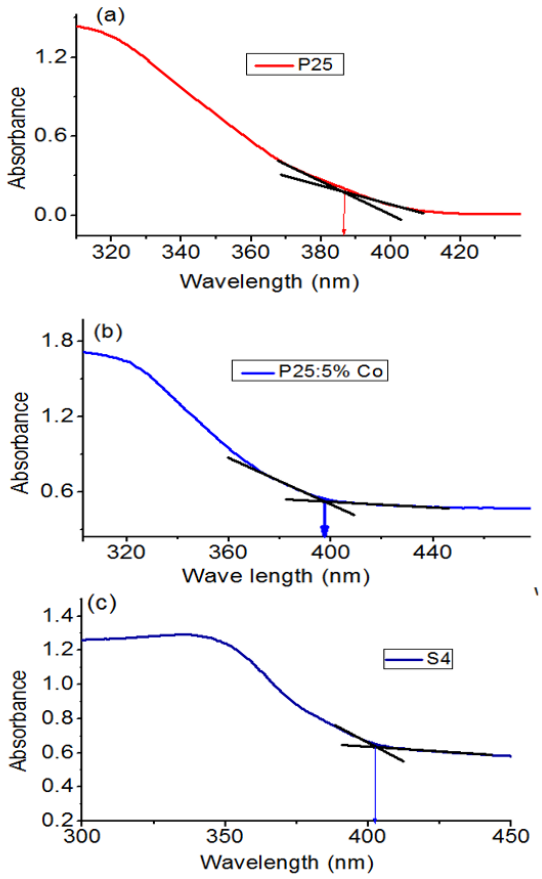

Figure 3.6: Analysis of the optical energy gap for P25 Degussa (a), P25:5%Co and S4 is prepared by the sol-gel method in (b) and (c), respectively.

3.1.4 Photocatalytic activity of TiO_2 nanopowders

3.1.4.1 Using mercury lamp

The photocatalytic activities of P25 Degussa, P25:x%Co doped and sol-gel samples were studied by observation the degradation of the Fenarimol powder (as a reference materials) dissolved in water (H_2O) as mentioned in section 2.1.3.
In this work, the photocatalytic activity experiments for all samples catalysts were repeated three times.

The photocatalytic degradation is shown in figure 3.7 for P25:x%Co doped and sol-gel powders when compared to commercially P25 Degussa.
All curves of studied samples can be described as the pseudo first-order kinetic reaction which follows Langmuir Hinshelowd model[115, 74].
The good linear relationship between $\ln\frac{C_0}{C}$ against time (t) was observed and the photocatalytic constant K extracted from the slope of the curve. That obtained the photocalalytic constant of the samples.
The results are shown in table 3.4. Under darkness, all catalyst samples have a little adsorption which can be neglected in the degradation.
However, it was shown that all catalyst samples exhibited significantly lower degradation photoactivity than P25 Degussa catalyst under the UV illumination.
Furthermore, the photocatalytic constant of P25 Degussa was found approximately 7.21 times higher than the direct photo degradation of Fenarimol powder under UV light illumination without P25 powder.
The results of the photocatalytic constant K for samples synthesized by the sol-gel method with the different surface area is given in table 3.4.
These results show that K constant decreases with decreasing the surface area of these samples.
On the other hand, the photocatalytic constant of P25 > P25:5%Co > P25:1%Co > P25:2%Co> P25:10%Co, respectively.

Table 3.4: Results calculated of the photocatalytic constant K(h^{-1}) of pure P25 Degussa and sol-gel powders. Also, P25:x%Co doped at different concentrations of Co (x= 1, 2, 5 and 10). All these samples are studied under mercury lamp as UV illumination and dankness in the same conditions.

Sample	$K_{Darkness}$	K_{UV}
Fenarimal	0.0412±0.001	0.212±0.02
P25Degussa	0.044±0.004	1.53±0.017
P25:1%Co	0.034±0.004	0.21±0.012
P25:2%Co	0.032±0.003	0.15 ±0.01
P25:5%Co	0.039±0.005	0.25±0.027
P25:10%Co	0.035±0.003	0.11±0.013
S1	0.039±0.01	0.39±0.03
S2	0.029±0.002	0.15±0.01
S4	0.037±0.004	0.19±0.01

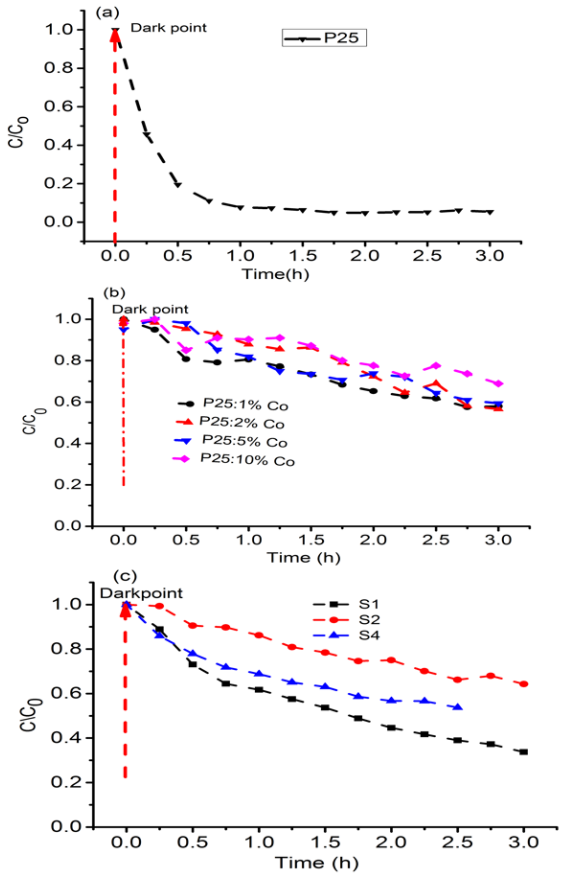

Figure 3.7: Degradation of pure P25 Degussa and sol-gel nanopowders. P25:x%Co doped with ddifferent concentrations of Co, respectively under UV illumination.

3.1.4.2 Using different wavelengths

There is no study available in the literature to highlight the photocatalytic activity of different TiO_2 samples by using different wavelengths in the range of 365 nm to 690 nm.

The photocatalytic activities of pure P25 Degussa, P25:x%Co doped with different concentrations of Co and different sol-gel powders are illustrated in figure 3.8 and figure 3.9 at different wavelengths, respectively.
These results indicate the photocatalyic degradation trends of P25 Degussa.
It was faster than the other samples and it has the best photocatalytic performance at low wavelengths specially 336 nm and 405 nm, respectively.
Furthermore, the degradation of P25 is faster than the other samples under 405 nm wavelength.
It is noticed that the photocatalytic degradation is not affected by applying the high wavelength as shown in figure 3.9.
The constant K of tested samples are calculated from the slopes of curves and they are illustrated in table 4.3.
The photocatalytic constant values under short wavelength 365 nm and 405 nm of P25 Degussa attain nearly 0.17 h^{-1} and 0.13 h^{-1}, respectively.
It illustrates P25 has higher K value than doped P25 samples, as well as, 5 times, 8 times, 5 times and 2 times for P25:1%Co, P25:2%Co, P25:5%Co and P25:10% Co, respectively. Furthermore, P25 has higher K than the value of sol-gel powders, there are 12 times, 18 times and 5 times for S1, S2 and S4 powders, respectively.
Moreover, the photocatalytic degradation of P25 and the tested samples are very small and nearly constant. Therefore, the K constant is not equal to zero under the high wavelengths.
Moreover, figure 4.3 characterizes the relationship between the constant K and different wavelengths of pure P25, sol-gel samples powders and P25:x%Co doped.
At shorter wavelengths, the K decreases with increasing wavelengths while it was more constant at the high wavelengths for P25 Degussa. This is the same behavior found for sample S4 powder and also similar to that of the P25:10%Co.

In our results, the photocatalytic constant increases at short wavelengths and becomes constant at high wavelengths, as shown in figure 4.3.

Table 3.5: Results calculated of the photocatalytic constant K(h^{-1}) for different TiO_2 nanopowders. There are P25:x%Co doped with different concentrations of Co (x= 1, 2, 5 and 10) and sol- gel powders under different wavelengths.

Wavelengths	365 nm	405 nm	436 nm	546 nm	690 nm
Fenarimal			0.030±0.001		
P25 Degussa	0.17±0.014	0.13±0.02	0.059±0.002	0.051±0.001	0.048±0.01
P25:1%Co	0.035±0.015	0.040±0.002	0.057±0.004	0.034±0.002	0.028±0.002
P25:2%Co	0.021±0.02	0.017±0.001	0.039±0.002	0.014±0.001	0.031±0.003
P25:5%Co	0.03±0.02	0.036±0.004	0.049±0.004	0.069±0.008	0.028±0.004
P25:10%Co	0.09 ±0.02	0.033±0.002	0.043±0.002	0.043±0.002	0.019±0.002
S1	0.014±0.01	0.022±0.003	0.036±0.001	0.04±0.004	0.019±0.003
S2	0.009±0.001	0.011±0.001	0.059±0.01	0.049±0.004	0.024±0.004
S4	0.036±0.001	0.028±0.002	0.033±0.003	0.033±0.001	0.018±0.002

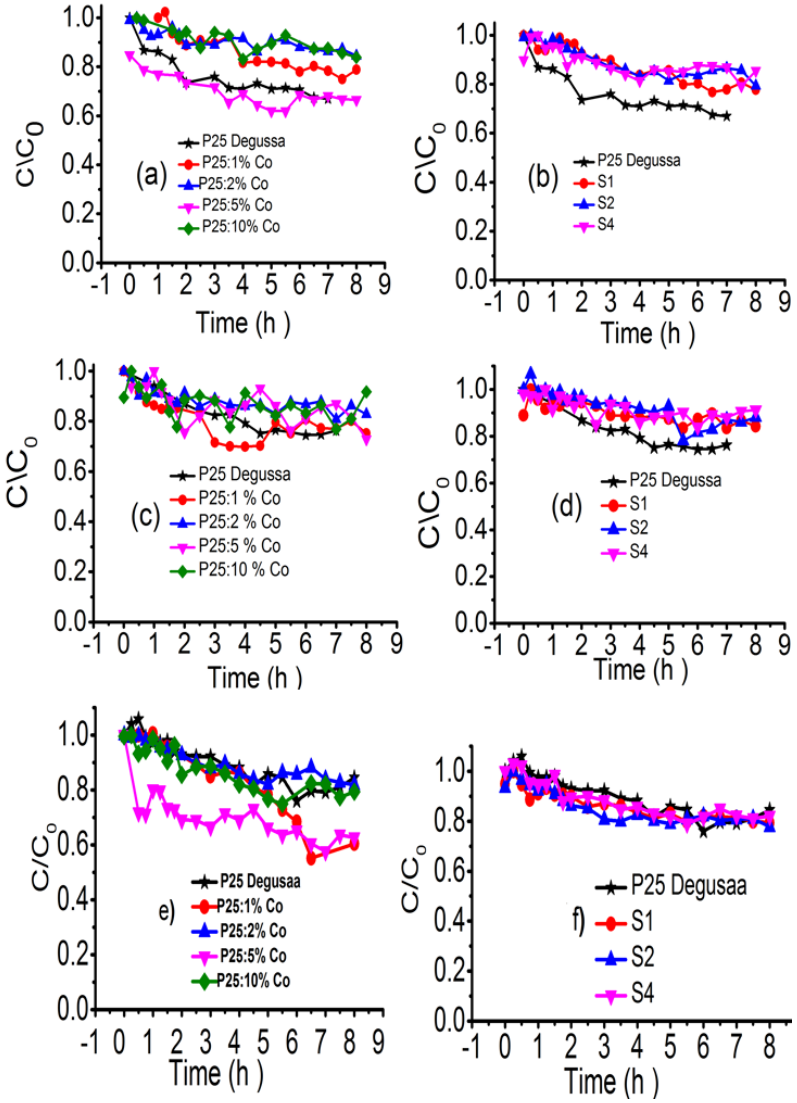

Figure 3.8: Photocatalytic degradation curves of P25 Degussa, P25:x%Co doped with different concentrations of Co (x= 1, 2, 5 and 10) and different sol-gel powders under different wavelengths at same conditions. There are 365 nm (a-b), 405 nm (c-d) and 463 nm (e-f).

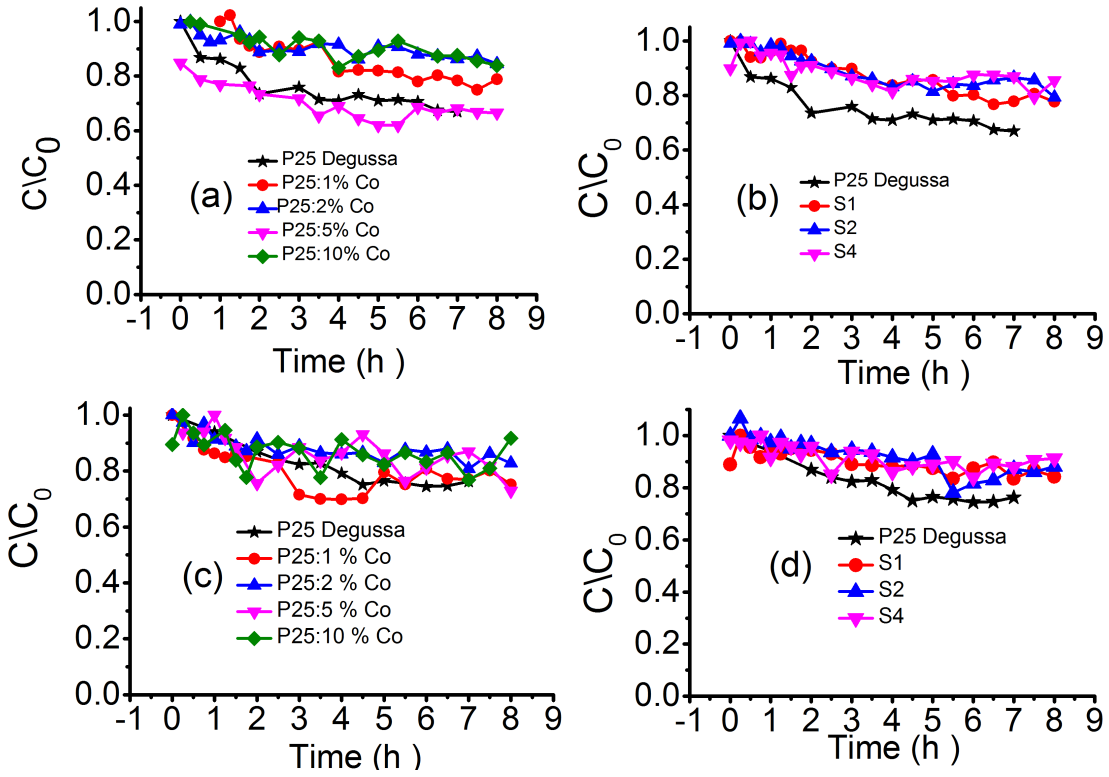

Figure 3.9: Photocatalytic degradation curves of P25 Degussa, P25 doped with different concentrations of Co and sol-gel powders under wavelengths 546nm (a-b) and 690 nm (c-d), respectively.

3.2 TiO_2 thin film

Many kinds of organic pollutants used to be degraded by TiO_2 materials.
The pure dyes are one of the important classes of pollutants for application of TiO_2 photocatalysts for wastewater purification.
To the best of our knowledge, there is no study in the literature dedicated to study the photocatalytic and electrochemical activity of a wide energy gap TiO_2 thin film in presence of applied electric field in order to remove different industrial dyes from water.
Methanol Blue(MB), Gentian violet (GV), Brilliant Green (BG), Methyl Orange(MO) and Eosin(EO) were used to verify the efficiencies of their removal from water.

There are two simultaneous effects that occur in water. One is the photocatalytic degradation of the dyes and the other is the electrochemical removing.
The photocatalytic and electrochemical performance of the synthetic TiO_2 thin film was studied by comparing the activities of TiO_2 p-type semiconductor thin films under three effects: UV illumination(UV), applied electric field(E) and UV illumination with electric field(UV+E) simultaneously under the same experimental conditions.

3.2.1 X-ray diffraction

Figure 3.10 shows the XRD pattern of deposited TiO_2 thin film on P-Si(100) as a substrate. The silicon wafer is a p-type semiconductor.
This XRD pattern displays characteristic peaks of TiO_2 anatase at $2\Theta = 25.27°$, 54.48°, 48.0° and 55.0°. These are attributed to TiO_2 anatase diffraction in planes (101), (200), (105) and (211), respectively[116].
In addition to these peaks, some peaks of $2\Theta = 38.5°$ and 61.68^o are also observed in this pattern which are attributed to TiO_2 anatase (004) and (213).
Furthermore, one peak appeared at $2\Theta = 56.36°$. This can be indexed to plane(220) of TiO_2 rutile phase.
The XRD pattern is consistent with the standard XRD data for tetragonal TiO_2 anatase phase, (JCPDS, no 21-1272) and tetragonal TiO_2 rutile (JCPDS, no 21-1276)[112].
Moreover, the small peak at $2\Theta = 32.97°$ is attributed to Si (200). This peak is agreement with the results presented in reference[117].

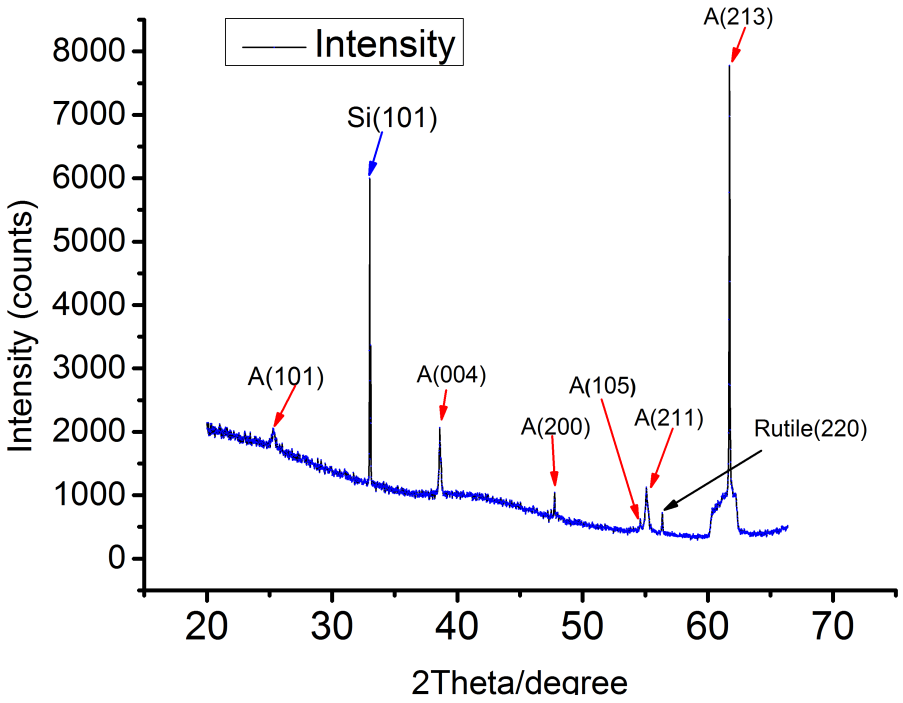

Figure 3.10: XRD pattern of the TiO_2 thin film deposited by the Chemical Vapor Deposited method. P-type-Si(100) was used as a substrate.

3.2.2 Photocatalytic activity of TiO_2 thin film

Figures 3.11 shows absorption spectra obtained by the UV-Vis spectroscopy in the range from 200 nm to 800 nm of different dyes without thin film in darkness.

The optical spectra of these dyes shows absorption in both UV and visible region with maximum peaks positions located at 664.5 nm, 465.07 nm, 622.04 nm, 581.51 nm and 516.68 nm for MB, MO, BG, GV and OS, respectively.
Furthermore, it is noted that there is no changes in the absorption with time of the dyes in the absence of TiO_2 thin film [118].
Figure 3.12 illustrates absorption spectra of studied dyes without thin film under UV illumination (direct photolysis). As shown in figure 3.12, plots a and e, Methanol Blue and Eosin show no interaction with UV radiation.
On the other hand, the absorption spectra of the Gentian Violet, Brilliant Green and Methyl Orange slightly decreases in UV radiation as shown in figures 3.12 b, c, and d respectively.

Another set of absorption spectra experiments were performed on the same way employing a few additional conditions. Namely, mercury lamp was used as a UV source, electric field created by voltage of 15 V (Electric field applied was 15 V/0.025 m = 600 V/m) and both UV+E were applied simultaneously.

These studies are shown in figures 3.13 and 3.14. All figures, (except figure 3.13) a which belongs to the methanol blue) show a bigger reduction for the absorption in the case of E+UV than when using only E. More details can be found in the appendix A.1.1.

More clarification for the photocatalytic degradation for the different dyes can be obtained. The absorption value is attributed to the area of the main peak which is calculated by fitting the curves to a Lorentz-Gauss shape.
In our experiments, the photocatalytic degradation efficiency of the studied dyes in the case photocatalysis and electrolysis simultaneously is higher than the case when using the photocatalysis or electrolysis alone.
It can be also sublined that the simultaneous application of photocatalysis and electrolysis is more effective than the pure sum of photocatalytic and electrolytic effect. So, some kind of synergetic effect can be confirmed in our studies.
In the following, there are results of dyes degradation after irradiation for 1 hour for different conditions of experiment. The dyes absorbtion is degraded from I = 1 or from 100 % at the beginning to 0.77%, 0.38%, 0.85%, 0.91% and 0.91% of MB, BG, MO, GV and EO, respectively in the case of the photocatalysis process .
In the same time, however, the degradation shows reduction in absorbtion to 0.29%, 0.38%, 0.54%, 0.83% and 0.84% in the case of the electrolysis process.
On the other hand, under two processes simultaneously, absorbtion decreases of studied dyes from 100 % to the 0.13%, 0.20%, 0.36%, 0.54% and 0.48% of MB, BG, MO, GV and EO, respectively.
Figures 3.15 a, b, c and d show the photocatalytic constants K of different dyes are obtained from equation 2.15 section 2.1.4.

As it follows from the results presented in table 3.6, the highest K constant was obtained from case of UV+E in comparison to case when only UV lamp or E field were used separately.
As shown, in the case of electrolysis and photocatalysis (UV+E), the K for MB is 4 times and 8 times higher than in the case of electrolysis (E) and photocatalysis (UV) processes used separately. However, K constant for GV is 2 times and 5 times higher than the E and UV, respectively.
Moreover, K of BG is increased to 3 times and 15 times of (UV+ E) processes in compare to processes UV and E. And for the MO, the K is 2 times and 7 times higher, respectively. Furthermore, K for OS is 6 times and 5 times higher.

Our results clearly show that the values of K constant for the UV+E case are much higher than for the E and UV cases, separately. It should be mentioned that this increase for different dyes. More details can be found in appendixA.1.2.

Table 3.6: Results calculated of the photocatalytic constant K(h^{-1}) of different dyes. There are Methanol Blue, Gentian Violet , Brilliant Green , Methyl Orange and Eosin, respectively with TiO_2 thin film under different effects.
There are:K_{NoTiO_2+UV} is photocatalytic constant of dyed without thin film, K_{UV} is photocatalytic constant under UV illumination, K_E is photocatalytic constant in the presence of electric field E and K_{UV+E} is photocatalytic constant with using UV illumination with electric field simultaneously, respectively in the same conditions.

Dyes	K_{NoTiO_2+UV}	K_{UV}	K_E	K_{UV+E}
Methanol Blue	0.001±0.004	0.25±0.02	0.60±0.04	2.04±0.13
Gentian Violet	0.05±0.01	0.09±0.01	0.22±0.003	0.46±0.03
Brilliant Green	0.12±0.02	0.16±0.02	0.99±0.04	2.45±0.14
Methyl Orange	0.12±0.003	0.162±0.01	0.68±0.03	1.13±0.05
Eosin	0.03±0.002	0.079±0.01	0.061±0.002	0.38±0.02

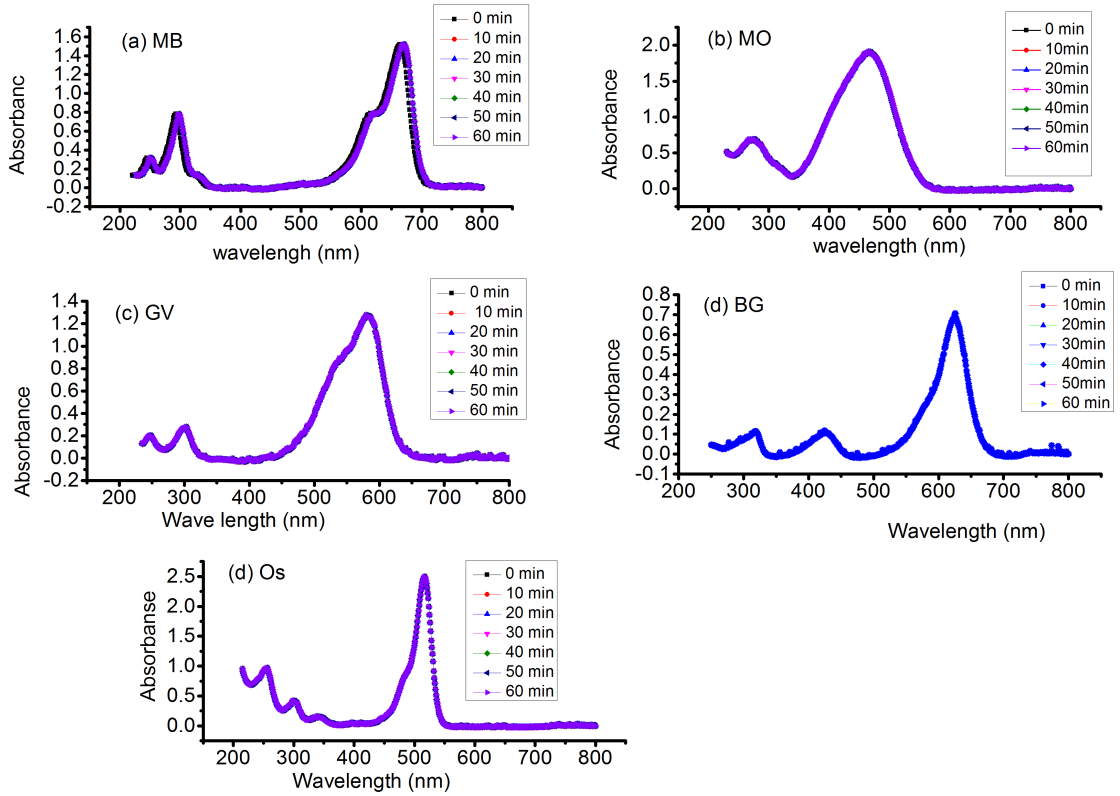

Figure 3.11: UV-Vis absorption spectra of diffident dyes under darkness without thin film at room temperature during 1 h in the range of 200 nm to 800 nm.

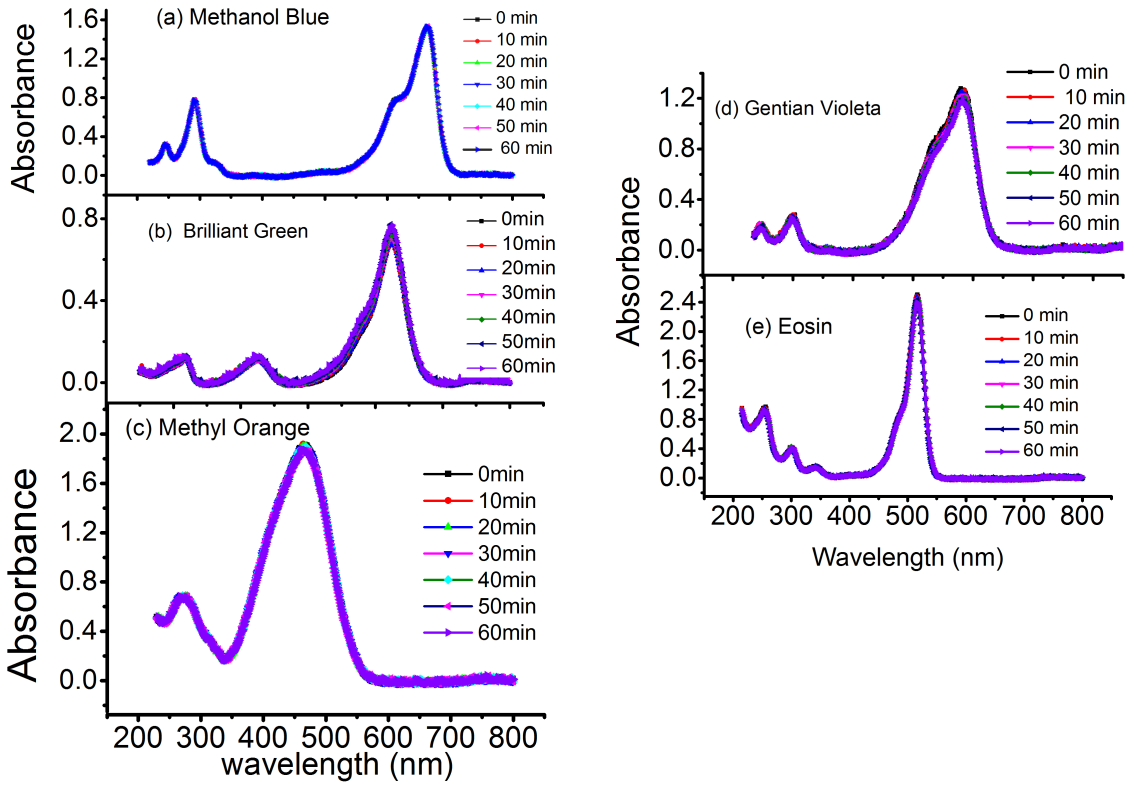

Figure 3.12: UV-Vis absorption spectra of Methanol Blue, Brillian Green , Methyl Orange, Gentian Violet and Eosin, respectively under UV illumination without TiO_2 thin film at room temperature during 1 h in the range of 200 nm to 850 nm.

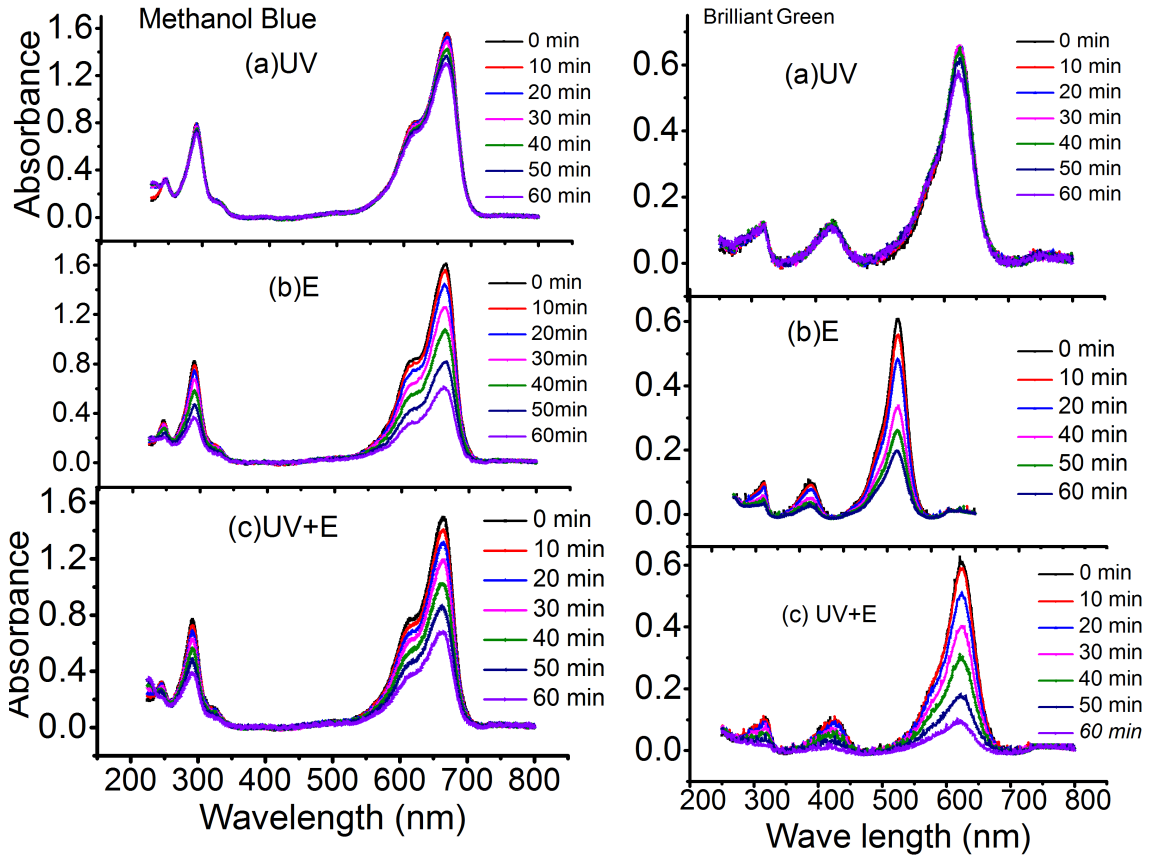

Figure 3.13: Absorption spectra of Methanol Blue and Brilliant Green with TiO_2 thin film under the different effects. There are UV illumination, the electrical field at 15V and UV illumination with electric field simultaneously at same conditions during 1 h.

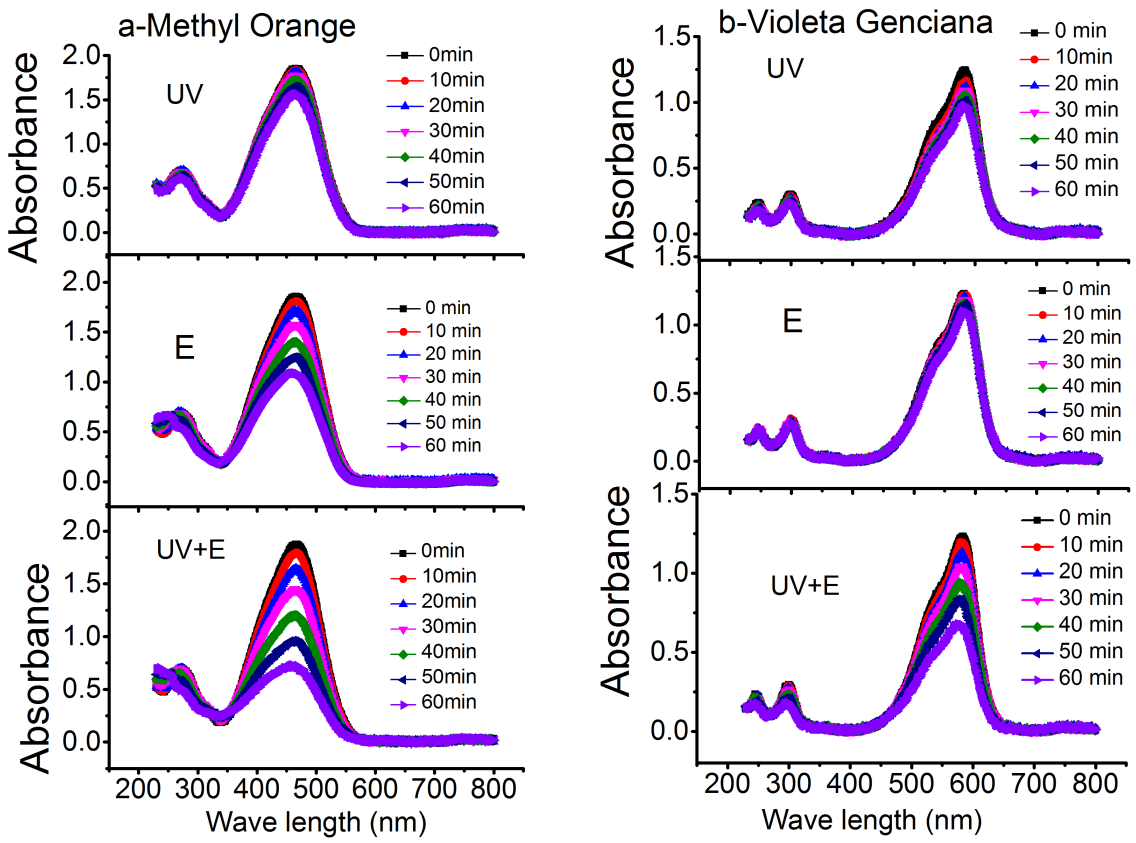

Figure 3.14: Absorption spectra of Methyl Orange and Gentian Violet with TiO_2 thin film under the different effects. There are UV illumination, applied electric field at 15V and UV illumination with electric field simultaneously at same conditions during 1h.

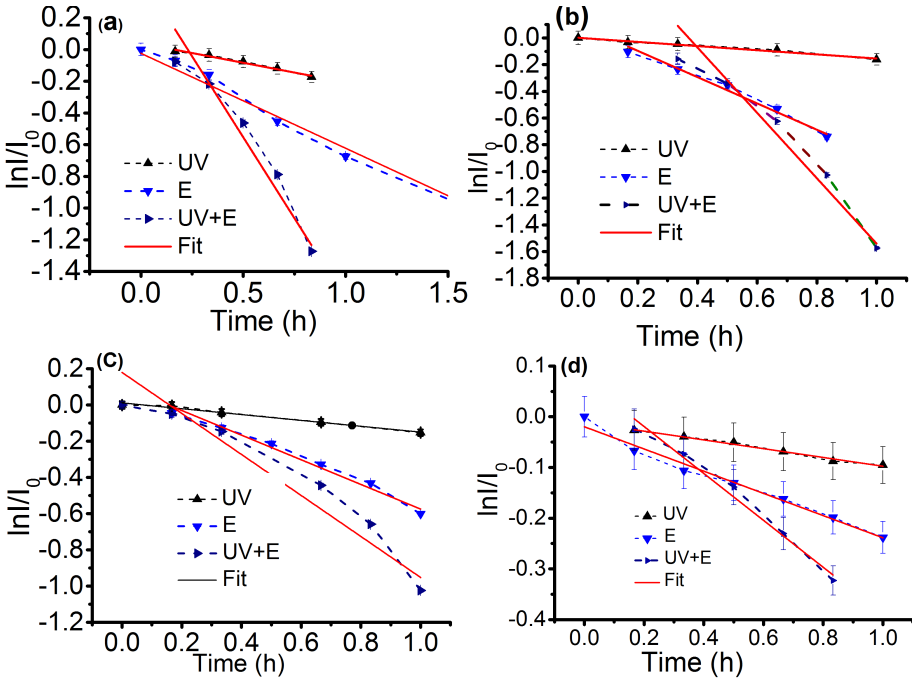

Figure 3.15: The photocatalytic constant of TiO_2 thin film under UV illumination(UV), electrical(E) and UV illumination with electrical field simultaneously(UV+E) at room temperature in the presence of Methanol Blue, Brilliant Green, Methyl Orange and Gentian Violet in a, b, c and d, respectively. Plot $\ln\frac{I}{I_0}$ as a function of radiation time to calculate K constant for different these dyes.

Chapter 4

Discussion

As it was already shown, the photocatalytic process is a many steps process. That includes light absorption, e-h excitation and recombination and adsorption of organic molecules on the photocatalyst surface. These molecules interact with excited electrons and holes which leads to further reactions steps of decomposition of these organic fragments.
In this part we study the influence of the surface area and porosity of nanopowders prepared using different chemical procedures on photocatalytic activity. The spectral dependence of photocatalytic constant and the influence of electrical field on photocatalytic activity of TiO_2 thin films are also investigated.
The photocatalytic activity studied here for different TiO_2 systems and analyzed in order to clarify the influence of different material parameters such as effective surface area, porosity, presence of dopants and external factors like electric field.

According to our knowledge, there is no study so far in literature highlighting the photocatalytic activity of TiO_2 p-type with applied electric field for a decomposition of different industrial dyes. These dyes covered by this chapter include Methanol Blue (MB), Gentian violet (GV), Brilliant Green (BG), Methyl Orange (MO) and Eosin (EO).

Our discussion here will include investigating the surface area and porosity for different powders and the photocatalytic activity of different dyes with different effects.

4.1 Surface area and porosity

The results of surface area and pore volume of TiO_2 nanopowder are listed in table 3.2. The structures studied here include the pure P25 Degussa and sol-gel nanopowders, as well as, P25 nanopowders doped with different cobalt.
The surface area of TiO_2 doped increases with increasing cobalt concentrations. However, this increase experiences an excess dopant amount deposited on the TiO_2 surface which in turn minimize the surface area [119].
The large surface area and wide pore size distribution may be enhanced the photocatalytic activity. The wide pores lead to ease diffusion of pollutant molecules on the catalyst powders [7].
In contrast, sol-gel powders have the smallest surface area and pores volume which results in a stronger particles aggregation.

Our analysis of the surface area of Co-doped TiO_2 powders shows that, the surface area does not change significantly with the concentrations.
Moreover, the TiO_2 phases show a clear independence on the Co concentrations within the temperature regimes used for the samples fabrication.

4.2 Analysis of energy gap

The energy gap values of different powders are investigated and listed in table 3.3. These values are plotted in figure 4.1. As shown there, the energy gap decreases with increasing the Co concentration compared to pure P25 Degussa [8, 113].
Basically, the addition of dopant creates an impurity level or most probably the formation of dopant electronic states within the TiO_2 energy gap structure.
In the current situation, the intermediate electronic states are mainly originated from Co^{+2} 3d states because of oxidation states in Co^{+2} contain no electrons in 3d orbitals. This means Co 3d states can overlap with the oxygen (O) 2p Ti near the valence band.

From our results, we can expect a decrease in energy gap with increasing the dopant concentration. This demonstrates that the addition of dopants introduces impurity levels which in turn changes the energy gap structure of the pure TiO_2. The optical absorption in the UV ($\lambda = 387$ nm) is attributed to the transitions from the valence band of O 2p to Ti 3d conduction band, while the impurity states of Co 3d can be overlapped with the O 2p state near the valence band.
Therefore, the low concentration of Co creates a slight variation in the energy gap [120, 8].
Our results are very well consistent with the last study presented in[113].
It proves that an observable change was introduced in TiO_2 band edges upon doping with different concentrations of Co.
Therefore, we can conclude that Co doping in TiO_2 may produce intermediate electron states which are originated from Co 3d and states in the energy gap.
These energy gap states result in the visible light photocatalytic activity of Co doped TiO_2 powders. This is due to electronic state density in the energy gap which increases with Co concentration.
In addition, this can be attributed to the overlap of impurities energy levels with O 2p Ti levels near valence band [8].
By using UV illumination electrons can be excited from valence band of TiO_2 to level states of Co near the valence band or from excited states of Co to conduction band of TiO_2.
Our results agree very well with those of reference [8], the density functional theory is used to calculate Co 3d state that is partially overlapped with O 2p states near the valence band. At lower concentrations of Co a slight variation of energy gap due to exchange interactions between s-d and p-d states causes an upward shift of valence band edge. This indicates that Co impurities have been successfully incorporated into TiO_2 crystal lattice [121].

On other hand, the results of the energy gap for sol-gel samples are shown in figure 4.1 (b). As shown here, the energy gaps of S1 and S2 powders slightly increases comparing to P25 Degussa nanopowders.
On the other hand, the energy gap of S4 has an opposite behavior. This can be attributed to a higher anatase (58%) existing in S2 causing a shift of absorption spectrum towards shorter wavelengths.

On the other side, an increase in the rutile percentage will shift the absorption spectrum towards longer wavelengths [7].
The crystallite size plays a role in the energy gap variation of the powder.
Our results showed that energy gap of the S1 and S2 increases with decreasing crystallite size in these powders [122, 2, 123, 124].
However, the energy gap decreases with increasing crystallite size for S4 indicating red of the absorption spectrum [125]. This phenomenon in semiconductor nanomaterials is known as quantum size effect[10].

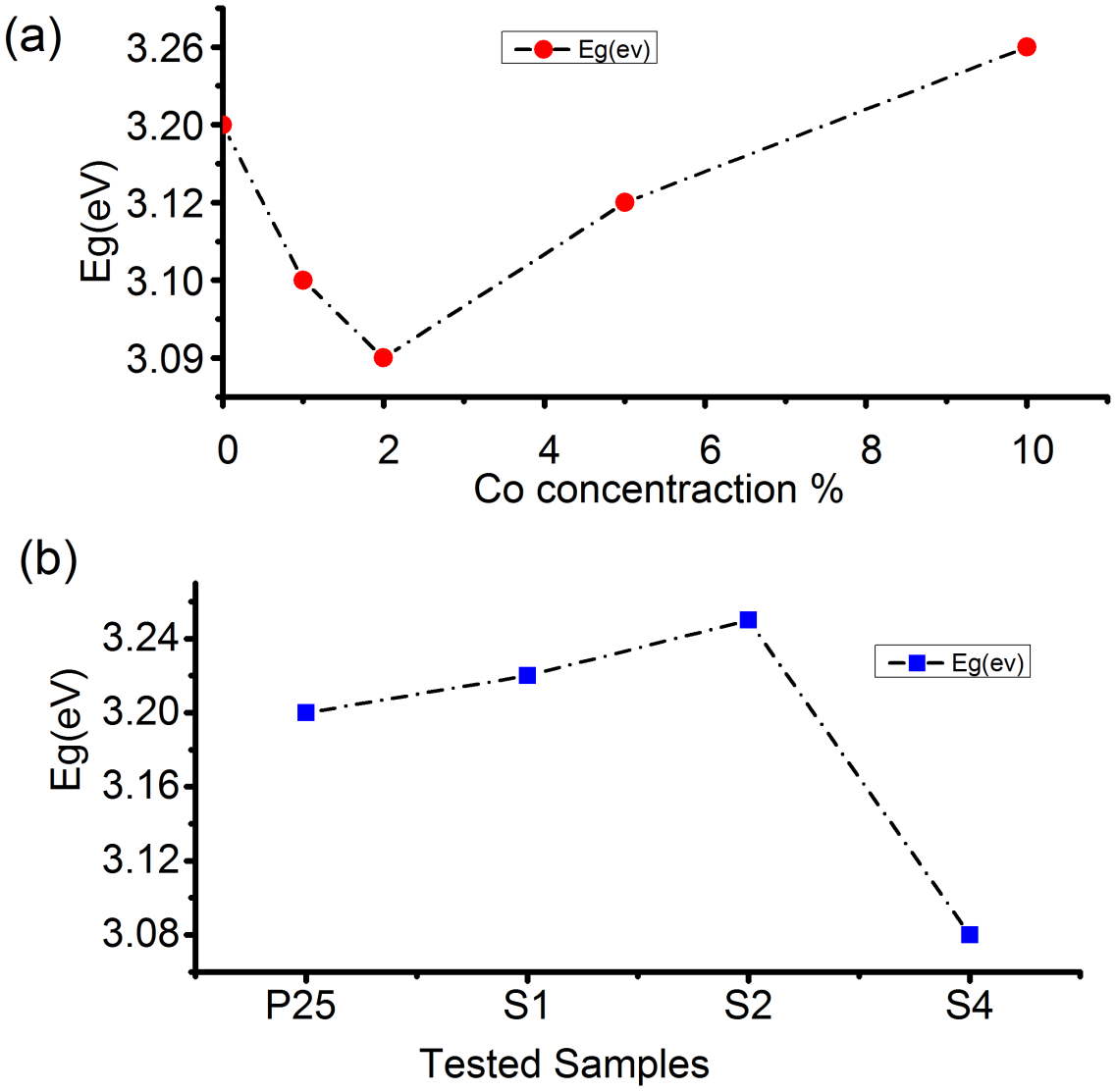

Figure 4.1: (a) The optical energy gap(E_g with different Co concentrations of (x= 1, 2, 5 and 10). (b) E_g of the pure P25 powderand also samples S1, S2 and S4 fabricated the sol-gel method

4.3 The photocatalytic activity of TiO_2 nanopowders with using mercury lamp

The results of the photocatalytic activity for studied samples are listed in table 3.4 and illustrated in figure 4.2. It is clear that P25 Degussa has the highest photocatalytic constant K compared to the other powder samples.
In spite of several studies of photocatalytic activities for different materials, including P25 Degussa nanopowders, it is not clear yet why this P25 powder has one of the highest photocatalytic activity constant. There are some hypotheses about this fact, for example it can be due to positive interaction between anatase and rutile particles in this powder. Another reason is the special contact between anatase and rutile phases. This maybe enough to enhance the separation of electron and holes carries and result in increasing photocatalytic efficiency of P25 Degussa[126, 127, 128].

On the other hand, the samples of P25:x%Co doped with different concentrations of Co(x= 1, 2, 5 and 10) exhibited significantly lower photocatalytic activity than the commercially P25 Degussa.
More specifically, the photocatalytic activity for P 25 doped catalysts decreases with increasing Co concentrations (1%, 2%, 5% and 10%).
This demonstrates that a high concentrations of Co ions act as e-h recombination centers leading to decrease in the photocatalytic efficiency[8].
This means the optimal concentration of doping ions should make the thickness of the space charger layer substantially equal to the light penetration depth is as demonstrated in reference[9].
The extremely high concentration of doping ions leads to narrowing the space charge layer and the light penetration depth exceeds the space charge layer thickness. Therefore, e-h pairs recombination become easier and hence further addition of cobalt lead to a progressive photocatalytic activity reduction.
In addition, the photocatalytic constant of P25 doped catalysts decrease with increased doping concentration because the excess doping ions occupy the grain boundaries as well as a deposit on the TiO_2 surface of the catalyst preventing the particles. This causes an increase in the recombination rate since the distance between the trapping sites decrease[7].
However, P25:5%Co has the highest K compared to other doped samples. That is maybe attributed to the slight improvement of the electron structure which is associated with an improvement in the visible absorption.

In addition, figure 4.2 shows the results of photocatalytic activity studies for the sol-gel powders presented in section 3.1.4.1 with different surface areas.
This results illustrate K constant decreases with increasing surface area. The large surface area is usually associated with large crystal defects which consequently favors e-h recombination and leads to reduce photocatalytic activity[27, 10].

Furthermore, the crystallite size plays a role in the photocatalytic efficiency. This K constant is lower for the powder that has the small crystallite size than the other powders. This is due to quantum size which influences the photocatalytic degradation[10].

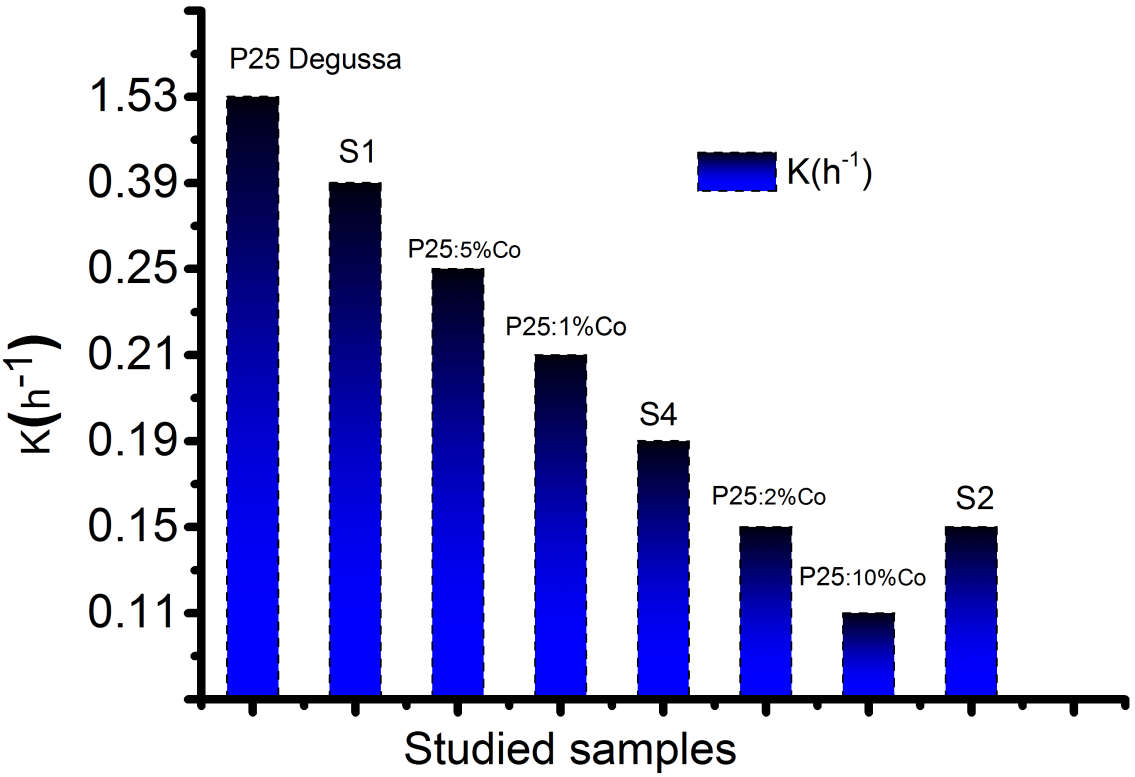

Figure 4.2: The photocatalytic constants K of the studied samples under UV illumination.

4.3.1 Spectral properties of the photocatalytic constant

The results of the photocatalytic degradation of studied samples are illustrated in figures 3.8 and 3.9. The photocatalytic degradation is low and nearly constant for all samples.
Furthermore, the photocatalytic degradation of P25 Degussa is faster than the other samples under the low wavelengths. This indicated that P25 powder has the best photocatalytic performance. However, the photocatalytic degradation is low and nearly constant at high wavelengths. Moreover, the K constant as a function of different wavelengths is shown in figure 4.3.
At different wavelengths, K constant of sol-gel samples especially S1 and S2 increases with 365 nm and 405 nm, while K is constant at higher wavelengths. However, S4 possesses the same behavior of P25 Degussa.

This can be attributed to the short wavelengths have enough energy to excite an electron from the valence band to the conduction band of TiO_2.
So, the K constant is very strong in TiO_2 powders at short wavelengths 365 nm and 405 nm. However, this K constant is steady at high wavelength due to the fact the energy is not sufficient in this case.
In contrast, the photocatalytic constant increases at low wavelengths and it becomes more steady in P25:x%Co doped with different concentrations of Co (x= 1, 2, 5 and 10) at higher wavelengths. An exception, P25:10% Co shows the same behavior as pure P25. This can be explained by the electron has a sufficient energy to transport from the TiO_2 valence band to the mid-level near the valence band at low wavelength.

All wavelengths have the energy in the range of the TiO_2 energy gap.
For all calculations and analysis, the K constant is normalized by the real incident light intensity.
The normalization is done by using the equations 4.1 and 4.2, respectively.

$$K_{Normalized} = \frac{K}{I_{Real}} \tag{4.1}$$

where K is photocatalytic constant for studied samples under different wavelengths and I_{Real} is the absorption of the wavelength. It is calculated from the following equation:

$$I_{Real} = I \times T_{Filter} \tag{4.2}$$

where I is the integrated area of the wavelength peak and T_{Filter} transition percentage of the filters.

The normalized values are listed in table 4.1. This table shows the photocatalytic for the studied samples.
P25 Degussa has a higher K constant at low wavelengths near the valence band, however, the K is decreased at higher wavelengths. This is due to the excited electron can easily move from the valence band to mid-level near the valence band.
The normalized values of K constant listed in table 4.1 correspond to the energy levels inside the energy gap. It should be noted that, these levels are not native energy levels created by defects of crystal structure because of impurities or crystal distortions on TiO_2 surface nanopowders. These levels are only corresponding to spectral energies emitted by high-pressure mercury lamp. These visible lines are cut out by the optical filter.
Photocatalytic constants K may not be in exact correspondence to resonance constant, when photons energy exactly equal to the difference between impurity energy level and energy of the conduction band.
However, this experiment clearly shows the presence of electronic levels inside the energy gap and the possibility to use visible part of the light spectrum for photocatalytic decomposition of pollutants by TiO_2 nanopowders in water.

More detailed analysis of the data in table 4.1 shows that similar behavior is observed for all pure powders. There are P25 Degussa, S1, S2 and S3, respectively.

For P25:x%Co with concentrations 2 and 5, a higher value of $K_{Normalized}$ is at 405 nm in compare to 365 nm. It can be concluded also that P25:5% Co is very similar to P25 Degussa.
Moreover, the $K_{Normalized}$ values decrease at 436 nm and 546 nm for all samples. However, all samples have a higher $K_{Normalized}$ at 690 nm than the others 436 nm and 546 nm.
For all samples the lowest $K_{Normalized}$ was observed at 546 nm. It should be also emphasized that for the TiO_2 thin films the experiment with incident light (created by laser with adjustable wavelength) of energy a little bit lower than energy gap shows k = 0. This fact can be attributed to absence the additional energy levels inside the energy energy gap due to more perfect crystal structure of thin films.

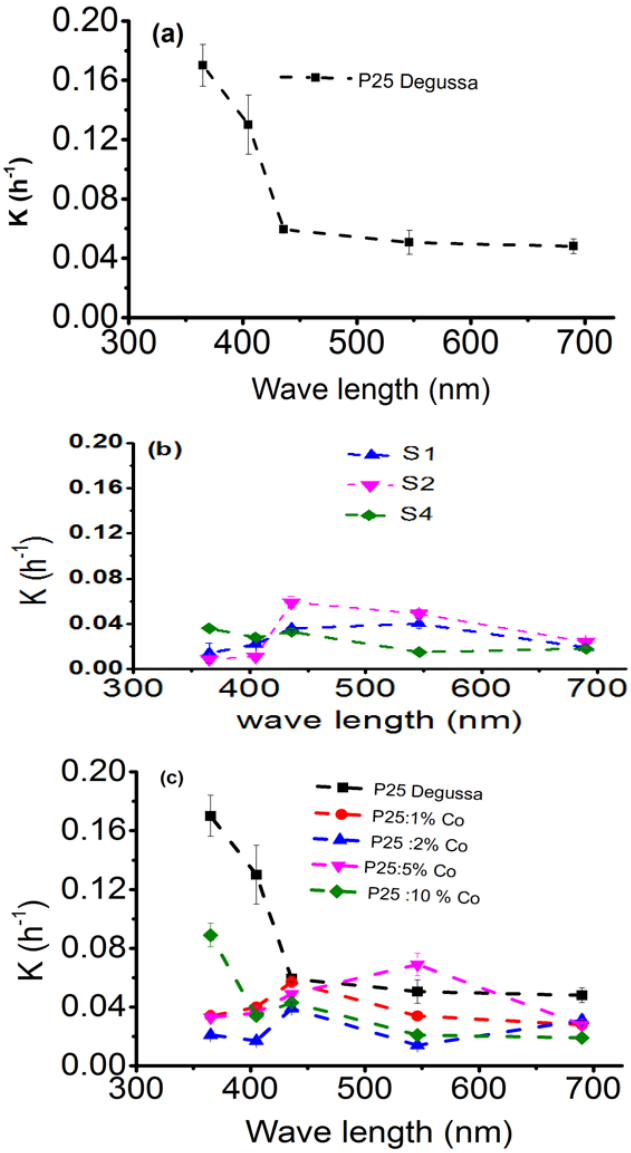

Figure 4.3: Photocatalytic constant K as a function of different wavelengths of (a) P25 Degussa, (b) sol-gel powders and P25:x%Co doped with different concentrations of cobalt (x= 1, 2, 5 and 10), respectively at room temperature in the same conditions.

Table 4.1: The results normalization of the photocatalytic constant K$\times 10^7$ for studied samples at different wavelengths.

Wavelength	365 nm	405 nm	436 nm	546 nm	690 nm
P25 Degussa	885	250	12.1	2.97	420
P25:1%Co	117	76.8	12.1	1.99	245
P25:2%Co	110	327	8.31	0.83	271
P25:5%Co	175	683	104	4.05	245
P25:10%Co	462	65	9.1	1.2	17
S1	72.9	42.3	7.67	2.35	16.6
S2	45.8	21.1	12.6	2.87	21.01
S4	188	53.8	7.03	0.88	15.7

4.4 Photocatalytic decomposition of different dyes

Dyestuffs represent a class of organic pollutants that absorb visible light.
Electron transfer processes take place between dyes and semiconductors, especially TiO_2 have been studied[129, 130]. When incident light have energy higher than or equal to the energy gap. The electron excites from the VB to CB bands.
As it was already described, this transport occurs in three steps as follows:
First, TiO_2 photocatalyst absorbs energy and generates photoexcited e-h pairs in the bulk. Then, the photoexcited carries are separated and migrate to the surface without recombination.
Finally, the adsorbed species are reduced and oxidized by photogenerated electrons and holes to produce H_2 or O_2.
In the system of the photoelectrochemical cell (PEC) (section 2.3.3 and figure 2.6. The dyes are exposed to UV illumination excitation as well as the TiO_2 surface thin film. The dye injects electrons to the TiO_2 surface and it converts to cationic radicals dye*.
In this case, the photoinduced electrons react with the dioxygen adsorbed on the TiO_2 surface and generate a series of active species such as $O_2^{-\cdot}$, H_2O_2 and $OH^{\cdot}$, as depicted in figure 4.4 a and b.

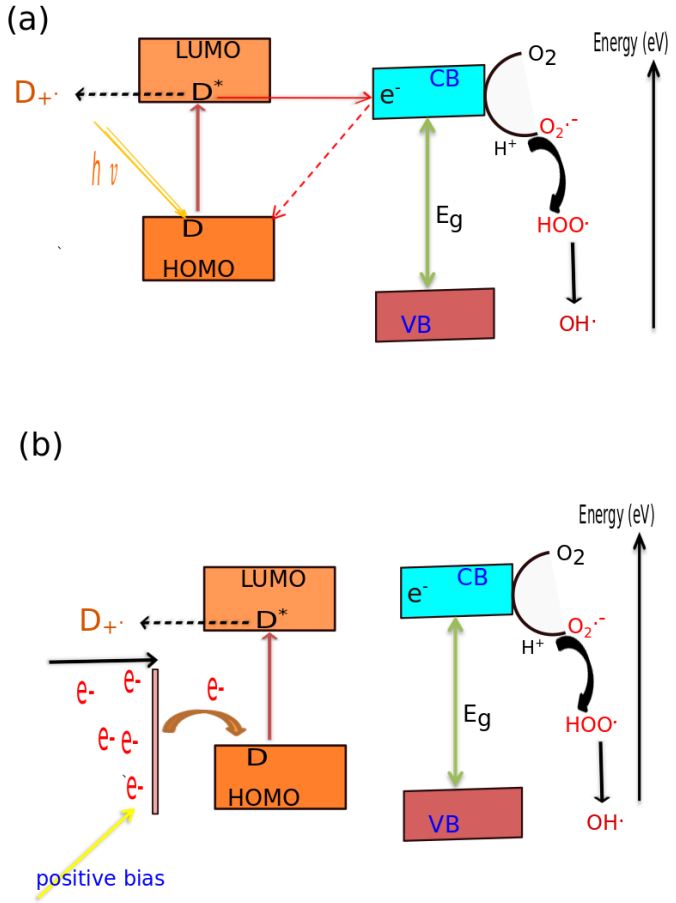

Figure 4.4: Schematic diagram illustrating the photocatalytic of dyes (a) and TiO_2 p-type semiconductor thin film with dyes using UV illumination(b).

The electron transfers very fast from the TiO_2 surface to the oxidized dyes. This is due to the reduction in the oxidized dye by Ti [131].
The PEC cell includes TiO_2 p-type thin film which is employed as a photo-anode or (photoelectrode). Gold metal wire was used as a cathode. Both the cathode and anode were connected to the external circuit to create e-h pairs in the dyes electrolyte.
This configuration is illustrated in figure 2.6. This configuration of PEC cell permits different kind of experiments in order to emphasize the main processes that occur in PEC cell during dyes decomposition.
Firstly, in the absence of thin film and without any electrical field the direct photolysis under UV irradiation can be studied and respective K constants of decomposition can be established.
Secondly, in presence of thin film without electrical field photocatalytic, decomposition can be studied under UV irradiation.
Thirdly, in absence of UV light but presence of electric field, direct electrolysis is the main process.
Finally, all processes can be studied at the same time in the presence of all factors, namely, in presence of thin film, electric field and UV irradiation.

When a positive bias is applied between electrodes, it causes electrolysis in parallel with photocatalysis in water.

As it can be seen from table 3.6 in section 3.2.2 and figure 4.5, dyes degradation processes occur at significantly higher speed that reflects in higher degradation constants.

In this case, a positive bias causes migration of the electron(e) to catalysis surface while the holes(h^+) go through the bulk solution.
In this process, the dye accepts an electron from the TiO_2 surface. Then, the electron excites dyes molecule and converts it into a cationic dye.
After that, the electrons are transferred from the excited dye to TiO_2 conduction band.

All the results of UV-Visible absorption of studied dyes under UV illumination without thin film are shown in figure 3.12.
In the system of MB and EO no degradation was observed. However, the absorption spectra of the other dyes GV, BG and MO slightly decreased.
This indicates that, the oxygen pump into the solution causes dye excitation and enhances their photodegradation. This degradation increases in presence of the H^+ and OH^- radicals.
Besides, an excited molecule dye is considered as an electron donor (for example O_2) to form dye cations which are decomposed subsequently by a superoxide radical anion $O_2^{-\cdot}$ or by dissolved (O_2)[132].

In the system of TiO_2 thin film /dyes (in the presence of TiO_2 thin film photocatalyst), the photo degradation is detected.
This is indicating that dyes interact with active radicals which is created on the TiO_2 surface in the result of e-h interaction with H_2O and consequent interaction between these dyes and active radicals.

Upon UV illumination, the intensity of absorption spectra slightly decreases with increasing radiation time without wavelength shift of the band.
This is because photo-degradation processes take place in these experiments, as it illustrated in figures 3.13 and 3.14.

All the results of the photocatalytic K constant of studied dyes are listed in table 3.6. All the results show that TiO_2 mediated dyes photodegradation process play an important role when compared to direct photolysis because the K constant in the system of TiO_2 thin film/dyes is much higher than the K constant without thin film.
For example, the photocatalytic constant of the TiO_2/MB»MB, TiO_2/GV> GV, TiO_2/BG> BG, TiO_2/MO> MO and TiO_2/EO> EO.
This is due to the e-h transfer and interaction with H_2O at the photocatalyst surface and consequent dyes interaction with these active species.
This transmission plays an important role in the dyes photo degradation.
It can be also indicated by the oxidation potentials of excited dyes varies from -0.33

V for Methanol Blue and 1.15 V for Eosin, respectively[133].
Moreover, Brilliant Green and Methyl Orange have 0.3 V and -1.16 V for excited singlet states of vs NHE and PH=7, respectively[134, 135] and that of the TiO_2 conduction band is -0.52 V[136].

From our results, the electron transfer that occurs from the GB and thin film is more effective than the electron transfer from other dyes. That is consistent with the results on degradation constant of GB which is higher than the other dyes [137] except that of MB which has a higher photocatalytic constant.

Furthermore, upon the applied electric field, the degradation processes of all dyes are very effective because the concentration of the dyes decreasing rapidly. This degradation is higher than the degradation when using UV illumination alone. The photocatalytic results indicated that all dyes with catalysis thin film by applying the electric field showed higher photocatalytic constant than that with UV illumination alone. The highest photocatalytic activity is obtained when the UV illumination and electrical field are applied simultaneously.
Compared to the other dyes, the BG is the highest K constant which is attributed to BG has the highest oxidation state.

All the results of the photocatalytic constants of all dyes with thin film are listed in table 3.6.
From this table, it is clearly seen that the K constant depends on the UV illumination and electric field.
As found here, K constant increases with applied UV illumination and electric field simultaneously.
This is attributed to the increase in e-h carriers which participate in the photocatalytic reaction.

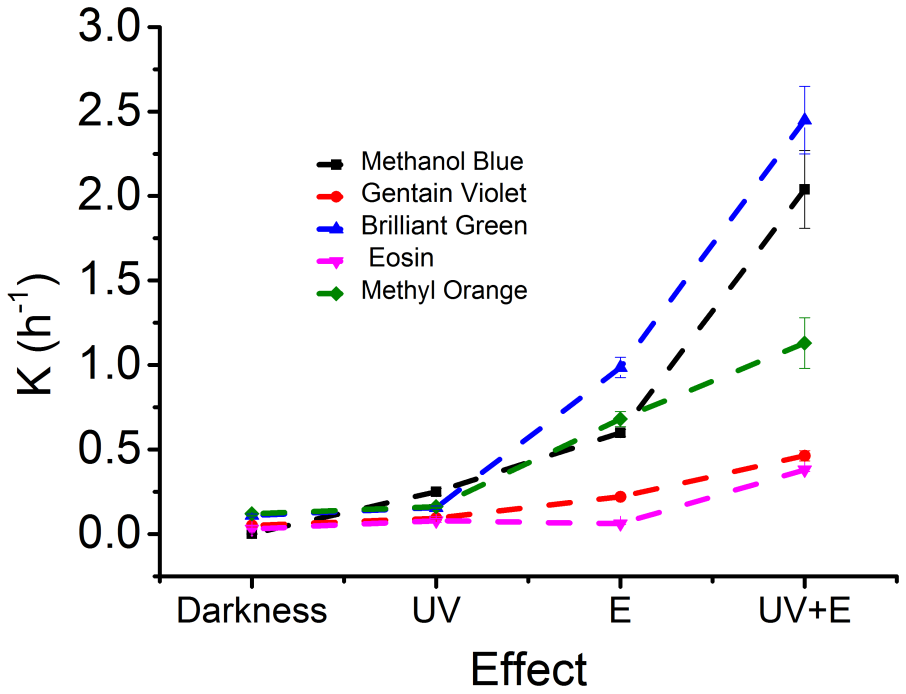

Figure 4.5: This curve summarizes the relationship between the photocatalytic constant of TiO_2 thin film using different dyes as electrolytes under darkness, UV illumination (UV), applied electric field (E) and UV illumination with electric field (UV+E) simultaneously, respectively in the same conditions.

This study illustrates the significant dependence of the photocatalytic activity and photocatalytic constant on the electric field.
The electric field separates the e-h pairs, as a consequence, the lifetime of the single carriers increases. However, the photocatalytic constant is lower when using UV illumination because of the e-h pairs recombination becomes very often.
This is shown in figure 4.5 which indicates a higher K_{UV+E} than K_{UV} and K_E.
As a consequence, the better performance found when the UV illumination and electric field are applied simultaneously. This can be attributed to produce e-h pairs and then separate them during applied two effects simultaneously.
Furthermore, the electric field has a stronger photo absorption than UV illumination. As a result, more photogenerated carriers will lead to higher photocatalytic activity.

The recent study shows that the photocatalytic constant dependent not only on the characteristics of dyes, but also it can be significantly influenced by the TiO_2 features and also the applied electrical field.

It should be also noted that in according with our findings some kind of synergetic effect can be revealed. Namely, photocatalytic constant in presence of UV irradiation and electric field(E) simultaneously is greater than the sum of the photocatalytic constants for UV and applied electric field separately, according to this relation $K_{UV+E} > K_{UV}+K_E$.

We assume that, the electric potential across the TiO_2 surface and H_2O attached to the oxide surface result in e-h pairs separation.
In this case lifetime of e-h pairs can be significantly increased and recombination will be suppressed.

Chapter 5

Summary and Conclusion

The main aim of this work was to investigate the spectral dependence of the photocatalytic constant of several titanium dioxide systems.

Series of TiO_2 powders were synthesized by sol-gel method by varying process parameters. These parameters represent changes in the process of adding of H_2O and HCl acid during the sample preparation experiments.
The process of the powder sample preparation also includes an increase in the fabrication temperature from room temperature for the samples S1 and S2 to 40°C for the sample S4.
This process changed particle size, surface area and polymorph structure which has been demonstrated by direct determination of these parameters affecting the photocatalytic activity of TiO_2.

On the other hand, the effects of dopants on the electronic states and the photocatalytic constant were studied by employing P25 Degussa, doped with different concentrations of Co.
The XRD patterns of P25:x%Co revealed the formation of the anatase and rutile phases without any impurity phases of Co within the sensitivity of XRD.
The content of the anatase phase increases when th doping concentration of Co increased.
Moreover, the surface area of P25 Degussa doped with different concentrations of Co showed no specific changes.

On the other hand, the energy gap reduction for doped samples indicates that Co has been successfully incorporated into the TiO_2 crystal lattice.
From the results shown above, we can conclude that Co doping in P25 Degussa causes no significant change in the band edge. However, it may introduce electronic states near the valence band edge in the electronic structure of TiO_2.

The results showed that P25 Degussa has the highest photocatalytic constant compared to 25 doped with cobalt (Co) and pure sol-gel TiO_2 powders.
This is attributed to the special interaction between the anatase and rutile phases under UV illumination.

As it follows from Figure4.2 for P25 Degussa powders, the photocatalytic constant is 1.53 h^{-1}. However, it is 0.21 h^{-1}, 0.15 h^{-1}, 0.25 h^{-1} and 0.11 h^{-1} for P25:x%Co with different concentrations of Co (x= 1, 2, 5 and 10), respectively.
The obtained values of the photocatalytic constant of the sol-gel powders were 0.39 h^{-1}, 0.15 h^{-1} and 0.19 h^{-1} for the samples S1, S2 and S4, respectively.
These samples have different surface areas which are 6.4m^2g^{-1}, 73.5 m^2g^{-1} and 8.6 m^2g^{-1} for S1, S2 and S4 compared to the one of P25 Degussa which is 57 m^2g^{-1}.
Also, these samples have different crystallite sizes which were 24.4 nm, 10.75 nm and 33.98 nm for S1, S2 and S4 compared to the one of 25.6 nm of P25 Degussa.
The efficiency of the photocatalytic activity is mainly dependent on the crystalline quality, the surface area and crystallite size of the powdered samples prepared by the sol-gel method.

The photocatalytic constant decreases in these powders compared to P25 Degussa, probably due to minor crystalline quality (P25 Degussa powders were prepared at significantly higher temperatures) and coexisting anatase and rutile crystal modifications.
This conclusion can be made because both surface area and crystallite size of sol-gel powders and P25 Degussa are of the same order.
Furthermore, the sample S1 powder showed the highest photocatalytic constant compared to the series S2 and S4 powders, respectively.

On the other hand, the spectral dependence of the photocatalytic constant was studied for TiO_2 nanopowders including P25 Degussa, sol-gel samples and P25 Degussa doped with different concentrations of Cobalt.

As it follows from Table 4.1 for all spectral lines presented in the light of mercury lamp some photocatalytic activity in nanopowders was observed.
Detailed analysis shows the presence of electronic states inside the main energy gap between valence and conduction bands of TiO_2. These states can produce electron-hole pairs under radiation with wave lengths higher than that of the corresponding energy gap.
It can be seen from Table 4.1 that for the wavelength λ=365 nm the normalized photocatalytic constant K is higher for P25 Degussa (K=885) powder, but with increase of Co concentration K increased from about K= 117 to K= 462 when Co concentration changed from 1% to 10%. For λ =405 nm, for the sample P25:5%Co K is higher (K= 683) than for the P25 Degussa (K = 250). The same was observed for λ=436 nm.
For λ=546 nm all values of K are relatively low. Finally, for λ=690 nm relatively high values of K for all Co doped samples, as well as, for P25 Degussa sample are observed. This behavior of K can be interpreted in terms of the existence of additional energy levels inside the main energy gap of TiO_2 and these levels can be changed by changing the Co concentration.

Additionally, the decomposition of different dyes by TiO_2 p-type semiconductor thin film prepared by the Chemical Vapor Deposition was investigated at different experimental conditions. Different dyes were used to study the photocatalytic constant of the degradation process that occurs on the surface of TiO_2 thin films deposited on a Si p-type substrate.
These dyes are Methanol Blue(MB), Gentian Violet(GV), Brilliant Green(BG), MethylOrange (MO) and Eosin(OS).

In the absence of the TiO_2 thin film, no change in the absorption spectrum of the dyes was observed. This indicates that the TiO_2 thin film plays an important role in the dye decomposition process via the H_2O splitting on the TiO_2 surface under UV illumination.
These dyes were successfully degraded by TiO_2 thin film. The decrease of the absorption amplitude at each time can be explained by breaking down molecule bonds of the dyes.

This process is associated with an adsorption of the dye molecules on the thin film surface and, consequently, with its decomposition which causes notable changes of the solution color.
It was observed that the dye decomposition process also takes place without any UV illumination, but in the presence of an electrical field and in the presence of an electrical current provoked by this field. It means that the electrochemical process of the dye decomposition has a significant role which is comparable or even higher than photocatalysis. Respective degradation constants are listed in Table3.6.

It should be noted that simultaneous application of UV irradiation and electrical field results in an additional increase of the degradation constant K leading to $K_{UV+E} > K_{UV} + K_E$.
This acceleration is attributed to the interaction between the dyes and the TiO_2 surface.
This study sheds light on the role of the electric field that it plays on the photocatalytic activity and, consequently, on the photocatalytic constant.
This role results from its effect on the e-h pairs separation and by increasing their lifetimes. These lifetimes become even higher when using UV associated with E.

Throughout this study, the existence of the synergetic effect was confirmed. This effect can be interpreted in the framework of e-h pair separation in the electric field and, as a result, in an increase of their lifetime, even when this field was relatively small.

This synergetic effect of the electrical field and UV illumination may explain the high photocatalytic constant obtained for the Brilliant Green compared to the other dyes.

Appendix A

Appendix

A.1

Appendix A

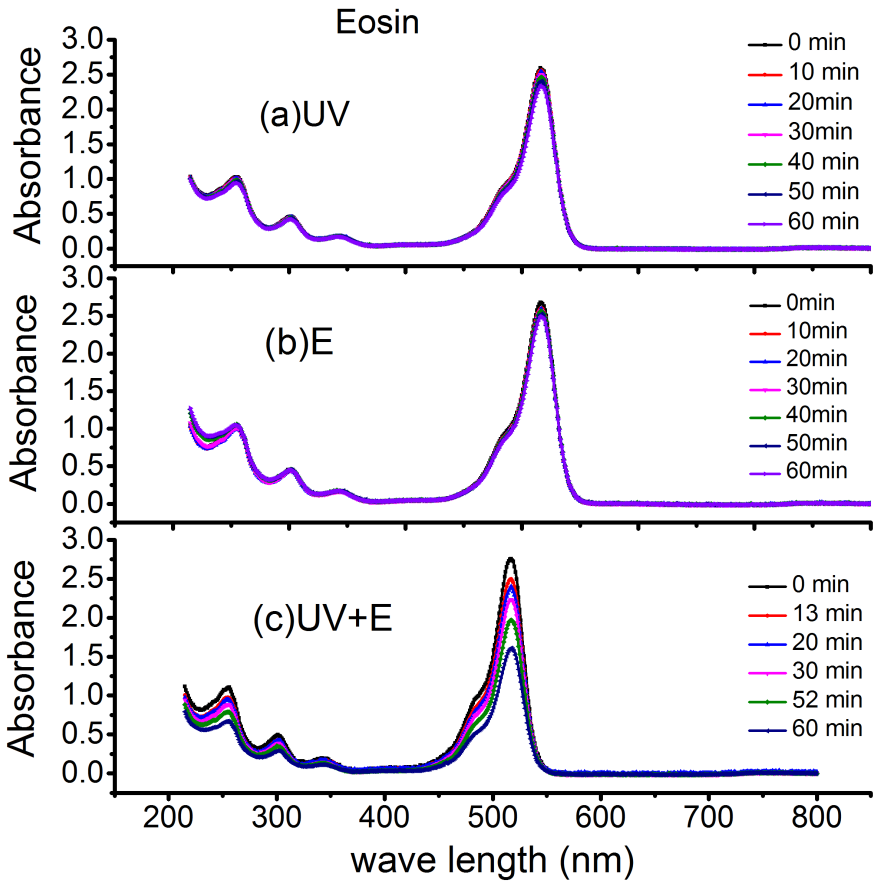

Figure A.1.1: UV-Vis absorption spectra of Eosin with TiO_2 thin film under UV illumination, the electrical field at 15V and UV illumination with electrical field illumination simultaneously, respectively at same conditions during 1h.

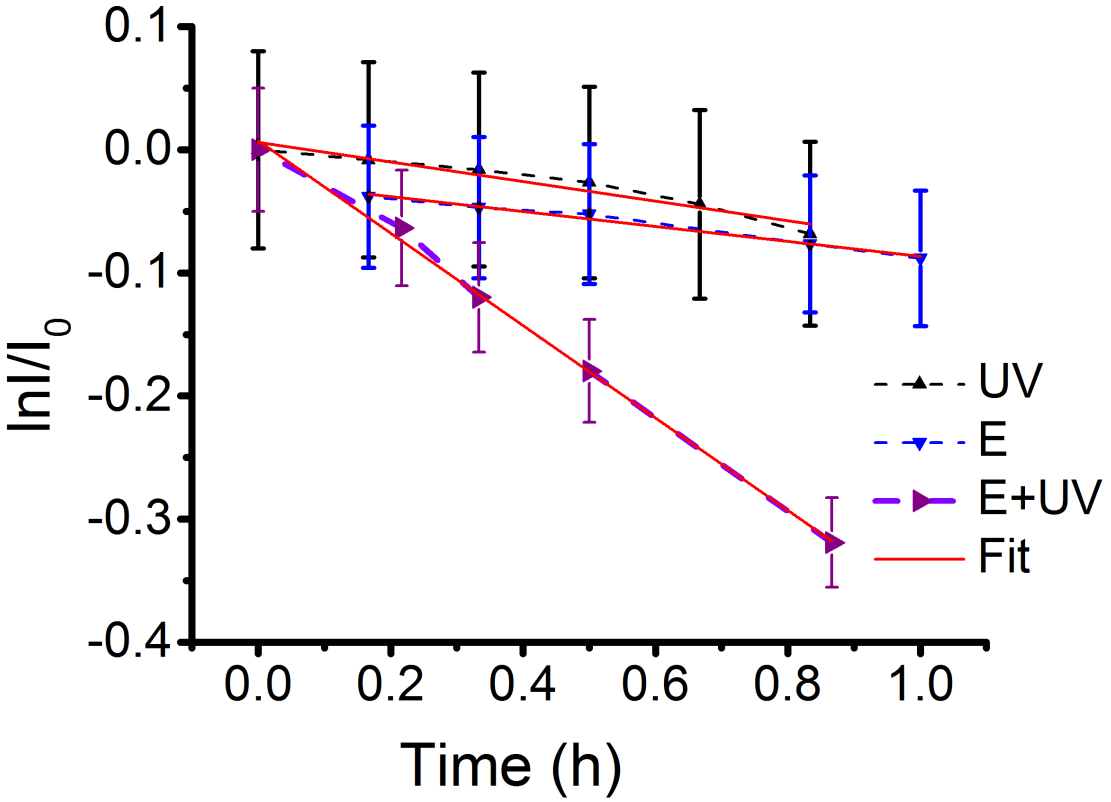

Figure A.1.2: The photocatalytic constant of TiO_2 thin film with Eosin (OS) under three effects. There are UV illumination(UV), applying electric field (E) and UV illumination with the electrical field(UV+E) simultaneously at same conditions. Plot $\ln\frac{I}{I_0}$ as a function of radiation time (h) to calculate K constant.

Bibliography

[1] Fujishima A and Honda K. "Electrochemical photolysis of Water at a Semiconductor Electrode. In Nature, 238(1972): 37-38.

[2] Gupta S M and Tripathi M."A review of TiO_2 nanoparticles."In Chinese Science Bulletin 56 (2011):1639 - 1657.

[3] Schneider J., Matsuoka M., Takeuchi M., Zhang, J., Horiuchi, Y., Anpo, M., and Bohnemann, D.W: "Understanding TiO_2 Photocatalysis: Mechanisms and Materials." In Chemical Reviews 114(2014): 9919 – 9986

[4] Cen J., Wu Q.,Liu M., Orlov A. "Developing new understanding of photoelectrochemical water splitting via in-situ techniques: A review on recent progress." In Green Energy and Environment 2 (2017): 100- 111.

[5] Bessergenev VG., Pereira RJ., Mateus MC., Khmelinskii IV., Vasconcelos DA., Nicula R., Burkel E., Do Rego AB., and Saprykin AI. "Study of Physical and Photocatalytic Properties of TiO_2 thin Films Prepared from Complex precursors by chemical vapour deposition." In Thin Solid Films, 503 (2006): 29 – 39.

[6] Asahi R., Taga Y., Mannstadt W., and Freeman A J. "Electronic and optical properties of anatase TiO_2." In Physical Review B. 61 (2000): 7459- 7465.

[7] Khan H. and Berk D. "Characterization and mechanistic study of MO^{+6} and $V^{+}5$ codoped TiO_2 as a photocatalyst." In Journal of Photochemistry and Photobiology A: Chemistry 294 (2014): 96-109.

[8] Jiang P., Xiang W., Kuang J., Liu W., and Cao W. "Effect of cobalt doping on the electronic, optical and photocatalytic properties of TiO_2." In Solid State Sciences 46 (2015): 27-32.

[9] Zhou W.,. Liu Q.,. Zhu Z., and Zhang J. "Preparation and properties of vanadium-doped TiO_2 photocatalysts."In Journal of Physics D: Applied Physics 43(3)(2010):035301.

[10] Gorska P., Zaleska A., Kowalska E., Klimczuk T., Sobczak JW., Skwarek E., Janusz W., and Hupka J. "TiO_2 photoactivity in Vis and UV light: the influence of calcination temperature and surface properties." In Applied Catalysis B: Environmental 84(3-4) (2008): 440-447.

[11] Linsebigler AL., Lu G., and Yates Jr J.T. "Photocatalysis on TiO_2 surfaces: principles, mechanisms, and selected results."In Chemical Reviews 95 (1995): 735-758.

[12] Gaya UI and Abdullah AH. "Heterogeneous photocatalytic degradation of organic contaminants over titanium dioxide: A review of fundamentals, progress and problems." In Journal of Photochemistry and Photobiology C: Photochemistry Reviews 9 (2008): 1-12.

[13] Mills A., Davies RH., and Worsley D ."Water purification by semiconductor photocatalysis." In Chemical Society Reviews, 22(1993): 417-425 .

[14] Qu Y. and Duan X."Challenge and perspective of heterogeneous photocatalysts." In Chemical Society Reviews 42(2013):2568-2580.

[15] Pelaez M., Nolan NT, Pillai SC., Seery MK., Falaras P., Kontos AG., Dunlop PS., Hamilton JW., Byrne JA., O'shea K., Entezari MH. "A review on the visible light active titanium dioxide photocatalysts for environmental applications." In Applied Catalysis B: Environmental.125(2012):331 - 349.

[16] Samsudin EM., Goh SN., Wu TY., Ling TT., Hamid SB., and Juan JC. "Evaluation on the Photocatalytic Degradation Activity of Reactive blue 4 using Pure Anatase Nano-TiO_2." In Sains Malaysiana 44(2015): 1011–1019.

[17] Shon H., Phuntsho S., Okour Y., Cho DL., Kim KS., Li HJ., Na S, Kim JB., Kim JH. "Visible light Responsive Titanium Dioxide (TiO_2)." In Journal of the Korean Industrial and Engineering Chemistry.19 (2008):1-16

[18] Tachikawa T., Fujitsuka M., and Majima T. "Mechanistic insight into the TiO_2 photocatalytic reactions: Design of new photocatalysts." In Journal of Physical Chemistry C.111(2007): 5259-5275.

[19] Cozzoli P D., Comparelli R., Fanizza E ., Curri M.L., and Agostiano A . "Photocatalytic activity of organic-capped anatase TiO_2 nanocrystals in homogeneous organic solutions." In Materials Science and Engineering C 23(2007):707 - 713 .

[20] Chatterjee D., and Dasgupta Sh ." Visible light induced photocatalytic degradation of organic pollutants." In Journal of Photochemistry and Photobiology C: Photochemistry Reviews : 6(2005):1389-5567.

[21] Pfaff G., P. and Reynders P . "Angle-Dependent Optical Effects Deriving from Submicron Structures of Films and Pigments." In Chemical reviews 99 (1999): 1963-1982.

[22] NN Greenwood, A Earnshaw. "Chemistry of the elements." Oxford: Butterworth-Heinemann;1997.

[23] Hoffmann MR., Martin ST., Choi W. and Bahnemann DW. "Environmental applications of semiconductor photocatalysis." In Chemical reviews 95, no. 1 (1995): 69-96.

[24] Bhatkhande D S., Pangarkar V G., and Beenackers, A A. "Photocatalytic degradation for environmental applications–a review."In Journal of Chemical Technology and Biotechnology: International Research in Process, Environmental and Clean Technology, 77(1)(2002): 102-116.

[25] Kudo A and Miseki Y. "Heterogeneous photocatalyst materials for water splitting." In Chemical Society Reviews 38.1 (2009): 253-278.

[26] Fujishima A and Zhang X."Titanium dioxide photocatalysis: present situation and future approaches". In Comptes Rendus Chimie, 9 (2006): 750 - 760

[27] Carp O. , Huisman C.L., and Reller A. "Photoinduced reactivity of titanium dioxide." In Progress in Solid State Chemistry 32 (2004) :33 - 177.

[28] Fuertes V C., Negre CF A., Oviedo M B., Bonafe F P. , Oliva F.Y., and Sanchez C.G. "A theoretical study of the optical properties of nanostructured TiO_2" In Journal of Physics: Condensed Matter. 25 (2013): 1-7.

[29] Chen X. and Mao S S. "Titanium Dioxide Nanomaterials: Synthesis, Properties, Modifications, and Applications." In Chemical reviews 107 (2007): 2891-2959.

[30] Zhang H. and Banfield J F. " New kinetic model for the nanocrystalline anatase-to-rutile transformation revealing rate dependence on number of particles." In American Mineralogist 84 (1999): 528-535.

[31] Hu Y., Tsai H.L, and Huang CL. "Effect of brookite phase on the anatase–rutile transition in titania nanoparticles." In Journal of the European Ceramic Society 23 (2003) :691 - 696.

[32] Van de Krol R. and Goossens A." Structure and properties of anatase TiO_2 thin films made by reactive electron beam evaporation."In Journal of Vacuum Science and Technology A: Vacuum, Surfaces, and Films 21 (2003): 76-83.

[33] Banerjee S., Gopal J., Muraleedharan P., Tyagi AK. and Raj B. "Physics and chemistry of photocatalytic titanium dioxide: Visualization of bactericidal activity using atomic force microscopy." In Current Science 90 (2006): 1378-1383.

[34] Park J Y., Lee C., Jung KW., and Jung D. "Structure related photocatalytic properties of TiO_2." In Bullution of the Korean Chemical Society 30 (2009):402-404.

[35] Fujishima A., Zhang X., and Tryk DA. "Titanium dioxide photocatalysis" . In Journal of Photochemistry and Photobiology C: Photochemistry Reviews. C 1 (2000): 1-21.

[36] Fujishima A., Zhang X., Tryk DA. "TiO_2 photocatalysis and related surface phenomena. In Surface Science Reports 63 (2008) 515-582.

[37] Sakai H., Baba R., Hashimoto K., Fujishima A., and Heller A. "Local detection of photoelectrochemically produced H_2O_2 with a "Wired" horseradish peroxidase microsensor."In The Journal of Physical Chemistry 99 (1995)11896-11900.

[38] Ikeda K., Sakai H., Baba R., Hashimoto K., and Fujishima A. "Photocatalytic reactions involving radical chain reactions using microelectrodes." In The Journal of Physical Chemistry B 101 (1997) 2617-2620

[39] Wang R., Hashimoto K., Fujishima A., Chikuni M., Kojima E., Kitamura A., Shimohigoshi M., and Watanabe V, "Light-induced amphiphilic surfaces." In Nature 388 (1997) 431-432.

[40] Choi W., Termin A. and Hoffmann M R."The role of metal Ion dopants in quantum-sized TiO_2: correlation between photoreactivity and charge carrier recombination dynamics." In The Journal of Physical Chemistry 98 (1994) 13669-13679.

[41] AsahiR., Morikawa T., Ohwaki T., Aoki K. and Taga Y. "Visible-light photocatalysis in nitrogen-doped titanium oxides." In Science, 293 (2001): 269-271.

[42] Naeem K. and Ouyang F., "Preparation of $Fe3^+$ doped TiO_2 nanoparticles and its photocatalytic activity under UV light." In Physica B: Condensed Matter, 405 (2010): 221-226.

[43] Colon G., Maicu M., Hidalgo M.C. and Navio JA. "Cu-doped TiO_2 systems with improved photocatalytic activity." In Applied Catalysis B: Environmental, 67 (2006): 41-51.

[44] Long R., English NJ. "Tailoring the electronic structure of TiO_2 by cation codoping from hybrid density functional theory calculations." In Physical Review B, 83 (2011): 1-5.

[45] Borgarello E., Kiwi J., Graetzel M., Pelizzetti E. and Visca M. "Visible light induced water cleavage in colloidal solutions of chromium-doped titanium dioxide particles." In Journal of the American Chemical Society, 104 (1982): 2996-3002.

[46] Iwasaki M., Hara M., Kawada H., Tada H., Ito S. "Cobalt ion-doped TiO_2 photocatalyst response to visible light." In Journal of Colloid and Interface Science, 224 (2000): 202-204.

[47] Klosek S. and Raftery D. "Visible light driven V-doped TiO_2 photocatalyst and its photooxidation of ethanol." The Journal of Physical Chemistry B, 105 (2001): 2815-2819.

[48] Zhu J., Chen F. , Zhang J., Chen H. and Anpo M. "$Fe3^+$-TiO_2 photocatalysts prepared by combining sol–gel method with hydrothermal treatment and their characterization." In Journal of Photochemistry and Photobiology A: Chemistry, 180 (2006): 196-204.

[49] Ibhadon A O. and Fitzpatrick P. "Heterogeneous photocatalysis: recent advances and applications." In Catalysts 3 (2013): 189-218.

[50] Haynes WM and Lide DR. "CRC handbook of chemistry and physics: a ready-reference book of chemical and physical data. CRC Press 2011.

[51] de Levie R. "The electrolysis of water." In Journal of Electroanalytical Chemistry 476 (1999): 92–93

[52] Berg H. "Johann Wilhelm Ritter-the founder of scientific Electrochemistry." Review of Polarography 54 (2008): 99–103.

[53] Zhang J., Zhang L., Liu H., Sun A. and Liu RS. "Electrochemical technologies for energy storage and conversion." New York: Wiley; 2012.

[54] Mavroides JG., Kafalas JA., Kolesar D F. "Photoelectrolysis of water in cells with $SrTiO_3$ anodes." In Appliy Physics 28 (1976): 241-243.

[55] Watanabe T, Fujishima A, and Honda KI. "Photoelectrochemical reactions at Sr TiO_3 single crystal electrode." In Bulletin of the Chemical Society of Japan 2 49(1976): 355-358.

[56] Liao CH., Huang CW., and Wu J. "Hydrogen Production from Semiconductor-based Photocatalysis via Water Splitting." In Catalysts 2(4) (2012) : 490-516

[57] Walter M G., Warren E L., McKone J R., Boettcher, S W., Mi Q., Santori E A.and Lewis N S. "Solar water splitting cells." In Chemical Reviews 110.11 (2010): 6446–6473.

[58] Wu J., Walukiewicz W., Yu K M., Ager Iii, J W., Haller EE., Lu H., Schaff WJ, Saito Y and Nanishi Y. "Unusual properties of the fundamental band gap of InN." In Applied Physics Letters 80 (2002): 3967-3969.

[59] Lutterotti L., Bortolotti M., Ischia G., Lonardelli I., and Wenk HR. "Rietveld texture analysis from diffraction images."In Z. Kristallogr. Suppl 26 (2007): 125-130.

[60] Lutterotti L., Matthies S., Wenk HR., Schultz AS., and Richardson Jr JW. "Combined texture and structure analysis of deformed limestone from time-of-flight neutron diffraction spectra."In Journal of Applied Physics 81 (1997): 594-600.

[61] Rietveld H. "A profile refinement method for nuclear and magnetic structures." In Journal of Applied Crystallography 2.2 (1969): 65-71.

[62] Rietveld H M. "Line profiles of neutron powder-diffraction peaks for structur refinement." In Acta Crystallographica 1 (1967): 151-152.

[63] Lutterotti L., Ceccato R., Dal Maschio R., and Pagani E. "Quantitative analysis of silicate glass in ceramic materials by the Rietveld method." In Materials Science Forum Bd. 278 Aedermannsdorf, Switzerland:Trans Tech Publications 1984-, (1998): 87-92.

[64] Lutterotti L and Scardi . "Simultaneous structure and size strain refinement by the Rietveld method." In Journal of applied Crystallography 23 (1990): 246-252.

[65] Barrett EP., Joyner LG., and Halenda PP. "The Determination of Pore Volume and Area Distributions in Porous Substances. I. Computations from Nitrogen Isotherms. " In Journal of the American Chemical Society 73 (1951): 373-380 .

[66] Sing S K. "Reporting physisorption data for gas/solid systems with special reference to the determination of surface area and porosity (Recommendations 1984)." In Pure and applied chemistry 57 (1985): 603-619.

[67] Brunauer S. "The Adsorption of Gases and Vapors." In University Press Oxford 1(1945).

[68] Brunauer S.,Emmett PH., and Teller E. "Adsorption of gases in multimolecular layers." In Journal of the American chemical society 60 (1938): 309-319.

[69] Roquerol J., RODRIGUEZ RF., and Sing KS. "Characterization of Porous Solids III."In Elsevier, Amsterdam(1994).

[70] Leofanti G., Padovan M., TozzolaG., and Venturelli B. "Surface area and pore texture of catalysts." In Catalysis Today 41 (1998): 207-219.

[71] Rouquerol J., Avnir D., Fairbridge CW., Everett DH., Haynes JM, Pernicone N, Ramsay JDF, Sing KSW., and Unger KK . "Recommendations for the characterization of porous solids (Technical Report)." In Pure and Applied Chemistry 66 (1994) : 1739-1758 .

[72] Sing K ."The use of nitrogen adsorption for the characterisation of porous materials.Colloids and Surfaces A." In Physicochemical and Engineering Aspects (2001)187-188 .

[73] Gregg SJ and Sing KS. Adsorption Surface Area and Porosity. In Academic Press, London (1982).

[74] QourzalS., Barka N., Tamimi M., Assabbane A., and Ait-Ichou Y. "Photodegradation of 2- naphthol in water by artificial light illumination using TiO_2 photocatalyst: Identification of intermediates and the reaction pathway." In Applied Catalysis A: General 334 (2008): 386-393.

[75] Bessergenev VG., Mateus MC., Vasconcelos DA., Mariano JF., Botelho do Rego AM. , Lange R., Burkel E. " TiO_2:(Fe, S) thin films prepared from complex precursors by CVD, physical chemical properties, and photocatalysis." In International Journal of Photoenergy (2012).

[76] Bessergenev VG., Mateus MC., Botelho do Rego AM., Hantusch M., Burkel E." An improvement of photocatalytic activity of TiO_2 Degussa P25 powder." In Applied Catalysis A: General 500 (2015): $40 - 50$.

[77] Park S J., Kang Y C., Park J. Y., Evans Ed. A., Ramsier R D., Chase G G. "Physical Characteristics of Titania Nanofibers Synthesized by sol-gel and Electrospinning Techniques." In Journal of Engineered Fibers and Fabrics 5 (2010).

[78] Wang Y., He Y., Lai Q., Fan M ." Review of the progress in preparing nano TiO_2: An important environmental engineering material. In Journal of environmental sciences 26(2014): 2139-2177.

[79] Henrist C., Dewalque J., Mathis F., Cloots R ." Control of the Porosity of Anatase Thin Films Prepared by EISA: Influence of Thickness and Heat Treatment. In Microporous and Mesoporous." In Materials 117 (2009): 292–296.

[80] Hernandez–Martinez AR., EstevezM., Vargas S., and Rodriguez R. "New polyurethane-anatase titania porous hybrid composite for the degradation of azo-compounds wastes. In Composites part B : In Engineering 44 (2013): 686-691.

[81] Chen Z., Zhao G., Li H., Han G., and Song B. "Effects of water amount and pH on the crystal behavior of a TiO_2 nanocrystalline derived from a sol–gel process at a low temperature." In Journal of the American Ceramic Society 92 (2009): 1024-1029.

[82] Gupta S M and Tripathi M. "A review on the synthesis of TiO_2 nanoparticles by solution route." In Central European Journal of Chemistry 10 (2012): 279-294.

[83] Schmidt H. "Chemistry of material preparation by the sol-gel process." In Journal of Non-Crystalline Solids 100 (1988): 51-64.

[84] Vorkapic D., and Matsoukas T. "Effect of temperature and alcohols in the preparation of titania nanoparticles from alkoxides." In Journal of the American Ceramic Society 81 (1998): 2815-2820.

[85] Cenovar A., Paunovic P., Grozdanov A., Makreski P., and Fidanccevska E. "Preparation of nano-crystalline TiO_2 by Sol-gel method using titanium tetraisopropoxide (TTIP) as a precursor." In Advances in Natural Science: Theory and Applications 2 (2012): 133-142.

[86] Sayilkan F., Asiltuer M., Sayilkan H., Oenal Y., Akarsu M., and Arpac E. " Characterization of TiO_2 Synthesized in Alcohol by a Sol-Gel Process: The Effects of Annealing Temperature and Acid Catalyst." In Turkish Journal of Chemistry 29 (2006): 697-706.

[87] Vinogradov A V., and Vinogradov V V.. "Low-temperature sol–gel synthesis of crystalline materials." In RSC Advances 4 (2014): 45903-45919.

[88] Brinker C J and Scherer GW. " Sol–gel science: the physics and chemistry of sol – gel processing." In Academic Press: United Kingdom, 1990.

[89] Brinker C. J and Scherer G W. " Gelation and gel structure." In Journal of Non-Crystalline Solids 70 (1985): 301-322

[90] Matsumoto Y., Murakami M., Shono T., Hasegawa T., Fukumura T., Kawasaki M., Ahmet P., Chikyow T., Koshihara SY., and Koinuma H., " RoomTemperature Ferromagnetism in transparent Transition metal-doped Titanium dioxide." In Science 291 (2001): 854 – 856.

[91] Herrmann JM."Heterogeneous photocatalysis: fundamental and applications to the removal of various types of aqueous pollutants." In Catalysis today 53 (1999): 115– 129.

[92] Chambers S A. "A potential role in spintronics." In Materials Today 4 (2002): 34 -39.

[93] Van Santen R A., Tranca I., and Hensen E J ." Theory of surface chemistry and reactivity of reducible oxides." In Catalysis Today 244 (2015): 63 - 84.

[94] Bessergenev VG., Khmelinskii IV., Pereira RJ., Krisuk VV., Turgambaeva VV., and Igumenov IK. " Preparation of TiO_2 films by CVD method and its electrical, structural and optical properties." In Vacuum 64 (2002): 275-279.

[95] Chang HT., Wu NM., and Zhu F. "A kinetic model for photocatalytic degradation of organic contaminants in a thin-film TiO_2 catalyst." In Water Research 34 (2000):407-416.

[96] Bessergenev VG., Ivanova EN., Kovalevskaya YA., Gromilov SA., Kirichenko VNand Larionov SV. " Electrical Properties of Conductive In_2S_3 and In_20_3 (S) Films Prepared from the In($S_2COC_3H_7 - i_5o$)3 Volatile Precursor." In Inorganic chemistry 6 (1996): 592-596

[97] CG Borman, RG Gordon. In Journal of the Electrochemical Society 12.(1989) : 3820-3828.

[98] Bessergenev VG. " The use of complex compounds in chemical vapour deposition." In Journal of Physics: Condensed Matter 16 (2004):531-552.

[99] Bessergenev VG., Mateus MC., Morgado IM., Hantusch M., and Burkel E. " Photocatalytic reactor, CVD technology of its preparation and water purification from pharmaceutical drugs and agricultural pesticides." In Chemical Engineering Journal 312 (2017): 306 - 316.

[100] Ganesh R., Boardman G D.,and Michelsen D. "Fate of azo dyes in sludges." In Water research 28 (1994) :1367-1376.

[101]] Weber EJ., and Adams RL. " Electrochemical monitoring of water remediation by metallic iron." In Environ Environmental Science and Technology 29 (1995): 113.

[102] Zhang T., Oyama T., Aoshima A., Hidaka H., Zhao J and Serpone N. " Photooxidative N-demethylation of methylene blue in aqueous TiO_2 dispersions under UV irradiation." In Journal of Photochemistry and Photobiology A: Chemistry 140 (2001): 163-172.

[103] Ollis DF., and Al-Ekabi H. " Photocatalytic purification and treatment of water and air: proceedings of the 1st International Conference on TiO_2 Photocatalytic Purification and Treatment of Water and Air. " In Elsevier Science Ltd; 1993 .

[104]] Serpone N., Sauve G., Koch R.,Tahiri H., Pichat P., Piccinini P., Pelizzetti E., and Hidaka H. " Standardization protocol of process efficiencies and activation parameters in heterogeneous photocatalysis: relative photonic efficiencies." In Journal of Photochemistry and Photobiology A: Chemistry 94 (1996): 191-203.

[105] Mohabansi NP., Patil VB., Yenkie N. " A comparative study on photo degradation of methylene blue dye effluent by advanced oxidation process by using TiO_2/ZnO photo catalyst. In Rasayan Journal of Chemistry 4. (2011): 814-819.

[106] PubChem (2013).Pubchem database. In National Center for Biotechnology Information. Available from: https://pubchem.ncbi.nlm.nih.gov/

[107] Saha TK., Bhoumik NC., Karmaker S., Ahmed MG., Ichikawa H., and Fukumori Y. " Adsorption of methyl orange onto chitosan from aqueous solution." In Journal of water resource and protection 10 (2010): 898.

[108] Balabanova M., Popova L., and Tchipeva R .(2004). "Dyes in dermatology". Disease-a-Month 6. 50 (2004): 270-279

[109] Thakare Y D., and Jadhav MS. " Degradation of Brilliant Green dye using cavitation based hybrid techniques." In International Journal of Advanced Engineering Technology (2013): 31- 36.

[110] Bancroft., John; Stevens, and Alan. "The Theory and Practice of Histological Techniques (2nd ed.)." Longman Group Limited eds. (1982).

[111] Srivastava V, Singh PP. " Eosin Y catalysed photoredox synthesis: a review. " In RSC Advances 50. (2017): 31377-31392.

[112] Seery MK., George R., Floris P., Pillai SC. "Silver doped titanium dioxide nanomaterials for enhanced visible light photocatalysis." Journal of photochemistry and Photobiology A: Chemistry 189 (2007): 258-263.

[113] Kaushik A., Dalela B., Kumar S., Alvi, P.A. and Dalela, S. " Role of Co doping on structural,optical and magnetic properties of TiO_2." In Journal of Alloys and Compounds 552 (2013): 274-278.

[114] Hanaor D A., and SorrellC C. "Review of the anatase to rutile phase transformation." In Journal of Materials science 46 (2011): 855-874.

[115] Asenjo NG., Santamaria.R., Blanco C., Granda M., Alvarez P., and Menendez R. " Correct use of the Langmuir–Hinshelwood equation for proving the absence of a synergy effect in the photocatalytic degradation of phenol on a suspended mixture of titania and activated carbon." In Carbon 55 (2013) 62-69

[116] Kim TW., Jung M., Kim HJ., Park TH., Yoon YS., Kang WN., Yom SS., and Na HK. "Optical and electrical properties of titanium dioxide films with a high magnitude dielectric constant grown on p-Si by metalorganic chemical vapor deposition at low temperature." Applied physics letters 64 (1994): 1407-1409.

[117] Kang BC., Lee SB., and Boo JH. "Growth of TiO_2 thin films on Si (100) substrates using single molecular precursors by metal organic chemical vapor deposition." Surface and Coatings Technology 131 (2000): 88-92.

[118] Wu T., Liu G., Zhao J., Hidaka H., and Serpone N. "Evidence for H_2O_2 generation during the Ti$_O$2-assisted photodegradation of dyes in aqueous dispersions under visible light illumination." In The Journal of Physical Chemistry B 103, (1999): $4862 - 4867$.

[119] Degenhardt J., and McQuillan AJ. "Mechanism of oxalate ion adsorption on chromium oxide-hydroxide from pH dependence and time evolution of ATR-IR spectra." In Chemical physics letters 311 (1999): 179-184.

[120] Liu X., Geng D., Wang X., Ma S., Wang H., Li D., Li B., Liu W., and Zhang Z. " Enhanced photocatalytic activity of Mo-[001] TiO_2 core-shell nanoparticles under visible light." In Chemical Communications(46) (2010): 6956-6958.

[121] Bouloudenine M., Viart N., Colis S., Kortus J., and Dinia A. "Antiferromagnetism in bulk Zn_{1-x} Co_x O magnetic semiconductors prepared by the coprecipitation technique." In Applied Physics Letters 87 (2005): 052501.

[122] Wunderlich W., Oekermann T. , Miao L., Hue N T.,Tanemura S., and Tanemura M. "Electronic properties of nano-porous TiO_2 and ZnO-thin films comparison of simulations and experiments." In Journal of Ceramic Processing and Research 5(2004):343-354.

[123] Paxton AT and Thien-Nga L."Electronic structure of reduced titanium dioxide." In Physical Review B 57 (1998): 1579-1584.

[124] Kenta Y., Nanbara T., Yamasaki J, and Tanaka N. "Oxygen release and structural changes in TiO_2 films during photocatalytic oxidation." In Journal of applied physics 99 (2006).

[125] Khan H and Berk D. "Selenium modified oxalate chelated titania: Characterization, mechanistic and photocatalytic studies." In Applied Catalysis A: General 505 (2015): 285-301.

[126] Bickley RI., Gonzalez-Carreno T., Lees JS., Palmisano L., and Tilley RJ. "A structural investigation of titanium dioxide photocatalysts." In Journal of Solid State Chemistry 92 (1991):178-190.

[127] Hurum DC., Agrios AG., Gray K A., Rajh T. and Thurnauer MC."Explaining the enhanced photocatalytic activity of P25 Degussa mixed-phase TiO_2 using EPR." In The Journal of Physical Chemistry B 107 (2003): 4545-4549.

[128] Hurum DC., Gray KA., RajhT. and Thurnauer MC. "Recombination pathways in the Degussa P25 formulation of TiO_2: Surface versus lattice mechanisms." In The Journal of Physical Chemistry B 109 (2005): 977-980.

[129] Vinodgopal K., and Prashant V K. "Photochemistry of textile azo dyes. Spectral characterization of excited state, reduced and oxidized forms of acid orange 7." In Journal of Photochemistry and Photobiology A: Chemistry 83(1994): 141-146

[130] Qu P., Zhao J., Zang L., Shen T., and Hidaka H. "Enhancement of the photoinduced electron transfer from cationic dyes to colloidal TiO_2 particles by addition of an anionic surfactant in acidic media. Colloids and Surfaces A".In Physicochemical and Engineering Aspects 138 (1998): 39-50.

[131] Youngblood WJ., Lee SH., Kobayashi Y., Hernandez-Pagan EA., Hoertz PG., Moore TA., Moore AL., Gust D., and Mallouk TE. "Photoassisted overall water splitting in a visible light-absorbing dye-sensitized photoelectrochemical cell." In Journal of the American Chemical Society 131 (2009): 926-927.

[132] He J., Zhang M., and Shen T. "Photoinduced intermolecular and intramolecular actions between eosin and porphyrin." In Science in China Series B: Chemistry 40 (1997): 380-388.

[133] Bogdos MK., Pinard E., and Murphy JA. "Applications of organocatalysed visible-light photoredox reactions for medicinal chemistry." In Beilstein journal of organic chemistry 14(2018): 2035-2064.

[134] Ghica ME and Brett CM. "Poly (brilliant green) and poly (thionine) modified carbon nanotube coated carbon film electrodes for glucose and uric acid biosensors." In Talanta 130 (2014): 198-206.

[135] Yang H., Liang J., Zhang L., and Liang Z . "Electrochemical oxidation degradation of methyl orange wastewater by Nb/PbO_2 electrode." In Int Journal Electrochem Sci 11 (2016): 1121-1134.

[136] Fujishima A., Rao TN., and Tryk DA. "Titanium dioxide photocatalysis." In Journal of photochemistry and photobiology C: Photochemistry reviews 1 (2000): 1-21.

[137] Yin M., Li Z., Kou J., and Zou Z. "Mechanism investigation of visible light-induced degradation in a heterogeneous TiO_2/Eosin Y/Rhodamine B system." In Environmental science and technology 43 (2009): 8361-8366.

Declaration of Authorship

I hereby declare I have prepared the present work on my own and wrote it without help from others, except the tools I have specified and sources used for this.

Adwaa Ahmed
26.06.2020, Rostock